Coherent Scattering from Colloidal Dispersions

by

ANDREW G. MUDDLE

This degree is submitted for the degree of Doctor of Philosophy of the University of London and a diploma for membership of Imperial College of Science and Technology.

Department of Chemical Engineering and Chemical Technology, Imperial College, Prince Consort Road, London, SW7 2AZ.

January 1986.

Acknowledgements

I would like to thank Dr. P.G. Cummins, Dr. J.S. Higgins and Dr. E.J. Staples for the interest, guidance and support that they have provided throughout the course of this work.

I am indebted to Unilever Research for the CASE Award and the opportunity and facilities for this research. On numerous occasions during my research colleagues at Unilever Research have provided both intellectual and material assistance and their contribution is gratefully acknowledged. I am much indebted also to Institut Max von Laue-Paul Langevin, neutron committees for their steady support.

I would like to thank Dr. E.J. Staples for the use of his light scattering data.

Finally, I would like to express my appreciation to Mr. Paul Johnson for his invaluable technical assistance in producing the figures included, and to Julia Holman for typing the manuscript.

CONTENTS Page No:

Abstract 5

Preface 6

Figures and Tables 7

CHAPTER 1 - Introduction

(1) Surfactants 9
  (a) Anionic
  (b) Cationic
  (c) Nonionic
  (d) Zwitterionic
(2) Micellization in Aqueous Solution 10
(3) The Krafft Point 11
(4) Solubilization 11
(5) Thermodynamics of Micelles 11
  (a) Introduction
  (b) Thermodynamics of Micellar Solution
  (c) Alkyl-Chain Packing Constraint (packing term)
(6) Concentrated Surfactant Solutions 16
(7) Liquid Crystal Phases 18
  (a) Lamellar Phase (neat)
  (b) Hexagonal Phase (middle soap)
  (c) Cubic Phase (viscous isotropic)
  (d) Others
  (e) Inter Micelle Interactions
(8) Membrane Mimicry 23
(9) Techniques of Observation 24
  (a) Rheology
  (b) Nuclear Magnetic Resonance (N.M.R.)
  (c) Microscopy
  (d) Scattering Techniques

CHAPTER 2 - Scattering Theory

(1) Introduction 28
(2) Scattering Theory 28
(3) Scattering Cross Section Function 30
(4) Contrast 34
(5) Particle Scattering Factor 38
(6) Polydispersity 40
(7) Multiple Scattering 40
(8) Dynamic Light Scattering 41
(9) Interacting Particles 43
(10) Polydispersity 45

CHAPTER 3 - Colloid Interactions

(1) DLVO Theory 47
  (a) Repulsion Forces
    i. Electrical Potentials
      a. Ionisation
      b. Ion adsorption
      c. Ion dissolution
    ii. Hydration Forces
    iii. Hard sphere potential
  (b) Attraction Forces

Page No:

(2) Concentrated Dispersion Particle-Particle Interactions 53
(a) The Radial Distribution Function
(b) Relationship between g(r) and S(Q)
(c) The Potential of Mean Force
(d) Relation of S(Q) to Models of Particle-Particle Interactions
(e) Charged Hard Sphere Potential
(f) One Component Macrofluids

CHAPTER 4 - Techniques

Small Angle Neutron Scattering

(1) General Background 61
(2) Experimental Techniques 62
(3) Data Analysis 64

Photon Correlation Spectroscopy

(4) Introduction 65
(5) Apparatus 66
(6) Data Analysis 68

CHAPTER 5 - Light Scattering and Neutron Scattering from Concentrated Dispersions of Small Unilamellar Vesicles

(1) Introduction 70
(2) Theory 72
(3) Experimental 73
(a) Materials
(b) Preparation of Vesicles Dispersions
(4) Results and Discussion 77
(a) Neutron Scattering
(b) Comparison of Theoretical Models
(c) Light Scattering
(5) Conclusions 101

CHAPTER 6 - Polymerised Vesicles

(1) Introduction 102
(2) Experimental 104
(a) Materials
(b) Preparation of Polymerised Vesicles Dispersions
(3) Results 105
A. Electrolyte Effects 105
(a) Neutron Scattering
(b) Light Scattering
(c) Discussion
B. Osmotic Shock on Polymerised Vesicles 120
(a) General Background
(b) Disadvantages
(i) Preparation of Vesicles
(ii) Electrolyte Effects
(iii) Isotope Effects
(iv) Column Dilution
(c) Neutron Scattering
(i) Characterisation of the Dispersion
(ii) Sucrose
(iii) Glucose
(iv) Incorporation of Methanol in Bilayer
(v) Conclusions

Page No:

CHAPTER 7 - Viscoelastic Micellar Solution: A Study of the Transition from Rod-Like to Spherical Micelle

(1) Introduction 140
(2) Experimental 142
(3) Results 145
(4) Discussion of Results 157
(5) General Discussion 159
(6) Conclusion and Future Aims 160

REFERENCES

Chapter 1 167
Chapter 2 169
Chapter 3 171
Chapter 4 173
Chapter 5 174
Chapter 6 177
Chapter 7 178

NAME: ANDREW G. MUDDLE

TITLE: Coherent Scattering from Colloidal Dispersions

ABSTRACT

Small-angle neutron scattering and light scattering have been used to study the interactions between particles (diameter >10nm) prepared from surfactant molecules in an aqueous medium.

Vesicular dispersions may be regarded in many respects as conventional colloids. Concentrated dispersions of small unilamellar vesicles have been prepared covering a wide range of concentration. Data are reported on the single-particle form factor P(Q) and the interparticle structure factor S(Q) for dispersions up to 4% (w/v) solids. The interparticle potential is investigated by varying the net charge on the vesicles (via the lipids used in the preparation) and by addition of electrolyte. The integrity of the vesicles with varying concentrations allow S(Q) to be obtained by simple division of high- and low- concentration data. The overall behaviour of S(Q) and S(0) is in agreement with model predictions. The structure factors, S(Q), which have been determined have been compared with those calculated for a model hard sphere potential and the mean spherical approximation model for charged hard spheres interacting through an unscreened Coulombic potential.

A similar data analysis and modelling has been used for polymerised vesicle dispersions prepared by heat treatment of vesicles made from monomers with a polymerisable group. These particles have the advantage over phospholipid vesicles of long-term stability.

The main objective has been to gain some knowledge of the structure of biological membranes. The formation of vesicles permits the use of a colloid approach to obtain detail of inter-membrane interactions. The experiments exploiting the change of concentration of encapsulated material with time has given insight into permeability of lipid structures.

Structure in viscoelastic mixed micelle systems has been investigated using the neutron scattering technique with the aim of obtaining interparticle spacing and particle size parameters.

PREFACE

In general, dispersed colloid systems are characterised by two distances. One relates to the size such as the diameter of the individual particles comprising the system which are in the range ten to a thousand angstoms. The other characteristic distance gives the mean separation of particles in the dispersed system and thus can be much larger ten's to ten thousand's angstoms. Independent of precise details of the dispersed system under consideration these two distances together determine the macroscopic properties and must be determined by measurement in any description of the system. As examples, one might remark that in surfactant liquid crystal phases these two characteristic distances are of similar magnitude, while in the dilute and concentrated micellar regions the intermicellar distance may be several orders of magnitude larger than the intra-micellar spacing.

The intensity of scattered radiation depends on the size of the particle on the number density (inter-probing distance) and on the polarizibility of the particle compared with that of the medium in which it is suspended. Provided a wide wavelength range encompassing both neutrons and light is available, scattering would appear to be the technique of choice for determining these characteristic distances. Save in particular circumstance, this technique is non-invasive and non-destructive in that the radiation normally leaves the particle unaltered in structure.

The extension of the Q range with the introduction of neutron scattering in particular has given new importance to modelling the scattered intensity in the Rayleigh-Gans regions with the single particle form factor P(Q). In the past one was restricted to the wavelength range of 3000-9000Å by the use of conventional light sources. Large particles by colloidal standards could be studied in detail using light sources. These particles are prone to sedimentation and in some cases are close to being Mie scatters, while smaller particles were regarded as point sources according to Rayleigh law. The introduction of neutron scattering has changed this situation in a radical way - particles down to 10Å in diameter are now susceptible to detailed study.

In the thesis unusual shaped association colloids were studied using scattering techniques. Surfactants usually associate to form spherical micelles above the critical micellar concentration, however, the surfactants chosen for these studies formed bilayer shell structures called vesicles and rod-like micelles. In general surfactants liquid crystal phase behaviour mirrors the structure of the micelle in the dilute region, i.e. where lamellar phase is present at high concentration the surfactant in the dilute region may form vesicles, and where a hexagonal phase is observed then rod-like micelles may be present in the dilute solutions.

In Chapter 1 surfactant phase behaviour is described from the dilute region to liquid crystal phases, while Chapters 2 and 3 are intended to provide a background in the major concepts of scattering theory and colloid science respectively. Chapter 4 details the techniques used and the data analysis. In constructing the experimental section of the thesis the author has attempted to group the work under three main chapters (5,6,7) which can be read with their separate introductions and conclusions as independent texts by those reasonably familiar with the areas of neutron and light scattering and colloid science.

FIGURES AND TABLES

Figure 1: Hartley model of a spherical micelle.
Figure 2: Liquid crystal phases.
Figure 3: Typical surfactant water phase diagram.
Figure 4: The chemical structure of the phospholipid group of molecules.
Figure 5: Definition of the scattering vector.
Figure 6: Contrast difference between particle and solvent.
Figure 7: Interaction between spheres.
Figure 8: Radial distribution of particles.
Figure 9: Radial distribution function.
Figure 10: Small angle diffractometer D11.
Figure 11: Photon correlation spectroscopy system.
Figure 12: Vesicle interactions: attractive only.
Figure 13: Vesicle interactions: attraction and electrostatic repulsion.
Figure 14: Neutron scattering data for uncharged PC vesicles.
Figure 15: Neutron scattering data at high Q for charged vesicles.
Figure 16: Neutron scattering data at low Q for charged vesicles.
Figure 17: Neutron scattering data at low Q for charged vesicles in the presence of salt.
Figure 18: Neutron scattering at low Q for charged vesicles.
Figure 19: Structure factor S(Q) against Q for 90:10 vesicles.
Figure 20: Structure factor S(Q) against Q for 95:5 and 50:50 vesicles.
Figure 21: Structure factor S(Q) against Q for 90:10 vesicles modelled by hard-sphere and Hayter-Penfold model.
Figure 22: Plot of S(Q) against Q for 90:10 vesicles 4% in 0.01 mol dm^{-3} salt modelled by Hayter-Penfold and hard sphere models.
Figure 23: Plot of S(Q) against Q for 90:10 vesicles 4% modelled by hard-sphere.
Figure 24: Plot of incoherent scattering intensity as a function of concentration, PC:PS 90:10
Figure 25: Pair distribution function.
Figure 26: Diffusion data for charged vesicles.
Figure 27: Absolute intensity light scattering data for 90:10 PC:PS vesicles.
Figure 28: Ammonium salt.
Figure 29: Methods of polymerisation of surfactant bilayer.
Figure 30: Particle diameter versus sonication time.
Figure 31: Neutron scattering data at high Q for polymerised vesicles (sample 3) in the presence of various salt concentrations.
Figure 32: Neutron scattering data at high Q for polymerised vesicles (sample 3) at two concentrations.
Figure 33: Theoretical model for aggregation over a long time period.
Figure 34: Neutron scattering data at high Q for polymerised vesicles at two time periods.
Figure 35: Neutron scattering data for the gel phase.
Figure 36: Neutron scattering data for polymerised vesicles (G2) modelled by P(Q).
Figure 37: Particle size distribution for sample G2 obtained from the model P(Q) used to fit figure 36.
Figure 38: Neutron scattering data for sample G2 on addition of 10% sucrose over a time course.

Figure 39: Particle size distributions for sample G2 in the presence of 10% sucrose obtained from the fits to the data in Figure 38.
Figure 40: Comparison of G2 and the 10% sucrose 48 hour sample 7447.
Figure 41: The three dimensional phase diagram for SDS/TDPS/H_2O system.
Figure 42: The three dimensional phase diagram of SDS/TDPS/H_2O system showing where data had been collected.
Figure 43: Neutron scattering data at high Q for SDS/TDPS mixed micelles along line 1.
Figure 44: The spectral parameters associated with the data in figure 43.
Figure 45: Neutron scattering data at high Q for SDS/TDPS along line 3.
Figure 46: The spectral parameters associated with the data in figure 45.
Figure 47: Neutron scattering data for 0.5% TDPS fitted with P(Q) and in the Guinier region.
Figure 48: Schematic diagram of the flow in shear experiments.
Figure 49: Neutron scattering data perpendicular and parallel to the flow direction for 0.03M CTAB in 0.4M KBr.
Figure 50: Neutron scattering data perpendicular and parallel to the flow direction for the TDPS/SDS system (2% SDS and 6% TDPS) (a) low shear, (b) high shear.
Table 1: Lipid ratios and concentrations.
Table 2: Interparticle spacing and number density for 90:10 vesicles.
Table 3: Effective diameters and second cumulant.
Table 4: Preparation of polymerised vesicles.
Table 5: 10% sucrose added to G2 polymerised vesicles. Fitting parameters for the data over the time course.
Table 6: 30% sucrose addition to G2 polymerised vesicles. Fitting parameter for the data over the time course.
Table 7: 10% glucose addition to G2 polymerised vesicles. Fitting parameter for the data over the time course.
Table 8: 30% glucose addition to G2 polymerised vesicles. Fitting parameter for the data over the time course.
Table 9: 10% sucrose with 10% methanol added to G2 polymerised vesicles. Fitting parameter for the data over the time course.
Table 10: 30% sucrose with 10% methanol added to G2 polymerised vesicles. Fitting parameter for the data over the time course.
Table 11: Sample preparations for the various solutions observed by neutron scattering.
Table 12: Micelle dimension obtained from fits using Guinier plots.
Table 13: Micelle dimension obtained from the peak in I(Q) data.

CHAPTER 1 - INTRODUCTION

This thesis is a study of association colloids by both neutron and light scattering. The surfactants of interest form unusual shaped particles, whereas most surfactants associate to form spherical shaped aggregates.

From the brief description above, researchers in the field will immediately understand and take for granted the problems to be solved in the area. However, any newcomer to the area may need more of an understanding of the elementary terms used in surfactant chemistry, micellization, liquid crystal phases and colloid science.

This chapter is an elementary glossary of the surfactant properties, describing surfactant types, dilute micellar and concentrated micellar solution properties and finally liquid crystal phases, while scattering theory and colloid interactions are dealt with in chapters 2 and 3 respectively.

(1) Surfactants

These are amphiphilic molecules, i.e. they have regions in the same molecule that vary enormously in their interaction with water. One part of the molecule is hydrophilic in nature and is commonly referred to as a "head group". This region is freely associated with water and is insoluble in hydrocarbons. It may be anionic or cationic and may have associated counter ions. The second part of the molecule is essentially hydrophobic in nature and is referred to as the "tail group". This group commonly occurs as a hydrocarbon chain and may be saturated or unsaturated. As a consequence of this dual property within the molecules they are said to be amphipathic, i.e. that they will tend to orient themselves such that the head groups are associated with water whilst the tail groups are away from it. At interfaces, such as the air-water interface, the molecules will adopt the configuration in which the head groups are in the water and the tail groups point away from the interface, they are said to be surface active.

Four groups of surface-active agents have been distinguished:-

(a) Anionic (the most common surfactants) includes soap and synthetic surfactants such as the linear alkyl sulphates. This type of surfactant is partially dissociated in aqueous solution and the hydrophilic portion is, as the name suggests, negatively charged.

(b) Cationics are similar to anionics. They dissociate in solution but now the hydrophilic portion carries a positive charge.

(c) Nonionic. This group of surface active agents do not dissociate but commonly derive their hydrophilic property from polyhydroxy or polyethoxy structures. The overall solubility of these materials depends on the extent of hydration of the hydrophilic moiety. The water molecules are associated with the ether oxygens by hydrogen bonding. Depending on the nature of the hydrophobic group, at least four to six ethylene oxide units per molecule are required to produce a water soluble surfactant.

(d) Zwitterionics have the potential for being both anionic and cationic, the relative contribution being dependent on the pH of the dispersing medium.

(2) Micellization in Aqueous Solution

In dilute solution surfactants act as normal electrolytes. As the concentration of surfactant is increased from zero a sudden change in the physical properties of the solution is observed. The conductance of the ionic surfactant solution however remains relatively high showing that ionic dissociation is still occurring. McBain (1,2) and Hartley (3) attributed these changes to a sudden onset of molecular association into what they term a micelle (Figure 1).

The concentration of surfactant at which this process occurs is referred to as the critical micelle concentration (C.M.C.). It must be recognised, however, that there may be a range of values for the C.M.C. depending on the physical property used to detect it.

(3) The Krafft Point

The formation of micelles is temperature dependent; below a certain value the micellar solution phase separates.

This behaviour is exactly analogous to polymer blend phase separation at the upper critical solution temperature (U.C.S.T.). From an observation of this behaviour with temperature it is possible to define a point below which micelles are insoluble. This point is called the Krafft point. It should be noted that this refers to the behaviour of the micelles and that in some systems a lower consolute solution temperature is also observed.

(4) Solubilization

Organic components are found to be much more soluble in mixed systems of solvent and surfactant than in solvent systems alone. In a system where there might be a driving force for phase separation (or precipitation) the surfactant acts by adsorbing at the interface and reduces this force.

The solubilized molecules are then incorporated into the micelles. Nonpolar molecules are incorporated into the core while semipolar molecules act like normal surfactants. Polar molecules can adsorb at the surface and decrease the hydrocarbon/water contact. The formation of microemulsions (4) is closely related to solubilization as the minor solvent is solubilized by surfactant. These are clear, low-viscosity fluids that contain oil, water and surfactants.

(5) Thermodynamics of Micelles

(a) Introduction

Simple theories have been developed to account for many of the observed physical properties of variously shaped micelles and of bilayer vesicles. Early thermodynamic treatments of micelle solutions involved the law of mass-action (5) and that

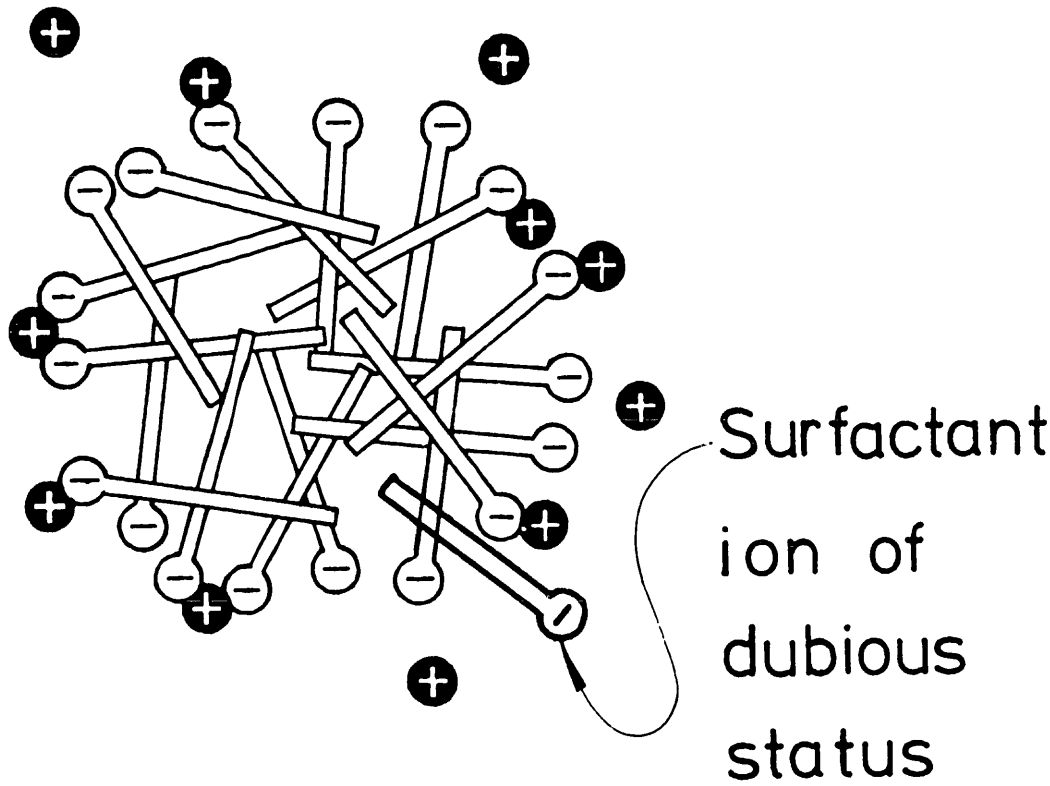


Figure 1: Hartley Model of a Spherical Micelle.

of the charged-phase (6) approaches. Subsequently a small system/multiple (7) equilibrium approach was applied to ionic surfactants and gave similar results. None of these analyses deal with interactions between micelles nor do they describe in detail the role of the counterions. The counterion in these approaches is divided into two distinct classes, bound and free, where the fraction of bound counterion neutralizes the charged micelle. However, this approach is an over-simplification as there must be a range of "boundness". In later theories (8) the role of geometric constraints is necessarily emphasized as in the absence of any such constraints, spherical micelles will be thermodynamically more favourable. From classical thermodynamics, micellization leads to non-ideal solutions which can be accounted for by the introduction of activity coefficients.

(b) Thermodynamics of Micellar Solution

The thermodynamics of dilute solutions of surfactants is fairly well understood given certain "reasonable" assumptions. The main one is the so-called "pseudo-phase approximation" (9) in which no micelles are assumed to occur below the C.M.C. Above the C.M.C. all additional surfactant molecules form micelles. The behaviour of the chemical potential or activities of the various solute species, when the temperature and the solution composition are altered is the main concern. This activity determines the macroscopic properties and gives an insight into the state of surfactant at the molecular level in solution.

The distribution of aggregates is determined by the law of mass action, which is:-

$$\mu^{\circ}_n + \frac{k_B T}{N} \text{ Ln } \frac{(X_n)}{N} = \mu_1^{\circ} + k_B T \text{ Ln } X_1 \qquad \text{Equation 1(1)}$$

N is aggregation number

k_B is Boltzmann constant

T is temperature

X_n is mole fraction of amphiphile

Each aggregate is considered to be a distinct species each characterised by its own self free energy $N\mu^{\circ}_{n}$.

The chemical potential of different aggregates, μ°_{n}, have contributions from four major effects.

μ°_{n} = "bulk term" + "surface term" + "curvature term" + "packing term".

The bulk term is constant and is a measure of the hydrophilic free energy of removing long hydrocarbon tails from water into an assumed oil-like phase. The oil-like phase is made up of all tails forming the interior of the micelle.

Micellar thermodynamics are mostly dominated by the requirements of the environment around the hydrophilic group. Early models (10) promoted the idea that water adjacent to hydrocarbon chains is more structured than the bulk water. However, later research explained the spectroscopic and thermodynamic properties of non-polar solutes in water in terms of van der Waal's interactions.

The surface term has several contributions which are in competition. At the surface there will be some contact between hydrocarbon and water. Reduction of this surface contact will be energetically favoured but will only be achieved at the expense of reducing head group separation.

This head group separation is controlled by forces which include steric, hydration and electrostatic forces. These contending forces will lead to an optimal area a_o per head group.

The curvature term includes a correction to the "effective" surface tension. In the case of ionic surfactants, corrections to the electrostatic contribution is added. A Debye screen length, which is the distance that the electrostatic repulsion force penetrates the solvent from the surface of the micelle, has to be considered along with the mean radius of curvature.

The above thermodynamic treatment imposes no model restrictions on micelles, however, consideration of simple geometric limitation further constrains the number of possible micelle geometries.

(c) Alkyl-Chain Packing Constraint (Packing term)

The shape of micelles in the region of the C.M.C. and at concentrations approaching the liquid crystalline phase are of considerable interest.

At the lower concentration the shape of the micelle is dependent on the type of surfactant and various other solution conditions (concentration, electrolyte levels, temperature). At higher concentrations, however, intermicelle effects become important.

Following assumptions that water is excluded from the centre of the micelle, the maximum diameter of a micelle of any geometry is restricted to twice the "all-trans" length of the alkyl chain.

In a dilute environment the micelle shape is determined by the surface area per molecule (a), at the micelle/water interface, and the interface curvature. For a spherical micelle, the volume of the surfactant alkyl-chain (v), micelle radius (r) and a are related through

$$v = \frac{ar}{3} \qquad \text{Equation 1(2)}$$

The radius (r) is limited by the "all-trans" length of the alkyl chain (l_t) while v is invariant. The surface area per molecule, a, cannot fall below a certain value, a_o, known as the critical packing area. Therefore, a spherical micelle will not be able to form unless the surface area $a > a_o$. This gives a critical condition (1c) for the formation of spheres:-

$$\frac{v}{a_o\, l_c} > 1/3 \qquad \text{Equation 1(3)}$$

For rod-like micelles we have

$r = 2v/a_o$; $v/a_o l_c < 1/2$ Equation 1(4)

This type of analysis yields the general trend:

$\longleftarrow$ Increasing area per head group

spherical > cylindrical > bilayers > inverted structures.

With the overall prediction of formation of various shaped micelles being:-

Spherical micelles	$v/a_o l_c < 1/3$
Cylindrical micelles	$1/3 < v/a_o l_c < 1/2$
Bilayers (or vesicles)	$1/2 < v/a_o l_c < 1$
Inverted structures	$v/a_o l_c > 1$

In summary the area occupied by the head group is of vital importance to the shape of the micelle. Thus any driving force that induces a change in head group configuration (e.g. electrostatic or hydration forces) may produce a transition in the particle shape and manifest itself in the macroscopic properties of the dispersion. The limiting head group area for spherical and cylindrical micelles can be estimated by assuming a C-C bond length of 1.25Å and using known densities for alkanes and this yields values of $\sim 70Å^2$ and $47Å^2$ for spheres and rods respectively.

It should be possible to extend these theories of micelle shapes to account for mesophase formation by addition of appropriate terms for intermicellar forces. Paresegian (11) has already successfully described the hexagonal/lamellar transition of ionic surfactants using Poisson-Boltzmann theory.

(6) Concentrated Surfactant Solutions

As the concentration of a micellar solution is increased from the C.M.C. towards the liquid crystal phase, two types of behaviour occur. The

first category (Type 1), which includes most single surfactant/water systems, shows no dramatic change in solution properties up to the saturation limit. Above this limit additional surfactant remains as a crystalline solid or forms a liquid crystalline phase. The properties of Type 1 can be linearly related to the properties at low concentration.

As indicated, there is no advantage in carrying out studies at high concentration since molecular/micellar information can in general be obtained from the dilute region. Information on micelle-micelle interactions however can be extracted from this concentrated region (12). These interactions, both electrostatic and hydrostatic, are large in magnitude.

In some surfactant systems as the concentration increases the micelle size increases, and a transition to anisotropic micelles may occur. The shape of the anisotropic micelles is thought to be related to the structure of the nearest liquid-crystal phase. For example, near the cubic phase spherical micelles exist, adjacent to the hexagonal phase cylinderical micelles occur, whereas those bordering the lamellar phase form platelike micelles or vesicular structures.

This second category (Type 2) of solutions is much more complex and usually occurs with mixtures of surfactants and additives, often in the presence of salt. In Type 2 solutions sharp increases in viscosity are observed well below saturation. Above the phase boundary additional surfactant separates as liquid-crystal phases. The equilibration time of these two phase solutions is very long and so many measurements are performed on non-equilibrium systems. Addition of salt increases the viscosity and lowers the boundary for mixed surfactants. Concentration ranges of Type 2 solution can be as low as 0.1%. These solutions can also be viscoelastic, i.e. on shearing energy is stored in the system to be released at some later stage.

Most researchers into these systems have explained these unusual properties as arising from the existence of large rod-shaped micelles (13) which form a network, so giving rise to viscoelastic effects. As the composition of the mixed micelle approaches the liquid-crystal phase boundary so the highest viscosities are measured in this region. One of

the rheological properties of these solutions is that the viscosity increases with shear rate. This phenomenon cannot be explained by the existence of rod-like micelles but can be explained by assuming the existence of an equilibrium between large rod-shaped micelles and small spherical micelles (13). In this dynamic equilibrium rod-shaped micelles are formed from collisions between small micelles. Factors that reduce electrostatic repulsion between small micelles increase the rate of collision therefore the equilibrium moves towards a larger proportion of rod-shaped micelles. High concentration also moves the equilibrium towards more or longer rods through more collisions.

(7) Liquid Crystal Phases

Three liquid crystal phases have been cited in the literature: (i) Lamellar, (ii) Hexagonal and (iii) Cubic, and are mainly concerned with an attempt to understand the behaviour of biological membranes. This work has been carried out in excess water where the liquid-crystal phase is in equilibrium with the aqueous phase.

(a) Lamellar Phase (neat)

In the lamellar phase (14,15,16) (Figure 2) the surfactant molecules are packed in bilayers with water layers sandwiched between them. The surfactant molecules are arranged so that the head groups are in contact with the aqueous medium. The thickness of the water layer can vary depending on the percentage of water in the system, but the layer spacings appear to remain equal. This is also the case with the surfactant layers, where the thickness here depends on the surfactant chain length. The thickness of the bilayer of surfactant is generally about 10-30% less than the length of two "all trans" surfactant chains.

(b) Hexagonal Phase (middle soap)

The hexagonal phase (16) (Figure 2) consists of rod-shaped micelles of a certain ill-defined length arranged in a hexagonal array. Depending on the conditions, water (normal)

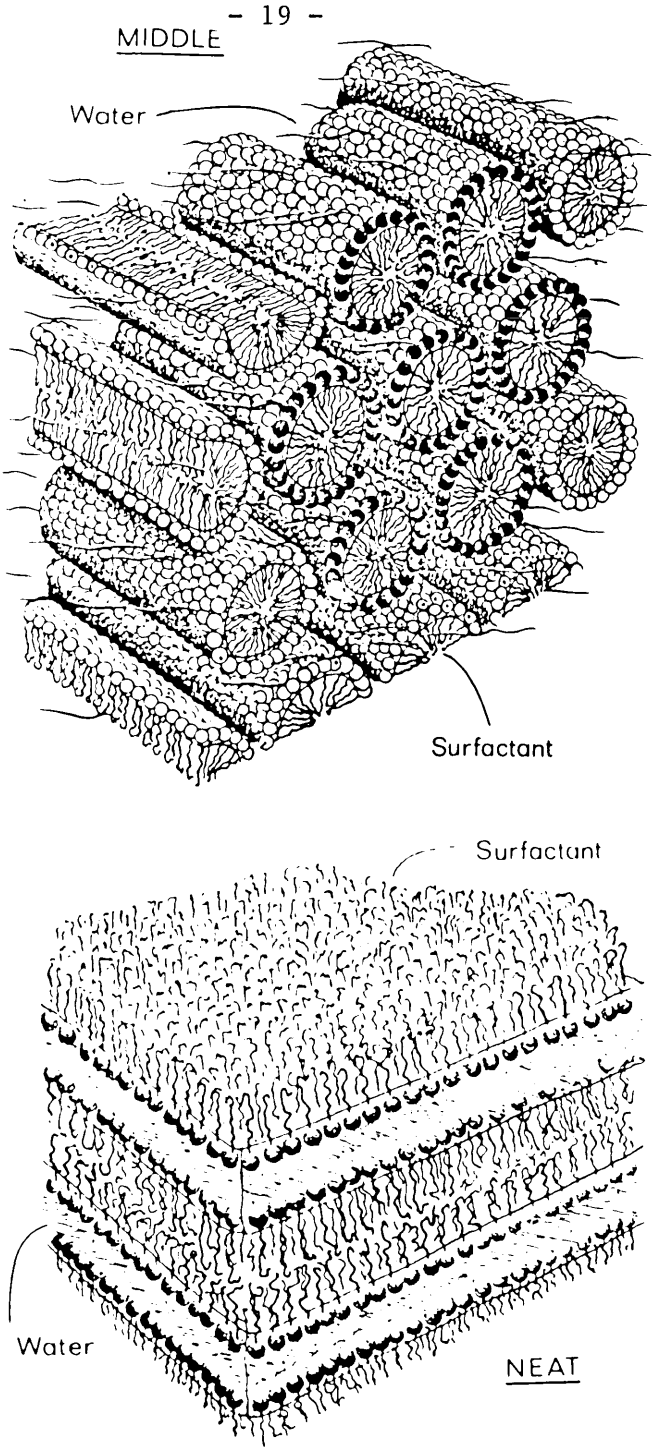


Figure 2: Liquid crystal phases. (a) schematic design of hexagonal (middle) phase. Surfactant cylinders of indefinite length packed hexagonally in aqueous continuous; (b) schematic diagram of lamellar (neat) phase. Alternating surfactant bilayers of indefinite extent (reprinted from "Anionic Surfactant" Chapter 2 with kind permission from G.J.T. Tiddy).

or surfactant (reversed) may be the continuous phase. As with the lamellar phase the radius of the normal hexagonal phase is limited to 70-90% that of the thickness of two "all-trans" surfactant chains. In the reversed hexagonal phase, however, the water cylinder diameter is usually in the range of 10Å-20Å, while the surfactant continuous region separating the aqueous cylinders is approximately 1.5 times the thickness of a fully extended chain.

(c) Cubic Phase (viscous isotropic)

The cubic phase (17) structure is not well established and there seems to be more than one inferred structure. One proposed structure for these phases involves normal (water continuous) micelles or reversed (alkyl-chain continuous) micelles packed in an array having cubic symmetry. This cubic array may be face-centred cubic, body centred cubic or primitive cubic. The second proposed structure has a continuous network of interconnecting rod-like structures. These can be water or surfactant continuous.

(d) Other Liquid-Phases

Surfactant and water "Gel" (18) phases are lamellar structures which occur at temperatures below the lamellar phase region and therefore have "solid-like" chains. These gel phases can have bilayers which can be tilted or they can be formed of mono-layers.

During research on numerous surfactants, at various concentrations, several unusual physical properties have been observed. These properties have been argued to arise from complex phase structures.

(e) Intermicelle Interactions

At high surfactant concentrations there are two significant forces on the systems, interactions and excluded volume. The latter is the major effect and may be considered singly for simplicity.

In a latex dispersion if the number of particles is increased there comes a point where no further particles can be added and structuring occurs. This point is referred to as an order-disorder transition and occurs independently of the shape of the particle.

In surfactant systems this transition is not observed due to the flexible nature of the micelle and its associated structure. Before the number of micelles reaches the order-disorder transition the system will convert into a more thermodynamically stable configuration. A phase change will occur generally to a liquid crystal phase. On passing through a phase boundary the concentration can still be increased as there is a range of concentrations over which these liquid crystalline phases occur. Although the phase is ordered it is not saturated. For spherical micelles this saturation condition occurs when the micelles pack into a face-centred cubic array. With this geometric restriction on the system a theoretically limiting volume fraction of 0.74 can be calculated. In the case of rod-shaped micelles a hexagonal array will occur with a limiting volume fraction of 0.91. Theoretically a lamellar phase can occur without an aqueous phase present so a limiting volume fraction of 1.0 is calculated. With lamellae it is impossible for two bilayers to pass through one another and therefore there is a tendancy for them to pack at any volume above the C.M.C.

The range of distances over which the bilayers may pack is governed by attractive and repulsive forces and since lamellae cannot pack at an infinite distance apart at any concentration above the C.M.C. the system is two-phase; a lamellar phase and water.

Due to the theoretical limits of the volume fractions associated with the three different liquid crystalline phases, when this value is approached the phase re-arranges to a more favourable phase. This is seen in most surfactant systems. Figure 3 shows one particular surfactant phase behaviour where several liquid crystal phases occur.

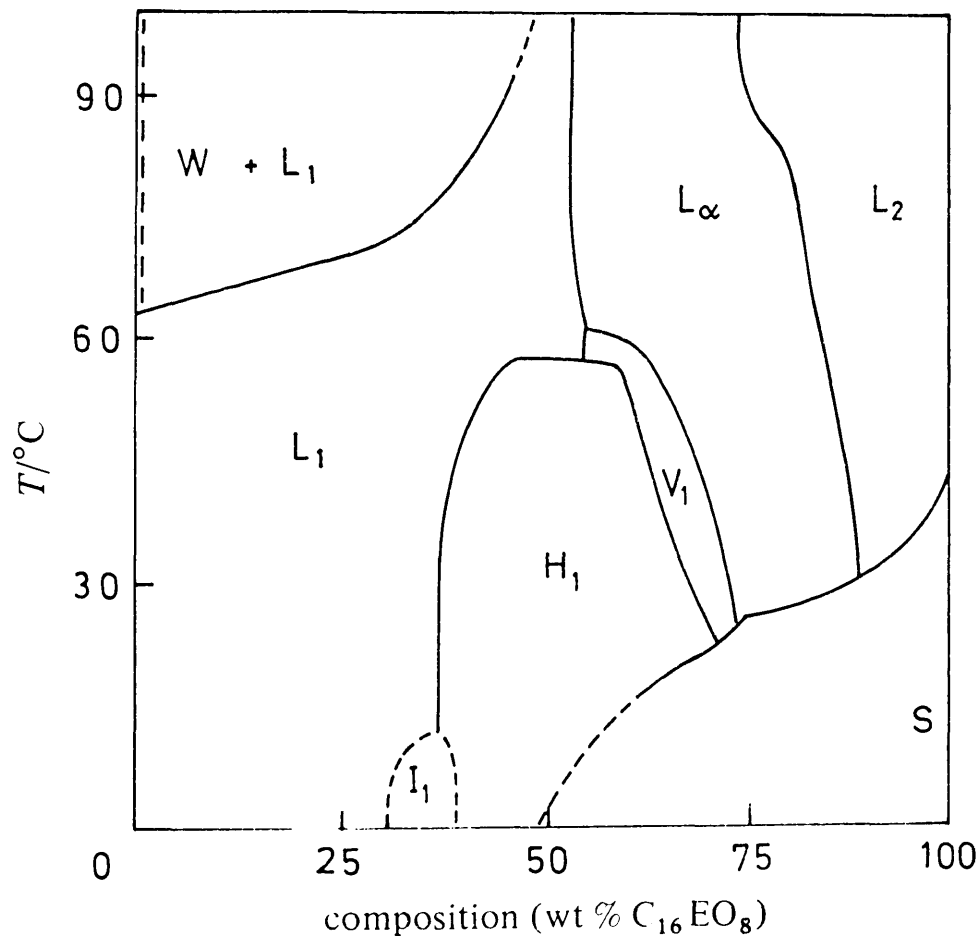


Figure 3: Phase diagram of a typical surfactant water system ($C_{16}EO_8$/water) over the temperature range 0-100°C (L_1, aqueous surfactant solution; W, very dilute surfactant solution; H_1 normal hexagonal, L_α lamellar; I_1 cubic-spherical micelles; V_1 normal-cubic-bicontinuous; L_2 surfactant liquid; S solid).

Since the assumption of hard-core interactions is only approximate a soft-core repulsion must be considered which extends over many micelle diameters. This force will be considered in detail in Chapter 3.

(8) Membrane Mimicry

The chemistry and physics of naturally occurring lipids presents a challenging and complex field for scientific exploration. Microscopic examination of plant and animal tissue reveals the fact that while cells differ markedly in shape, size and function, they still have certain fundamental characteristics in common. Each is bound by a fine membrane the main component of which consists of proteins and various lipids.

The term "lipid" or "fat" refers to esters of long chain fatty acids and alcohols or closely related derivatives. The main lipid component of animal cells is phospholipid of the general structure shown in Figure 4 where x is a nitrogenous base, usually: choline ($x=CH_2CH_2{}^{(+)}N(CH_3)_3$), ethanolamine ($x=CH_2CH_2{}^{(+)}NH_3$) or serine ($x=CH_2CH(COO^-)N^+H_3$). A wide range of acyl groups are found in naturally occurring glycerophospholipids, the most common having between 16 and 20 carbon atoms in the chain with up to four carbon-carbon double bonds.

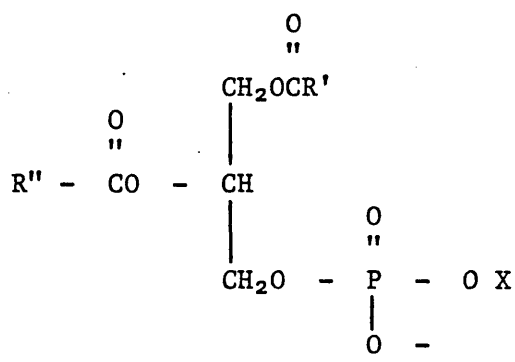


Figure 4: The chemical structure of the phospholipid group of molecules.

One of the major aims of molecular biology must be the elucidation of the structure of the cell membrane, for it is the outer membrane that ultimately determines the interaction between cell and the environment. It must have certain physical properties which include mechanical strength electrical insulation as a permeability barrier and it must remain intact for the lifetime of the cell.

The fluid-mosaic model of Singer-Nicholson (19) is an attempt to incorporate the various properties of biological membranes in a defined way. The model is based on the findings that proteins and lipids are more dynamic than previously suggested. The proteins and lipids form a "mosaic" if the surface of the membrane is viewed from above. The proteins are incorporated in a sea of lipid. Some of the proteins are arranged so that they pass completely through the lipid bilayer and others are confined to one half of the bilayer or the other. The lipid bilayer presents an effective permeability barrier whilst some proteins maybe the agents by which molecules may be transported (18) from one side to the other. The proteins are also responsible for the variety of enzymatic processes (19) that occur at the interface.

On dispersion in water, phospholipids do not form simple solutions, but adopt structures such as micelles, or a variety of other forms incorporating the lipid bilayer. A knowledge of these bilayers may provide insight into the function of cell membranes and interactions between phospholipid vesicles have been extensively studied as models for cellular and subcellular adhesion (20,21).

A number of dynamic properties can be expected for lipid molecules arranged in a bilayer. Firstly, there is the possibility of rapid internal motion within each lipid molecule. Secondly, lipid molecules might diffuse laterally in the plane of the bilayer, although the rates of this motion could be very different for those lipids associated with additivies (proteins) and those lipids which make up the bulk of the membrane. Thirdly, lipid molecules may be able to rotate rapidly as a whole about their long axes. Finally, there is a transfer from one side of the bilayer to the other, referred to as "flip-flop". Evidence for all these motions has been obtained using nuclear magnetic resonance and electron spin resonance (22,23).

(9) Techniques of Observation

In researching surfactants a great many techniques can be used. However, to draw any conclusions about any system at a particular concentration one has to correlate the results of several of these techniques. The physical nature of surfactant solution can range,

depending on the water content, from a pure solution through viscous slurry to solid phase materials. In the first instance a list of generally used techniques has been compiled which include surface tension, colligative properties (osmotic pressure, etc.), electrical conductivity, scattering techniques (x-ray, neutron and light) and electrophoresis.

(a) Rheology

Viscosity measurements which characterise resistance to deformation are useful over the total concentration range of surfactants. In the simple case of spherical micelles the dependence of viscosity on concentration was first demonstrated by Einstein. Information about particle shape and interactions can be derived, but at this point in time no information which relates viscosity to the fundamental structural unit of the phase is available from rheological measurements. For lamellar and hexagonal phases movement along the bilayers and rod length respectively is expected to be easy. Movement perpendicular to these directions involves modification of the packing in the systems. Cubic phases have no easy flow direction because the aggregates repel each other in a three dimensional network. In theory the cubic phase is more viscous than the hexagonal phase which is more viscous than the lamellar phase. Generally this is observed in practice (24,25) other more complex behaviour also occurs which obscures this pattern. Shear-thinning is observed when randomly orientated "crystallites" align on shear while shear-thickening occurs when new defects form and viscosity increase. At different shear rates both shear-thinning and shear-thickening can occur in the same sample.

(b) Nuclear Magnetic Resonance (N.M.R.) and other Spectroscopic Techniques

N.M.R. (26) is the most popular technique for studying surfactants because of the wide variety of nuclei that can be used (^{1}H, ^{2}H, ^{13}C, ^{14}N, ^{23}Na, ^{31}P, etc.). Information on both molecular orientation and mobility can be obtained in systems

where surfactant, water and counterions are all present. Most alternative spectroscopic techniques give similar information to N.M.R. Though often an added probe is necessary as the surfactant and water are insensitive to the radiation involved in the technique. The application of electron spin resonance (27) (E.S.R.) usually involves the addition of a paramagnetic spin probe. Care must be taken in these cases as the behaviour observed can apply to the probe and not to the surfactant. Raman and infra-red (28,29) spectroscopy can be used to study hydrocarbon conformations and water hydrogen bonding.

(c) Microscopy

Both electron and optical microscopy are extremely useful in the study of surfactant systems. Electron microscopy can be used to observe large surfactant aggregates in dilute solution, but has resolution problems when attempting to observe small micelles. The technique is useful if the phases exhibit distinct textures.

Optical microscopy using crossed polars is an inexpensive desktop technique for determination of phases.

(d) Scattering Techniques

When a beam of light is directed at a colloidal solution or dispersion some of the light may be absorbed (colour is produced when light of certain wavelengths is selectively absorbed), some is scattered, whilst the remainder is transmitted undisturbed through the sample.

Three areas of interest have been dealt with theoretically:-

(i) Scattering by small particles.
Rayleigh laid the foundation of light scattering by small spherical particles (<ca. $\lambda/20$). For a system of independent scatterers (point sources of scattered light distributed completely at random),

the emitted light waves have an equal probability of reinforcing or destructively interfering with one another. The amplitudes of the scattered waves add and subtract in a random fashion, with the result that the amplitude of the total scattered light is proportional to the square root of the number of scattering particles. Since the intensity of a light wave is proportional to the square of its amplitude, the total intensity of scattered light is proportional to the number of particles.

(ii) Scattering by large particles

The theory of light scattering is more complicated when one or more of the particle dimensions exceeds ca. $\lambda/20$. Such particles cannot be considered as point sources of scattered light, and destructive interference between scattered light waves originating from different locations of the same particle must be taken into account.

Mie (1908) elaborated a general quantitative theory for light scattering by spherical particles. The intensity of the light scattered at various angles is related to m, the ratio of the refractive index of the particles to that of the medium, and the parameter (30) $x = 2\pi r/\lambda$. Mie's theory has been extended by Gans to include certain non-spherical shapes.

(iii) Rayleigh-Gans Region

This region lies between the Rayleigh and the Mie region. Due to the relative short wavelength of thermal neutrons and the particle size range of most colloid systems this area has grown in interest for colloidal scientists. This thesis concentrates on the Rayleigh-Gans scattering region and its applicability to polydisperse dispersions.

CHAPTER 2 - SCATTERING THEORY

(1) Introduction

The techniques of small angle neutron (SANS), x-ray (SAXS) and light (SALS) scattering are all manifestations of interference phenomena as described by the equation:-

$$E_o = E_s \sum_i \rho_i \exp[-ik\,(\underline{r}_i.\underline{s})] \qquad \text{Equation 2(1)}$$

and where E_s and E_o are the scattered and incident electric field strengths, (in the case of x-rays and light), ρ_i is the fraction of the radiation scattered by the ith scattering element, $\underline{k}_o$, $\underline{k}_i$ are the incident and scattered wave vectors, $|\underline{k}| = 2\Pi/\lambda$, λ is the wavelength of radiation used) $\underline{r}_i$ is a vector from an arbitrary origin to the element i and s is the vector difference between vectors along the incident and scattered rays.

(2) Scattering Theory (30,31,32,33)

The differences between the various techniques are primarily related to the nature of ρ_i. For neutron scattering this is associated with the nature of the scattering nucleus, for x-ray scattering with electron densities and for light with polarizabilities or refractive indices.

If an incident wave of amplitude (ϕ_i)

$$\phi_i = \phi_o \exp(i\,\underline{k}_o \cdot \underline{r}) \qquad \text{Equation 2(2)}$$

interferes with a single point scatterer at the origin then the emitted scattered amplitude of waves at a distance R is:

$$\phi_{sc} = \frac{\phi_o\, a}{R} \exp(ikR) \qquad \text{Equation 2(3)}$$

where $a = Ae^{i\alpha}$ and A is the scattering length and α determines the phase with respect to the incident wave.

If the scatterer is not positioned at the origin but at position r then there is a phase step $(\underline{k}_i - \underline{k}_o).\ \underline{r}$ which has to be included.

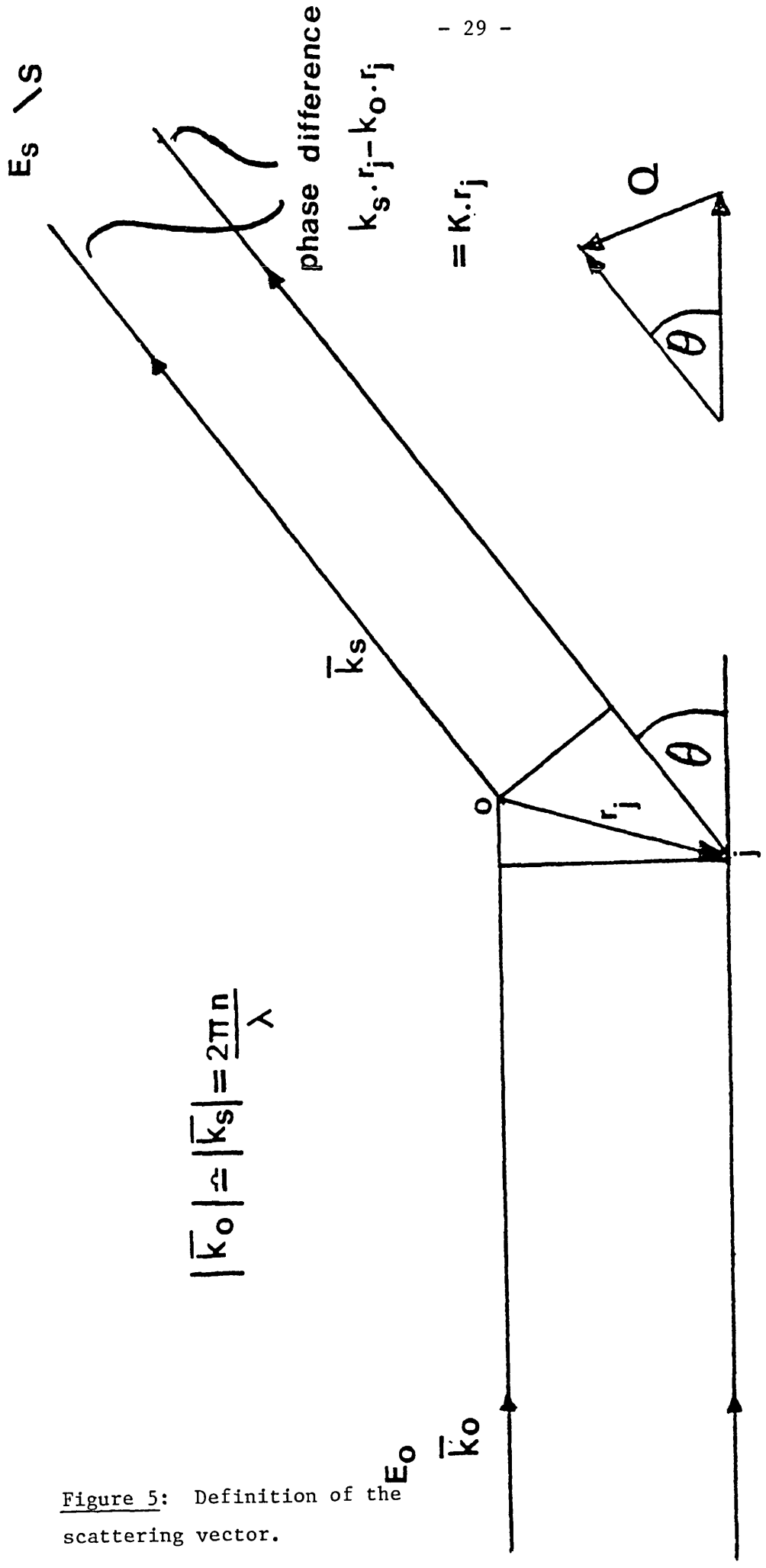


Figure 5: Definition of the scattering vector.

$\underline{k}_i$ is a wave vector in the direction of scattering. The scattered radiation from each point of the sample forms a parallel beam. By now introducing a scattering vector Q defined by $Q = \underline{k}_i - \underline{k}_o$ equation 2(3) may be written

$$\phi_{sc} = \frac{\phi_o a}{R} \exp \; Li(kR - \underline{Q}.\underline{r})\} \qquad \text{Equation 2(4)}$$

The scattering wave vector $\underline{Q}$ depends on the magnitude $(4\Pi/\lambda) \sin \theta/2$ where θ is the angle between $\underline{k}_i$ and $\underline{k}_o$.

If there are N particles in the system then the amplitude at R is the sum of the amplitudes

$$\phi_{sc} = \frac{\phi_o a}{R} \exp(ikR) \sum_{j=1}^{N} \exp(-i\underline{Q}.\underline{r}_j) \qquad \text{Equation 2(5)}$$

Any fluctuations in the scattering power of each individual particle must be taken into account. Introduction of the density function $\rho(r) = \Sigma\delta(\underline{r}-\underline{r}_j)$ which consists of point delta functions at the N scattering points enables the transformation of equation 2(5) and 2(6),

$$\phi_{sc} = \frac{\phi_o a}{R} \exp(ikR) \int \rho(r) \exp(-i\,\underline{Q}.\underline{r})\, d\underline{r} \qquad \text{Equation 2(6)}$$

Two important assumptions are made in deriving equation 2(6), the first is that the incident wave passes through the scattering volume with negligible reduction in intensity. This is called the Rayleigh-Gans approximation. Therefore, scattering is weak and no multiple scattering occurs. The second assumption is that the scattering centres have the same scattering amplitude, a_i. If this is not true, however, it can be taken into account in the density function, $\rho(r)$.

(3) Scattering Cross-Section Function

The power flow per unit area flux in the incident and scattered waves at any point averaged in time is proportional to $|\phi_i|^2$ and $|\phi_{sc}|^2$. The power scattered per steradian per unit area at a distance $\underline{R}$ from the scattering assembly is:-

$$\sigma(Q) = \frac{|\phi_{sc}|^2 R^2}{|\phi_i|^2} = aa^* \left| \int \rho(r) \exp(-i\underline{Q}.\underline{r})\, d\underline{r} \right|^2 \qquad \text{Equation 2(7)}$$

The function, $\sigma(Q)$, is called the differential scattering cross-section of the system. Introduction of the interparticle structure factor $S(Q)$

$$S(Q) = \frac{\left|\int \rho(r)\ \exp(-i\ Q.r)\ dr\right|^2}{\int \rho(\underline{r})\, d\underline{r}} \qquad \text{Equation 2(8)}$$

which specifies the correlations between the centres of different particles, simplifies the situation and allows equation 2(7) to be re-written in the form

$$\sigma(\underline{Q}) = aa^*\ S(Q)\ \int \rho(\underline{r})\ d\underline{r} \qquad \text{Equation 2(9)}$$

The term aa^* is equivalent to the single-particle form factor, $P(Q)$, and takes into account the physical nature of the scattering process. $\int \rho(\underline{r})$ dr takes into account the amount of scattering material present. If the system consists of discrete particles then the quantity $\int \rho(\underline{r})$ dr is equal to N, the number of particles in the scattering volume. The structure factor $S(Q)$ allows for interference effects and depends on the structure of the system.

For a dilute, non interacting system and for particles assumed to be isolated point scatterers, then $\sigma(Q) = aa^*N$ as $S(Q)$ tends to unity.

In neutron scattering theory the double differential cross-section $\delta^2\sigma/\delta\Omega\delta E$ represents the probability that neutrons will be scattered by an array of N particles with cross-section σ into a solid angle $d\Omega$ with energy change between E and δE. However, if the scattering is elastic, then only the differential cross-section $\delta\sigma/\delta\Omega$ is required. This is given by (34).

$$\frac{\delta\sigma}{\delta\Omega} = N\overline{(b-\bar{b})^2} + b^2 \left| \sum_i \exp(i\underline{Q}.\underline{r}) \right. \qquad \text{Equation 2(10)}$$

The first term is the incoherent cross-section. It is isotropic and does not depend on a phase term, therefore, no information can be obtained from it concerning the relative positions of the particles. The second term is the coherent cross-section which depends on the mean value of the scattering length and on interference effects between waves scattered from different particles. Information about the particle shape $P(Q)$ and the relative positions of the particles $S(Q)$ can be obtained from this term.

For light the Rayleigh ratio, R_θ, is equivalent to the coherent term of the differential cross-section in equation 2(10).

$$R_\theta = K\,cM\,P(\underline{Q}) \qquad \text{Equation 2(11)}$$

where K is a constant, c is the concentration, P(Q) is the single particle form factor, and M is the molecular weight. Light scattering is usually done in dilute solution and in this case the S(Q) is unity.

The structure factor, S(Q), was introduced through the theory of simple liquids which ha been well described in texts on the statistical mechanics of fluids (35).

Scattering from liquids or amorphous solids is observed since the density fluctuation is within the probing distance of . incident radiation. This is not, however, the case for gases. In liquid state theory the scattering from a system yields information on the time average position of the particles and any structure.

Liquids and amorphous solids may be considered by the same theory since in both cases the molecules are randomly orientated. The simple liquid theory involves a statistical mechanical method which is applied to a many-body system and requires a knowledge of the potential energy of the interactions between the particles. In application to colloidal systems this potential energy is given by the well known DLVO potential where the solvent properties appear as parameters in the potential of mean force. Often the solvent may be treated as a homogenous medium if the size of the scattering entity is sufficiently large.

The similarity between the structure in colloidal dispersions and that in liquids and amorphous solid was first recognised by Riley and Oster (36) and many workers have since used this observation (37,38).

With dynamic systems only intensity information can be produced and it follows from the Wiener-Khintchine theories that the Fourier inversion of S(Q) results in the density autocorrelation function.

$$S(\underline{Q}) = \frac{\int \exp(-i\underline{Q}.\underline{r})\,[\int \rho(\underline{r}_1)\,\rho(\underline{r}_1+\underline{r})\,d\underline{r}_1]\,d\underline{r}}{\int \rho(\underline{r})\,d\underline{r}} \qquad \text{Equation 2(12)}$$

For an assembly of point scatterers equation 2(12) can be manipulated to give

$$S(\underline{Q}) = \frac{\int \exp(-i\underline{Q}.\underline{r}) \left[\int \sum_i \delta(\underline{r}_1-\underline{r}_i) \sum_j \delta(\underline{r}_1+\underline{r}-\underline{r}_j) d\underline{r}_1\right] d\underline{r}}{\int \sum_i \delta(\underline{r}-\underline{r}_j) d\underline{r}} \qquad \text{Equation 2(13)}$$

$$= \frac{1}{N} \int \exp(-i\underline{Q}.\underline{r}) \sum_{ij} \delta(\underline{r}_i+\underline{r}-\underline{r}_j) d\underline{r} \qquad \text{Equation 2(14)}$$

$$= \frac{1}{N} \int \exp(-i\underline{Q}.\underline{r}) \left[N\,\delta(\underline{r}) + \sum_{ij} \delta(\underline{r}-[\underline{r}_j-\underline{r}_i])\right] d\underline{r} \qquad \text{Equation 2(15)}$$

The double summation consists of delta functions at the N(N-1) values of r to every interparticle spacing within the sample, and large N can be regarded as a continuous function with the quantity in the brackets in equation 2(15) replaced by $g(\underline{r})$, a pair correlation function. The pair correlation function can be defined as the probability of finding some particle at a distance r from an arbitrary reference particle.

For a sample of infinite extent equation 2(15) can be rationalised on a volume basis and written as:

$$S(Q) = 1 + \rho \int \exp(-i\underline{Q}.\underline{r}) g(r) d\underline{r} \qquad \text{Equation 2(16)}$$

$$= 1 + \rho \int [g(r)-1] \exp(-i\underline{Q}.\underline{r}) d\underline{r} + \rho \int \exp(-i\underline{Q}.\underline{r}) \qquad \text{Equation 2(17)}$$

where ρ = mean number density

The third term in 2(17) is responsible for the transmitted beam and is associated with the refractive index of the medium. This "forward" scattering will contribute to the small angle scattering through diffraction for very small samples widths.

$$\theta \hat{} \lambda/\text{sample widths} \qquad \text{Equation 2(18)}$$

In the region in Q space where this forward scatter does not affect S(Q) the function reduces to

$$S(Q) = S(0) \lim_{Q \to o} 1 + N \int \{g(r)-1\} \exp(-i\underline{Q}.\underline{r}) d\underline{r} \qquad \text{Equation 2(19)}$$

and using assumptions based on statistical thermodynamics this S(Q) has been identifed with the compressibility of the system (35).

The limiting expression (Q=0) is related to the compressibility through

$$S(0) = k_B T \beta \rho \qquad \text{Equation 2(20)}$$

where k_B is the Boltzmann constant, T is the absolute temperature and β is the isothermal compressibility

$$\beta = - \frac{1}{V} \left(\frac{\delta V}{\delta \rho} \right)_T \qquad \text{Equation 2(21)}$$

(4) Contrast

In any scattering process the scattering entity must be "seen" by the radiation to be scattered by it. In any diffraction imaging experiment, contrast allows us to observe the object in question.

The ability to alter the contrast to increase or decrease the scattering intensity has advantages. Obviously, if the scattering densities of particle and medium are identical the radiation will not be scattered. If the particle has regions of varying contrast then it would be possible to match out different areas of the particle with solvent, leaving other areas visible.

For x-ray's this type of experiment is possible but the contrast can only be varied by chemical substitution or addition of molecules with high electron density. For example, in the study of biological systems the contrast may be altered by varying the concentration of glucose or a salt in the surrounding medium. It is extremely likely that addition of these additives to the medium will alter the physical nature of the systems and in any case this technique can produce only a limited range of available contrast.

The problem of contrast variation using light scattering is that in choosing a solvent with a similar refractive index to the scattering particle the two species must automatically be of similar chemical nature. In the case of a polymer, the solvent would have to be hydrocarbon and its penetration into a particle will cause swelling. Therefore, the physical nature of the scatterers are altered. Recent research has been published where silica particles are suspended in various hydrocarbon solvents (39). The refractive index difference

between the particles and solvent is so small that the dispersion can be studied by means of light scattering up to high concentrations. Furthermore, optical density differences in the silica core were detected.

Neutron scattering would appear to be a prime technique for performing contrast variation experiments. Neutrons interact with nuclei in a way that is uncorrelated with their atomic number. In particular, neutrons are scattered with different scattering lengths by different isotopes of the same atomic element. Deuterium has a positive value of the scattering length, b, and hydrogen a negative value. The contrast of a particle or solvent can thus be changed by replacing hydrogen in the molecule for deuterium. This may involve partial or total substitution of hydrogen atoms and in some cases addition of certain percentages of deuterium. Since water is chemically the most interesting solvent and the scattering density of many chemical and biological materials falls within the two extremes of scattering lengths for H_2O and D_2O the scattering materials can be contrast matched by varying the ratio of these two isotopic waters.

For a neutron experiment the scattered intensity of a system is given by

$$I(Q) = \langle \left| \int_V (\rho(\underline{r}) - \rho_s) \exp(i\underline{Q}.\underline{r}) d^3r \right|^2 \rangle \qquad \text{Equation 2(22)}$$

where $\rho(\underline{r})$ is the local scattering length density associated with the material of interest and ρ_s is the mean scattering length density of the solvent.

The contrast ρ between the solvent and the scattering molecules or particles can be written as

$$\overline{\rho} = \frac{1}{V} \int_V \rho(\underline{r}) dr^3 - \rho_s \qquad \text{Equation 2(23)}$$

where the volume V, occupied by atoms of the molecule or particle, is that volume which is inaccessible to the solvent. For vesicles this is represented by a toroid. The local scattering density $\rho(\underline{r})$ may have the type of profile shown in figure 6.

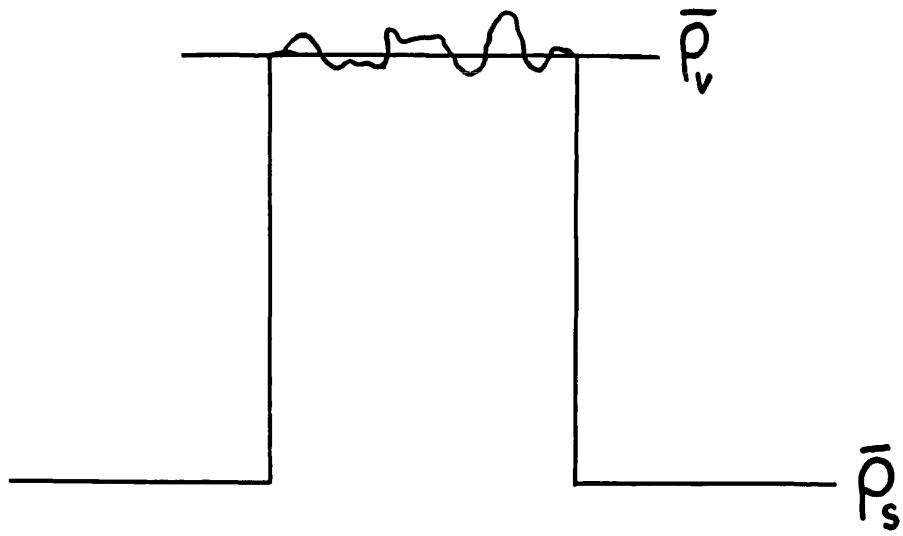


Figure 6: Contrast difference between particle and solvent. This schematic diagram shows there will be a variation in the contrast of any scattering entity. $\bar{\rho}v$ and $\bar{\rho}s$ are the mean scattering length densities.

The function $\rho(\underline{r})$ can be split into two parts:

$$\rho(\underline{r}) = \bar{\rho}_v - \rho_f(r) \qquad \text{Equation 2(24)}$$

where $\rho_f(r)$ is defined by

$$\int_v \rho_f(\underline{r})\, d^3r = 0 \qquad \text{Equation 2(25)}$$

is the fluctuation in scattering densities about the mean value $\bar{\rho}_v$.

In the limit of very small scattering angles Guinier's law represents the scattered intensity, I(Q), of a particle and is given by

$$I(Q) = I(0)\exp(-R_G^2Q^2/3) \qquad \text{Equation 2(26)}$$

$$\text{with } I(0) = (\bar{\rho}V)^2 \qquad \text{Equation 2(27)}$$

and R_G is the radius of gyration. The contrast ρ is given by the difference between the mean scattering length density of the particles $\bar{\rho}_v$, and of the solvent, ρ_s,

$$\rho = \bar{\rho}_v - \bar{\rho}_s \qquad \text{Equation 2(28)}$$

Extrapolation of a lnI versus Q^2 plot to (with the limitation that $QR_g<1$) the region where Q approaches zero will yield I(0).

$$I(0) = [(\bar{\rho}_v - \bar{\rho}_s)V]^2 \qquad \text{Equation 2(29)}$$

By varying the contrast $\bar{\rho}_s$ by changing the percentage of heavy water in the solvent there comes a point where $\bar{\rho}_p = \bar{\rho}_s$. This null point is called the "matching point" or isopicnic point. It must be noted that at this point the intensity of scattered neutrons is never reduced to zero as the $\bar{\rho}_v$ is only an average value. As a result a plot of $\sqrt{I_o}$ versus $\bar{\rho}_s$ does not pass through zero but rather exhibits a minimum.

In this discussion the assumption that $\rho_\rho(r)$ is independent of the contrast means that exchange of protons for deuterium is neglected. Exchange of labile protons on the particle puts limitation on the approach. If the exchange is uniform across the scattering particle, it would modify the contrast linearly and the analysis can proceed unaltered. If the particle exchanges protons easily the internal contrast is a function of contrast. If this is true then the separation in equation 2(24) first derived by Stuhrmann (40) will not apply.

(5) Particle Scattering Factor

For an isolated small sphere (radius $\bar{\nu}\lambda/20$) Rayleigh assumed that the particle scattering amplitude was a constant. For large particles the amplitude, however, is Q dependent. The single particle form factor, P(Q), represents the modification of the intensity caused by the finite size of the particle. The Q dependent P(Q) can be introduced into equation 2(9) and the cross-section becomes

$$\sigma(Q) = AA^* S(Q) P(Q) \int \rho(\underline{r}) dr \qquad \text{Equation 2(30)}$$

where

$$P(Q) = \frac{1}{V} \left| \int_V e^{-i\underline{Q}.\underline{r}} \, d\underline{r} \right|^2 \qquad \text{Equation 2(31)}$$

The expression is evaluated and averaged over all particle orientations. Due to averaging, P(Q) for assymetric particles cannot be introduced as a multiplicative factor in equation 2(30).

Information about the P(Q) of particles at the Q→0 region can be obtained from the widely used Guinier approximation [Equation 2(26)].

Information about the molecular weight of the particle and its radius of gyration is determined from the intercept, I(0), and the slope of the curve respectively [Equation 2(26)]. It must be emphasised that the concept of a radius of gyration is sound, whatever the form of the particle, although it may not relate simply to a physical dimension.

For a sphere with a sharp interface, however, the radius of gyration is related to the geometric radius, r, by

$$Rg^2 = \frac{3}{5} r^2 \qquad \text{Equation 2(32)}$$

Kratky and Porod (41) have given an approximate formula [Equation 2(33,34)] for particles in the form of narrow cylinders and thin discs which are derived from the Guinier approximation and which yield further parameters associated with these shapes.

$$P(Q) \text{ cylinder} = \frac{1}{QH} \exp(-Q^2 r^2/4) \qquad \text{Equation 2(33)}$$

where H is the half length of the cylinders

$$P(Q)\ \text{disc} = \frac{1}{Q^2r^2} \exp\frac{[-Q^2H^2]}{12} \qquad \text{Equation 2(34)}$$

where H is the thickness of the disc

In both these cases the equations are only valid in the region where QH<<1 and for Qr>>1. The thickness of the disc must be small compared to the radius and the radius of the cylinder must be small compared to its length.

The form factors for various shaped particles have also been calculated over a larger Q range and are given by (42,43,44).

$$P(Q)\text{sphere} = \left[\frac{3}{x^3}\{\sin x - x\cos x\}\right]^2 \qquad \text{Equation 2(35)}$$

$$P(Q)\text{shell} = \left[\frac{3}{x^3(1-\gamma^3)}\{\sin x - \sin(\gamma x) - x\cos x + x\cos(\gamma x)\}\right]^2 \qquad \text{Equation 2(36)}$$

where x = Qr : r = particle radius

$$\gamma = \frac{rin}{r} : rin = \text{particle inner radius} \qquad \text{Equation 2(37)}$$

$$P(Q)\ \text{cylinder (45)} = \int_0^{\pi/2} \frac{\sin^2(QH\cos\beta)}{Q^2H^2\cos^2\beta} \cdot \frac{4J_1^2(Qr\cos\beta)}{Q^2r^2\sin^2\beta} \cdot \sin\beta\, d\beta \qquad \text{Equation 2(38)}$$

Where H is the half length and J_1 (Qrsinβ) is a Bessel function of order 1.

$$P(Q)\text{disc} = \left(\frac{2}{Q^2r^2}\right) \cdot \left[1 - \frac{1}{Qr} J_1(2Qr)\right] \qquad \text{Equation 2(39)}$$

In the case of a random coil macromolecule the P(Q) is

$$P(Q)\text{coil} = \frac{2}{w^2}(e^{-w} + w - 1) \qquad \text{Equation 2(40)}$$

$$\text{where } w = \frac{Q^2s^2}{6} \qquad \text{Equation 2(41)}$$

Here s^2 is the mean square end to end distance of the macromolecule.

At high Q values the principal term in the particle form factor, P(Q), is $2\pi\rho s/Q^4$, where s is the external surface area. No matter what shape the particle is as long as it has a sharp surface boundary the scattering will fall as Q^4.

(6) Polydispersity

All colloidal systems are polydisperse, i.e. there is a distribution of particle sizes associated with each particular system. For a dispersion of non-interacting polydisperse particles the total scattered intensity will be given by

$$I_{TOT} \approx \sum_i N_i \langle A_i^2 \rangle P_i(Q) \qquad \text{Equation 2(42)}$$

$$\text{or } \alpha\ N \int_o^\infty A^2(i)\ P(Q,i)\ f(i)\ di \qquad \text{Equation 2(43)}$$

where A(i) is the scattering power of the ith component, P(Q,i) is the particle scattering factor of the ith component and f(i) fractional mass of the ith component.

The f(i) term is the distribution of particle sizes and the scattering power of each particle involves the density, volume, etc. If the particles are of the same material then the only term of importance is the volume. The scattering spectra will then be significantly affected by the larger size part of any number distribution.

(7) Multiple Scattering

In the description of scattering so far the percentage of radiation scattered is low and the process is dominated by single scattering events. If the concentration is high enough for this not to be the case then the system is said to be multiple scattering.

The main difficulty in any formulation of multiple scattering is the proper evaluation of phase relationships among the various individual wavelets which together define the resultant radiation field. It is thus evident that the mutual interaction amongst the various scatterers

plays a prominant role in any such evaluation of the resultant radiation field. Only in recent years have theoretical approaches been applied and considerable progress has been made in this direction. However, multiple scattering has been ignored in the research described in this thesis.

(8) Dynamic Light Scattering

In the case of N identical, spherical Brownian particles dispersed in a fluid medium. The scattered light (when illuminated by a laser light of wavelength, λ,) is largely due to the particle rather than the medium. The instantaneous value of the complex amplitude of the electric field is

$$E(Q,t) \alpha \sum_{i=1}^{N} \exp(i\underline{Q}.\underline{r}_i(t)) \qquad \text{Equation 2(44)}$$

This time or frequency term can be introduced into the density function, i.e. $\rho(\underline{r},t)$. Both $E(Q,t)$ and $\rho(\underline{r},t)$ describe the instantaneous random diffraction or 'speckle' pattern of the random arrangement of particles at time t. The consequent spectral power density is given by

$$I_s(\underline{Q},w) \alpha AA^* S(Q,w) \frac{1}{T} \int\int \rho(\underline{r},t)\, d\underline{r}\, dt \qquad \text{Equation 2(45)}$$

where $S(Q,w)$ allows for interference and "Doppler" effects which alter the angular and frequency distribution of the scattered light.

It is more relevant and simpler to consider a time analysis of the scattering process rather than a frequency analysis.

The simplest function by which a randomly fluctuating quantity can be characterised is its first order correlation function, $G^1(\underline{Q},\tau)$, defined by

$$G^1(\underline{Q},\tau) = \langle E_s^*(\underline{Q},t) \cdot E_s(\underline{Q},t+\tau) \rangle \qquad \text{Equation 2(46)}$$

where E_s^* is the complex conjugate and the brackets imply an ensemble average taken over all time (t).

The normalised electric field autocorrelation function is given by

$$g^1(\underline{Q},\tau) = \frac{\langle E_s^*(\underline{Q},t).\, E_s(\underline{Q},t+\tau)\rangle}{\langle |E_s(\underline{Q},t)|^2\rangle} \qquad \text{Equation 2(47)}$$

where for a stationary process $\langle |E_s(Q,t)|^2\rangle = I_s$, the time average intensity.

Substitution of equation 2(44) into 2(47) gives

$$g^1(\underline{Q},\tau) = F(\underline{Q},\tau)/S(Q) \qquad \text{Equation 2(48)}$$

where the intermediate scattering function or dynamic structure factor $F(Q,\tau)$ is given by (46)

$$F(\underline{Q},\tau) = \frac{1}{N\langle A^2\rangle} \sum_{i=1}^{N} \sum_{i=j}^{N} \langle A_i \exp(i\underline{Q}.\underline{r}_i(o)).\, A_j \exp(-i\underline{Q}.\underline{r}_j(\tau))\rangle \qquad \text{Equation 2(49)}$$

and the 'structure factor'

$$S(Q) \equiv F(Q,o) \qquad \text{Equation 2(50)}$$

In a sufficiently dilute dispersion, particle interactions are negligible so that the position and velocities of different particles are uncorrelated. The cross-terms ($i \neq j$) in equation 2(49) vanish, $S(Q) = 1$ and $F(\underline{Q},\tau)$ becomes the self scattering function $F_s(\underline{Q},\tau)$ which for spherical identical particles simply relates to the time averaged particle displacement.

$$g^1(\underline{Q},\tau) = F_s(\underline{Q},\tau) = \langle \exp(-i\underline{Q}.\Delta\underline{r}(\tau))\rangle \qquad \text{Equation 2(51)}$$

where $\Delta\underline{r}(\tau)$ is particle displacement.

The self intermediate scattering function $F_s(\underline{Q},\tau)$ is given by the Fourier transformation of the self space time correlation function $G_s(\underline{r},\tau)$).

$$F_s(\underline{Q},\tau) = \int_o^\infty G_s(\underline{r},t) \exp(i\underline{Q}.\underline{r})\, d\underline{r} \qquad \text{Equation 2(52)}$$

where $G_s(\underline{r},t)$ is the conditional probability that a particle located at the origin at time 0 will be at the position $\underline{r}$ at time t.

For a particle undergoing free isotropic diffusion, $G_s(\underline{r},t)$ obeys the diffusion equation

$$\frac{\delta G_s(r,t)}{wt} = D\,\nabla^2 G_s\,(\underline{r},t) \qquad \text{Equation 2(53)}$$

The spacial fourier transform of which yields

$$\frac{\delta}{\delta t} F_s(Q,t) = -Q^2 D_o F_s(\underline{Q},t) \qquad \text{Equation 2(54)}$$

and the solution of equation 2(54) is identical to 2(51) with the displacement related to the diffusion coefficient.

$$g^1(\underline{Q},\tau) = \frac{F_s(Q,t)}{(F(K,0)=1)} = \exp(-Q^2 D_o t) \qquad \text{Equation 2(55)}$$

The self diffusion coefficient, D_o, is given by the Einstein relation

$$D_o = R_B T/f \qquad \text{Equation 2(56)}$$

where the frictional constant (f) for stick boundary conditions is given by the Stokes relationship

$$f = 6\pi\eta a \qquad \text{Equation 2(57)}$$

where k_B is the Boltzmann constant, T is the absolute temperature, η is the shear viscosity of the solvent and a is the particle radius.

(9) Interacting Particles

In systems where the particle concentration is moderately high and if Coulombic electrosatic forces are present particles can interact with neighbours over large distances. These interactions cause correlations between both the position and motion of different particles. A second

indirect interaction is present and occurs when a velocity field generated by a moving particle affects another particle. These hydrodynamic interactions in the presence of long range Coulombic interactions are negligible and are ignored. For strong interactions the particles may actually crystallize in a lattice with spacings of many particle diameters. The structure factor, S(Q), associated with any order is now not unity.

The experimental diffusion coefficient measured, when the probing distance is large with respect to the mean interparticle spacing, is dramatically affected by the presence of structure and is given by (47,48).

$$Deff = D_o/S(Q). \qquad \text{Equation 2(58)}$$

Using the generalised Einstein relationship defined by

$$D(\phi) = \frac{1}{1-\phi} \left| \frac{d\mu}{dc} \right|_{P,T} \frac{1}{f(\phi)} \qquad \text{Equation 2(59)}$$

where ϕ is the phase volume, $1/1-\phi$ is the reference frame correction factor and corrects for solvent reverse flow in a finite system, $f(\phi)$ is the particle frictional coefficient, μ is the chemical potential and δc is the concentration fluctuation.

Researchers (49,50) have approximated the concentration dependence of the diffusion coefficient D as

$$D = D_o (1 + (K_I - K_F) \phi). \qquad \text{Equation 2(60)}$$

Here K_I is the time average light scattering second virial coefficient and K_F is the frictional second virial coefficient. It is in the frictional second virial coefficient that information about dynamic interactions is contained.

From Weissman's (51) research Pusey (52) has demonstrated the long time correlation function measured at low Q in low phase volume in strongly interacting systems contains two terms. The first an incoherent term which reflects the self diffusion coefficient of the particles and the

usual coherent term which is the mutual diffusion coefficient. His expression for $F(\underline{Q},\tau)$ is

$$F(\underline{Q},\tau) = \frac{\langle A\rangle^2}{N\langle A^2\rangle} \sum_{ij}\sum \langle \exp i\underline{Q}.[\underline{r}_i(o)-\underline{r}_j(\tau)]\rangle + \frac{\langle A^2\rangle-\langle A\rangle^2}{\langle A^2\rangle} \langle \exp i\underline{Q}.[\underline{r}(o)-\underline{r}(\tau)]\rangle$$

Equation 2(61)

$$= \frac{\langle A\rangle^2}{\langle A^2\rangle} F^I(Q.\tau) + \left[\frac{\langle A^2\rangle-\langle A\rangle^2}{\langle A^2\rangle}\right] F^I_s(\underline{Q}.\tau)$$

coherent incoherent Equation 2(62)

In this derivation it is assumed that the polydispersity in the scattering volume does not affect the packing arrangements or dynamics of the particles. The incoherent term arises from the change in scattering power within the coherence area (speckle) due to all the possible configuration of particle sizes on a fixed spacial arrangement of particles. The spectral power arises from polydispersity fluctuation whose dissipation relies on the self diffusion of particles.

Therefore any measured S(Q) or S(0) using dynamic scattering cannot be related to the true S(Q) or S(0) obtained by static scattering without a preconceived knowledge of the polydispersity distribution function.

In these systems two types of polydispersity should be included in the analysis, polydispersity in size (see next section) and polydispersity of interactions, which is not pursued in this work. Therefore, the dynamic S(Q) or S(0) determined in the study is assumed to be the true S(Q) or S(0).

(10) Polydispersity

In a polydisperse colloidal dispersion there will be a distribution of particle sizes and hence $|g^{(1)}(\tau)|$ will no longer be a single exponential. For non-interacting scatterers $|g^{(1)}(\tau)|$ is given by a sum of exponentials

$$|g^{(1)}(\tau)| = \int G(\Gamma) e^{-\Gamma\tau}\, d\tau$$ Equation 2(63)

where $G(\Gamma)$ is the appropriate normalised distribution of decay rates.

$$G(\Gamma) = \frac{\sum_i \langle I \rangle_i \, \delta(\Gamma - \Gamma_i)}{\sum_i \langle I \rangle_i} \qquad \text{Equation 2(64)}$$

and $\langle I \rangle_i = N_i \langle A_i^2 \rangle P_i(Q)$ Equation 2(65)

and $\Gamma_i = D_i Q^2$ Equation 2(66)

where $\langle I_i \rangle$ is the average intensity and D_i is the translational diffusion coefficient from which we obtain

$$\frac{\Gamma}{Q^2} = \frac{\sum_i N_i \langle A_i^2 \rangle P_i(Q) D_i}{\sum_i N_i z A_i^2 \rangle P_i(Q)} \qquad \text{Equation 2(67)}$$

If the $P_i(Q)$ is equal to 1 then for all i, Γ/Q^2 can be identified with the z averaged diffusion coefficient D_i.

The obvious solution to the polydispersity problem is a Laplace inversion of the experimental data to give $G(\Gamma)$. In general, data of unattainably high precision are necessary to perform this inversion in order to obtain reasonable degrees of accuracy.

CHAPTER 3 - COLLOID INTERACTIONS

(1) DLVO Theory

Over thirty years ago Derjaguin and Landau (53) and Verwey and Overbeek (54) independently put forward the theory which still provides the basis for our understanding of the stability of lyophobic colloids. The basic assumption of the DLVO theory is that the net energy of interaction between two bodies is obtained by a straightforward algebraic summation of the two component energies, namely:- repulsion and attraction.

Consider the case of rigid spherical particles of radius r, with a pair interaction potential V(x) where x = (R-2r)/2r and R the distance between the centres of the two particles. This potential energy of interaction between the two particles can be separated into parts, i.e.

$$V(x) = V_R + V_A \qquad \text{Equation 3(1)}$$

The repulsive interaction, V_R, arises from the overlap of electrical double layers and the attractive part, V_A, is attributed to the London - Van der Waals interactions.

(a) Repulsion Forces

i. Electrical Potentials

When an electrically neutral substance is dispersed in a polar medium there is normally a redistribution of charge at the interface. The origin of the charge at the interface will be dependent on the system under observation. However, three main sources should be described:-

a. Ionisation - a chemical change by which ions are formed from a neutral molecule. Examples are carboxyl and amino groups. The ionisation of such groups and consequently molecular charge depends strongly on the pH of the solution.

b. Ion adsorption - a net surface charge can be acquired by the unequal adsorption of oppositely charged ions. Cations are generally more hydrated than anions and tend to reside in the bulk aqueous medium. Surfaces are generally negative because these smaller anions have a tendency to be specifically adsorbed. At charged surfaces there is a preferential tendency to adsorb counter ions to lower the surface potential. It is possible for counter-ion adsorption to cause a reversal of charge.

c. Ion dissolution - ionic substances can acquire a surface charge by virtue of unequal dissolution of the oppositely charged ions of which they are composed. This type of charge accumulation is common in metal oxide or metal halide solutions. In an aqueous medium the metal ion salt is in equilibrium with a saturated solution of ions. Depending on the concentration of the ions in the medium the particle surface could have both positive or negative charge. The particular ion in excess is termed the potential - determining ion, since its concentration determines the electric potential at the particle surface. This redistribution of charge constitutes the electric double layer. Electroneutrality is, of course, always maintained. Charged colloidal species will have reversibly bound counter ions associated within the locality of the interface. Thermal motion produces a uniform distribution of these ions around the particle forming a diffuse cloud known as the "Gouy layer". Those ions that are irreversibly bound are considered to be in the "Stern layer". The thickness of the Gouy layer is defined as that distance from a surface associated with a 1/e decay (Debye length) in the surface potential. Since the layer forms spontaneously its free energy of formation is negative. The first approach (54) in calculating the potential used a simplistic model where the particles were represented as positively charged flat plates in contact with a solution of point charges. The solvent was assumed to influence the double layer only

through its dielectric constant. The potential ψ associated with the ions was calculated as a function of distance from the surface using a Boltzmann distribution and a charge density related to the potential through Poisson's equation. These theoretical calculations were rapidly extended by Derjagiun to a two bodied spherical system via a sphere-plate calculation (55). For interacting spheres no exact analytical solution of the Poisson-Boltzmann equation is available. Approximate solutions may be derived by assuming $\psi o < {}^{k_B T}/e$ (where ψo is the surface potential energy, e is the electronic charge and $k_B T$ has its normal meaning) and the Poisson-Boltzmann equation reduces to

$$\nabla^2\psi = \kappa^2\psi \qquad \text{Equation 3(2)}$$

κ is the Debye-Huckel reciprocal length parameter and is given by

$$\kappa = \sqrt{\frac{8\pi C\, e^2\, Z^2}{\varepsilon k_B T}} \qquad \text{Equation 3(3)}$$

ε is the dielectric constant of the suspending medium, Z is the valence of the ionic species in solution and C is the concentration (ions/cm^3) of the same species.

Approximate expressions for the interaction potential, V_R, have been derived from equation 3(2). When the ionic strengh is low then the limit $\kappa r \ll 1$ is valid and V_R becomes

$$V_R = \frac{q^2 e^2}{2\varepsilon r(1+\kappa r)^2}\,\frac{e^{-2\kappa r x}}{1+x} \qquad \text{Equation 3(4)}$$

Where qe is the electric charge on the particle, $x = (R-2r)/2r$ and R is the distance between the centres of the two particles. At high ionic strength, i.e. $\kappa r \gg 1$, V_R becomes

$$V_R = \left[\frac{\varepsilon r \psi o^2}{2}\right] \ln\{1 + \exp(-2\kappa r x)\} \qquad \text{Equation 3(5)}$$

Here the surface potential ψo is related to the charge qe through the expression

$$\psi o = \frac{(2k_B T)}{e} \sinh^{-1}\left[\frac{2\pi e\kappa^{-1} qe}{4\pi r^2 \varepsilon k_B T}\right] \qquad \text{Equation 3(6)}$$

The zeta potential, ψo, can be measured by electrophoretic mobility and is considered to be the potential at the "slipping plane" at the outer boundary of the "Stern layer". Even though the potential at the slip plane and the potential at the Stern layer have fundamental differences they are experimentally indistinguishable.

McCartney and Levine (56) have produced an expression for solving the Debye-Huckel equation in the limit $\kappa a >> 1$ and their modified form of the equation is

$$V_R = \frac{64\pi r (K_B T)^2 \varepsilon \gamma^2}{Z^2 e^2} \frac{H + r}{H + 2r} \ln\{1 + r/(H + r)] \exp(-\kappa H)\}$$

Equation 3(7)

where

$$\gamma = [\exp\left(\frac{Ze\psi o}{2k_B T}\right) - 1]/[\exp\left(\frac{Ze\psi o}{2k_B T}\right) + 1] \qquad \text{Equation 3(8)}$$

H = surface to surface separation.

ii. Hydration Forces

The hydration force which is considered to be a special repulsive force which is greater than electrostatic repulsion at separations less than about 20Å has been observed in colloidal dispersions (57). It is considered to be a consequence of the work required to remove water from the polar groups. This force of dehydration is likely to be characteristic of all interacting hydrophilic surfaces although it is not always recognised since at normal separations the electrostatic interaction dominates. At high electrolyte concentrations, however, the electrostatic forces

are screened and a single exponential decay function is observed. An empirical formula (which is derived from osmotic pressure measurements for lamellar phases, modified for spherical geometry) has been calculated by Rand and co-workers (58) to be

$$V_s = \pi a \xi^2 \, Po \exp(-H/\xi) \qquad \text{Equation 3(9)}$$

where ξ is the decay length and Po the osmotic pressure.

iii. Hard Sphere Potential

For the purposes of this work only spherical particles having a radius r and separated by a distance R will be considered.

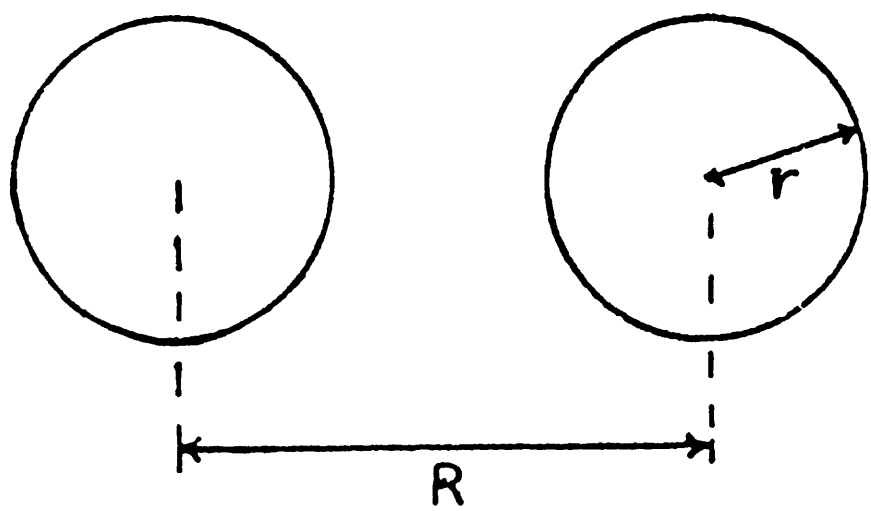


Figure 7 - Interaction between two spheres. The spheres have radius r with their centres separated by a distance, R.

The actual volume of a particle in this situation, V_p, is thus given by

$$V_p = (4/3)\pi r^3$$

and the total volume of particles in the system becomes

$$V = N_p V_p$$

with N_p the particle number concentration.

In attempting to consider the theoretical aspects of particle-particle interactions one of the simplest models to use is the hard sphere model, based on the idea of a hard sphere potential.

(b) Attraction Forces

The attraction between colloid particles is of similar origin to the forces introduced by Van der Waal to explain the behaviour of non ideal gases and liquids.

Expressions describing the attractive interaction as a function of separation between bodies of different geometries are available. All of these expressions may be represented as the product of a geometrical term and a material constant (A). This Hamaker constant derives from an extension of London's treatment of interaction forces to colloidal particles.

For the case of two spheres the attractive term, V_A, becomes

$$V_A = \frac{-A}{12}\left[(x^2+2x)^{-1} + (x^2+2x+1)^{-1} + 2\ln\left[\frac{(x^2+2x)}{(x^2+2x+1)}\right]\right] \quad \text{Equation 3(10)}$$

where $x = (R-2r)/2r$.

In obtaining the equation Hamaker made the assumption that there was a characteristic dipole frequency associated with the interaction between two identical spheres and it is this fluctuating charge distribution that produces the attractive forces. The Hamaker constant is given by

$$A = \frac{(\rho N a \pi)^2 \beta}{M} \quad \text{Equation 3(11)}$$

where β is a constant that represents the intermolecular attraction and M and ρ are the molecular weight and density respectively.

If the continuous medium was not a vacuum, A would be replaced by an effective value

$$A = A_{11} + A_{22} - 2(A_{11}A_{22})^{\frac{1}{2}} \quad \text{Equation 3(12)}$$

The subscript 11 and 22 refer to the particle and solvent respectively.

Vincent (59) has derived an expression which is applicable to the structure of vesicle particles. The attractive potential V_a comes from the attraction between particles surrounded by a "single sheath" adsorbed layer. In this case of a vesicle the "particle" is water, as it is the material which occupies the core volume of the particle. The sheath (i.e. the vesicle wall) is taken to be a mixture of hydrocarbon and water.

Discussion of interaction potential with respect to concentration vesicle experiments

In chapter five only the repulsive contribution to the interaction potential is considered for the concentrated vesicle analysis. Justification for this is given, for a single sheath vesicle, by Figures 12 and 13. Figure 12 represents the attractive contribution.

(2) Concentrated Dispersion Particle-Particle Interactions

The DLVO theory is strictly limited to dilute dispersion. In these dilute dispersions only occasional contacts occur between particles and hence the diffusional motion is only very marginally restricted. As the particle number concentration of the dispersion increases the volume of space occupied by these particles increases. A proportion of the total volume is an excluded volume, i.e. certain volume is occupied by the particle and some space between these particles is inaccessible to further particles. The main consequence of increasing the particle concentration is to increase the probability of interactive contact between the particles.

Although the DLVO theory is strictly limited to dilute concentrations it represents the only way of obtaining at higher phase volume a pairwise interaction potential of any meaning between two particles.

This has been utilised to explain the physics of simple liquids and also in recent work (60,61) to explain the properties of microemulsions and colloidal dispersions. The particle has an effective radius, R_{eff}, which is larger than its actual radius R. When two particles are

separated by a distance of $2R_{eff}$ the potential energy becomes infinite. The particles then have an effective volume fraction given by

$$\phi_{eff} = 4\pi R^3_{eff} N_p/3 \qquad \text{Equation 3(13)}$$

In a situation where the repulsive forces are dominant there is a strong dependence on the range of the repulsion R_{eff}, and as more particles are added each particle must interact with others with the resulting formation of a dispersion with a high degree of order. In some dispersions at low electrolyte concentration R_{eff} can be many times R. A description of the spatial arrangement in a dispersion, be it only an analogy to the states of matter "vapour-like" (random), "liquid-like" (loosely ordered), or "solid-like" (highly ordered) is extremely important. This may be obtained through the radial distribution function g(r).

(a) The Radial Distribution Function

The description of the structure may conveniently be carried out for spherical particles using the radial distribution function, g(r), which describes the probability of finding another particle at a distance r from a central reference particle.

On a macroscopic level the density of a dispersion is

$$\rho o = N_p/V$$

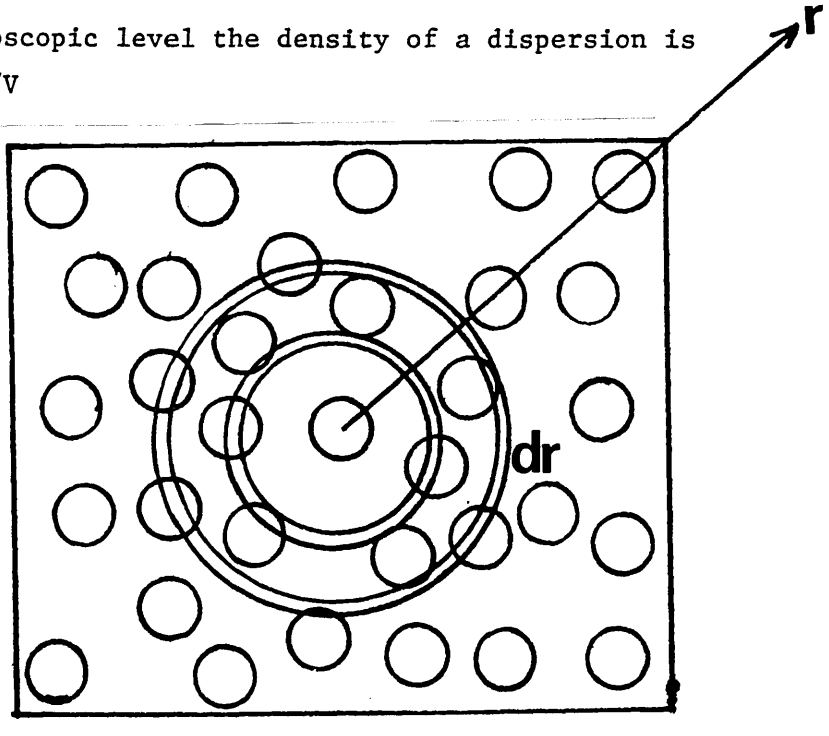


Figure 8 - Schematic illustration of the radial distribution of particles around a central particle. r is the distance from the central particle and dr is a small change in the distance.



Figure 9: Radial distribution function g(r) in a concentrated dispersion of spherical particles as a function of centre to centre separation.

However, on a microscopic level, if one proceeds outwards from the particle at the origin the density of particles in the immediate vicinity is zero. As r becomes very large the number density of particles in a shell of thickness dr must increase and approach ρo. Thus we can define a number density function $\rho(r)$ which for r greater than 2R must be zero and for $r \to \infty$ must be equal to ρo. Thus a distribution function of the form $g(r) = \rho(r)/\rho(o)$ appears reasonable.

Principal structural information is contained in the radial distribution function and the typical appearance of g(r) for a colloid dispersion is shown in Figure 9.

The definition of g(r) is such that for a random distribution of non-interacting particles, its value would be unity at all values of r. At short distances g(r) will be related to the interaction energy.

The term radial distribution function is usually used for the quantity

$$g(r) = 4\pi r^2 \rho(r) \qquad \text{Equation 3(14)}$$

(b) Relationship between g(r) and S(Q)

There are three principal routes to the radial distribution function: theory, computation and experiment.

The integrated intensity as a function of angle; S(Q) is related to g(r) by

$$S(Q) = 1 + \frac{4\pi\rho o}{Q} \int_o^\infty r[g(r)-1] \sin Qr.dr \qquad \text{Equation 3(15)}$$

where equation 3(15) was derived from equation 2(19).

The Fourier transformation of the structure factor leads directly to

$$g(r) = 1 + \frac{1}{2\pi^2 r\rho o} \int_o^\infty [S(Q)-1)\, Q \sin Qr.dQ \qquad \text{Equation 3(16)}$$

(c) The Potential of Mean Force

As both g(r) and S(Q) are a Fourier pair they both are related to the interaction potential

$$g(r) = \exp[\Phi(r)/KT] \qquad \text{Equation 3(17)}$$

where Φ is the potential of mean force between the particles such that

$$\Phi(r) = V(r) + \psi(r) \qquad \text{Equation 3(18)}$$

where V(r) is the pair potential for interactions between the particles and $\psi(r)$ is a perturbation potential which allows for the many-body interactions present in the system.

(d) Relation of S(Q) to models of Particle-Particle Interactions

As mentioned earlier the simplest model for interactions is the hard-sphere model. From the original theory of Percus and Yevick (60), S(Q) was obtained by Ashcroft and Lekner (61) in the form

$$S(Q) = \frac{1}{[1-N_p C(2QR_{eff})]} \qquad \text{Equation 3(19)}$$

with

$$C(2QReff) = -32\pi R^3_{eff} \int_0^1 \frac{\sin(2sQR_{eff})}{2sQR_{eff}} (\alpha+\beta s+\gamma s^3)s^2 ds \qquad \text{Equation 3(20)}$$

where α β and γ are given by

$$\alpha = (1+2\phi_{eff})^2/(1-\phi_{eff})^4 \qquad \text{Equation 3(21)}$$

$$\beta = -6\phi_{eff}(1+0.5\phi_{eff})^2/(1-\phi_{eff})^4 \qquad \text{Equation 3(22)}$$

$$\gamma = 0.5\phi_{eff}(1+2\phi_{eff})^2/)1-\phi_{eff})^4 \qquad \text{Equation 3(23)}$$

The hard-sphere model is incorrect as it ignores the essential particle-particle interactions. Softness can be incorporated into the potential via the theory of Barker and Henderson (64). In this approach the effective radius can be written in the form

$$Reff = R + \frac{R}{2} \int_2^\infty \{1-\exp[-V(r)/KT]\}d(r/R) \qquad \text{Equation 3(24)}$$

(e) Charged Hard Sphere Potential

Hayter and Penfold (37,65,66,67,68) calculated S(Q) by solving the Ornstein-Zernike equation in the mean spherical approximation (MSA). This modified potential has a hardcore and a soft surface which is the screened potential. Short-range attractive interactions are neglected.

The parameters which are in the S(Q) model are the volume fraction of particles, ϕ, the Debye-Huckel reciprocal length κ, the charge Z and the radius r.

(f) One Component Macrofluids

A macroion solution is a solution in which the effects of the ionic species is large enough to dominate many of the solution properties. The medium in which these particles are dispersed may then be treated as a uniform background, which has the physical characteristics necessary to ensure electroneutrality and appropriate dielectric properties, but is otherwise featureless. Recently a pioneer study by Hayter and Penfold showed that a pronounced interaction peak could be observed in sodium dodecyl sulphate (SDS) micellar solutions. They developed a mean spherical model of the interparticle structure S(Q) based on an interaction potential between micelles consisting of a hard sphere plus screened Coulombic potential. The weakly attractive van der Waals force in the basic DVLO potential was found not to affect the full potential. The hard core potential used in the structure factor S(Q) was calculated in closed form by solving the Ornstein-Zernike equation in the mean spherical approximation.

Their general statistical-mechanical computer simulation can be of use to the experimentalist interested in analysing many colloid systems under different experimental conditions using several parameters, namely the volume fraction, charge, particle diameter and the debye screening length.

The scattered intensity is thus calculated by summing all the scattered waves over all positions. However, by assuming that the solution is a OCM we may immediately exclude all atoms other than the colloidal particles.

The summation can be further split into two sums, the sum of j and k, self-part, in the same particle plus the sum over j and k belonging to different particles. By assuming that the particles are independently orientated (isotropic) the result is

$$I(Q) = S(Q)\langle F(Q)\rangle^2_Q + \langle F^2(Q)\rangle_Q - \langle F(Q)\rangle^2_Q \qquad \text{Equation 3(25)}$$

where

$$F(Q) = \sum_i b_j \exp(iQ.r_j) \qquad \text{Equation 3(26)}$$

is the single particle form factor and $\langle\ \rangle_Q$ is the ensemble average over all orientation with respect to Q.

The Ornstein-Zernike (OZ) equation involves the radial distribution function g(r) which is the excess probability over that for a random distribution of finding another particle at a certain distance from a reference particle. The total correlation function, h(r) = g(r) -1, measure the correlation between two particles while the direct correlation function, c(r), measures the direct influence of one particle on another with a third particle which is influential on both. The third particle's influence must be integrated over all possible positions of that particle leading to

$$h(r_{12}) = c(r_{12}) + \rho\int c(r_{13})h(r_{32})\, dr_3 \qquad \text{Equation 3(27)}$$

where r is the distance between particles and the labels indicate the particles 1,2 or 3. By using the Fourier transformation of h(r) or c(r), equations for the structure factor are obtained.

$$S(Q) = 1 + \rho\,\hat{h}(Q) \qquad \text{Equation 3(28)}$$

$$S(Q) = 1/[1 - \rho\hat{c}(Q)]$$

where the $\hat{x}$ (r) is the Fourier transform of x(r) and ρ is the number of particles in the dispersion. By applying boundary conditions to c(r) and h(r), using the mean spherical approximation (MSA) closure relations, S(Q) may be calculated.

The Percus-Yevick approximation assumes that there is an excluded volume term, in the case of hard sphere packing the particle cannot get closer than the diameter of the sphere. The Percus-Yevick hard sphere S(Q) has proved useful for uncharged systems. In the case of monodisperse and spherically symmetric particles,

$$\langle F^2(Q)\rangle_Q = \langle F(Q)\rangle^2_Q = P(Q) \qquad \text{Equation 3(29)}$$

and equation 3(25) becomes

$$I(Q) \alpha P(Q).S(Q) \qquad \text{Equation 3(30)}$$

Polydispersity can be introduced into equation 3(30) by convoluting the P(Q) with a distribution of some type depending on the system and replacing S(Q) by an effective value S_{eff} (Q) which takes into account polydispersity. Hayter and Penfold used an analytic solution to the problem of different screening conditions which is slightly different from Waisman who solved the problem of a screened Coulomb potential through an integral equation to a set of simultaneous non-linear algebraic equations.

Extraction of the P(Q) and S(Q) functions from I(Q) is possible by two methods. The first employed by Hayter and Penfold, involves calculation of S(Q) from the MSA solution and P(Q) from a model of the micelle.

Only two parameters are required, charge on the micelle and the aggregation number. These parameters are obtained by fitting the theory to the data. In micellar solutions this procedure is used as the micelle size varies with surfactant concentration and the dilute P(Q) cannot be obtained, as the micelles do not exist below the critical micellar concentration (CMC).

The second method can be used with non-association colloids, the P(Q) function can be obtained by experimental measurement of the scattering over the Q range of interest from a dilute dispersion. The subtraction of this spectra from a spectra of a concentration dispersion gives an experiment $S_{eff}(Q)$ which is unnormalised.

CHAPTER 4 - TECHNIQUES

Small Angle Neutron Scattering

(1) General Background (69,70,71,72)

Small angle neutron scattering analysis is a possible technique for studying structural features of colloidal size. Colloidal dimensions are in the range ten to several thousand Angstroms and are large compared to the wavelength of the neutron sources. Any scattering process is characterised by a reciprocity law, which gives an inverse relationship between particle size and scattering angle.

The importance of small angle neutron scattering for studying colloids has arisen due to the large differences in the scattering lengths of hydrogen and deuterium atoms.

Since the neutron is uncharged it interacts with the nucleus via nuclear forces. It carries a magnetic moment which can also interact with the nucleus and with the unpaired electrons in a molecule. This magnetic scattering is relatively weak and can be ignored in colloid systems. The nuclear interaction is strong and very short range.

For an isolated stationary nucleus, scattering is therefore spherically symmetric and energy independent and can be characterised by a single parameter, the scattering length b. Values of b vary randomly from nucleus to nucleus, from isotope to isotope and even with the spin state of the scattering nucleus. In particular, the values for ^{1}H and ^{2}D are of opposite signs.

The probing distances explored experimentally are determined by Q^{-1} where $Q = \frac{4\pi}{\lambda} \sin \theta/2$

λ is the neutron wavelength and θ the angle of scatter. If the instrument has a cold source, wavelengths of the order 10Å are obtained which yield probing distances up to several thousand Angstroms.

(2) Experimental Techniques

An elastic scattering experiment consists of scattering neutrons of known wavelength off the sample under investigation and measuring the intensity of the scattered neutrons as a function of scattering angle. If the scattering from the sample is isotropic then the intensity may be radially averaged and outputed as I(r) versus r where r is the position on the detector measured from the centre of the incoming neutron beam. From the sample to detector distance and the neutron wavelength r is converted to Q to give I(Q) versus Q.

If the scattering is anisotropic then it can no longer be radially averaged instead it must be analysed on a cell-by-cell basis. One method of analysing the scattering is to divide the detector into sectors which are parallel and perpendicular to any deformation axis. The sector angle is optimised to use the most of the detector as possible, without affecting, the intensity. However, to obtain the same statistical accuracy much longer measurement times must be used compared to an isotropic scatterer.

Neutrons with wavelengths in the range 4 to 15Å are generally used in small angle neutron scattering (SANS) and the maximum angle is less than 6° so that the Q range is of the order of 10^{-3} to 10^{-1} $Å^{-1}$. The actual Q range depends on the configuration of the diffractometer. Most experiments have been made on the instruments D11 and D17 at the Institut Laue - Langevin, Grenoble, France (73), while a number of other diffractometers have been used; these include Harwell (England) and the University of Missouri (USA).

Neutrons from the reactor are directed through a cold source (liquid hydrogen), which slows them to thermal velocities. The beam then passes through a curved neutron guide which removes unwanted fast neutrons and γ-rays. The "white" neutron radiation is then monochromated by passing through a helical slot velocity selector. The speed of the velocity selector is varied so a narrow distribution of neutrons of the appropriate wavelength travel through the slot while the rest are absorbed. On D11 two selectors are available with resolutions ($\Delta\lambda/\lambda$) of 10% and 50%. Only the narrow wavelength distribution selector was used in these experiments.

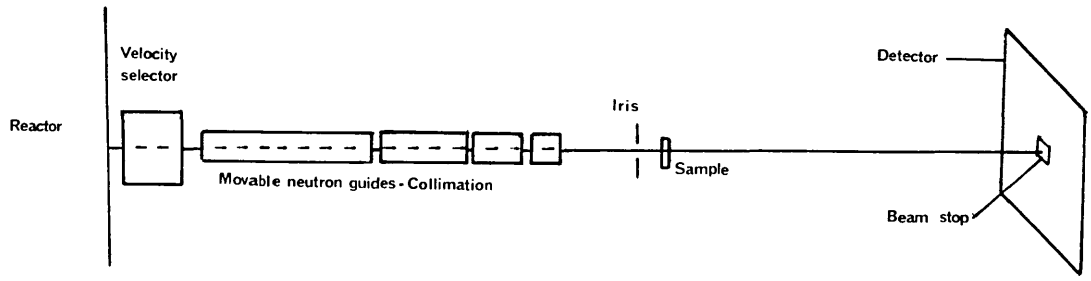


Figure 10: The small angle diffractometer D11. The main parts are the helical velocity selector, and the movable neutron guides and the detector. The collimator distance between the exit of the guide and the sample can be varied between 2m to 40m. The sample-detector distance can also be varied from -.7m to 40m.

The monochromated beam then passes through a number of collimators and diaphragms which are optional; thus changing the apparent position of the sources of neutrons from the sample. On D11 up to 40m of collimation are available. The less collimation used the higher the flux of neutrons, but the less defined the "parallel" beam of neutrons. The neutrons which are scattered by the sample are detected by a position-sensitive detector placed in a 40m long evacuated tube. The position of the detector can be varied from 1.3m to 40m from the sample. The detector is a BF_3 position sensitive detector with an array of 64 x 64, 1cm apart electrodes giving 4096 $1cm^2$ detector cells. The data are collected from each cell and stored on a designated computer.

Normally silica cells are used to contain the sample as silica has very little small angle scatter for neutrons. Their thickness is 1mm or 2mm. With concentrated dispersions, however, multiple scattering may be reduced by using smaller path length cells.

The experimental condition may be taken into account if a standard scatterer is placed in the beam, these are usually water or vanadium. A number of factors must be accounted for to obtain absolute intensities. These include detector efficiency ε, incident intensity ϕ and the solid angle of scatter Ω.

(3) Data Analysis

The measured scattered intensity, I(Q), is related to the differential cross-section, $d\sigma/\delta\Omega$ in the following way:

$$I(Q) = \phi\, \Omega o.\varepsilon.A.d.T.N. \left(\frac{d\sigma}{\delta\Omega}\right)_{coh} \qquad \text{Equation 4(1)}$$

where ϕ is the incident neutron flux, Ωo is the solid angle, ε is the detector efficiency, A is the area of the beam, d is the thickness of the sample, T is the transmission of the sample and N is the number of scatterers per unit volume.

The standard scatters incoherently then its scattered intensity Is(Q) is

$$Is(Q) = \phi\, \Omega o\, \varepsilon\, A\, d\, T_s\, N_s \left(\frac{d\sigma}{\delta\Omega}\right)_{incoh} \qquad \text{Equation 4(2)}$$

For an incoherent scatterer the scattered intensity is spread uniformly over 4π steradians and equation 4(2) becomes

$$Is(Q) \cong \phi \ \Omega o \ \varepsilon \ A \ \frac{(1-Ts)\,Ts}{\mathcal{L}_s \, 4\pi}$$

Substitution for $\phi \ \Omega \ \varepsilon \ A$ in equation 4(1) gives

$$I(Q) = Is(Q) \ \frac{d.T.4\pi}{Ts(1-Ts)} \ N \ \frac{(d\sigma)}{\delta\Omega \ coh} \qquad \text{Equation 4(3)}$$

$$I(Q) = DN \ \frac{(d\sigma)}{\delta\Omega \ coh} \qquad \text{Equation 4(4)}$$

where $D = Is(Q)_o \ 4\pi \ d.T./(1-Ts)Ts$

Photon Correlation Spectroscopy

(4) Introduction (32,33,74,75,76)

In recent years, with the development of relatively inexpensive, stable lasers of moderate power, intensity fluctuation spectroscopy has become a rapid growth area in research. Photon correlation spectroscopy (PCS) is a specialised intensity fluctuation spectroscopy method where a digital auto correlation function of intensity fluctuations yields a precise and rapid measurement of macromolecular diffusion coefficient.

It may be useful at this point to diverge and consider the difference between PCS and conventional light scattering. In the latter the scattered intensity from a large volume of a colloid dispersion is measured as a function of angle and if the sample is monodisperse a particle dimension is obtained. The scattering volume in a PCS experiment is very small and the scattered light intensity affected by Brownian motion. These fluctuations in intensity can be rationalised by analogy with x-ray scattering from a crystal. In a highly ordered crystal, x-rays give a diffraction pattern with a few intense maxima arising from in phase atomic scattering. In colloidal dispersion, however, the scattering centres have a random distribution. The diffraction pattern from the dispersion consists of maxima and minima of

varying size, position and intensity, which, due to the Brownian motion, fluctuate with time. In the detection of the scattered light the photomultiplier is observing one diffraction maxima (one coherence area) whose evolution in time will reflect the Brownian diffusion rates of the macromolecules. Time for a minimum to be replaced by a maximum at the detection point is similar to the time for a particle to diffuse one wavelength of light. This (coherence) time is in the order of microseconds to milliseconds for most colloid dispersions.

On this time scale the laser line width broadens and an examination of the spectral breadth of scattered light allows the particle size to be calculated within given constraints. There are two methods for analysing the time dependence of the detected light of randomly fluctuating intensity, through measurement of the frequency spectrum in the detector photocurrent or through measuring the time autocorrelation function of individually detected photons. These two methods are physically equivalent and represent a Fourier pair.

For either method of analysis two detection methods are possible to study the intensity fluctuation: homodyne and heterodyne. In the heterodyne method the scattered light is mixed at the detector surface with an excess of unscattered laser light. This process has been called "light-beating" or "optical-mixing" and the method is generally used in the frequency domain. In the homodyne method only the scattered light is studied and the scattered electric field beats against itself, hence the term "self-beat". All the experiments described in this text were PCS homodyne experiments.

(5) Apparatus

The apparatus consisted of an EMI 9863/100 KB photomultiplier and K7023 Malvern photon correlator with 48 delay channels. The optical source was a 5mW Spectra Physics helium-neon laser (λ = 6328Å). All the experiments were carried out at 25±0.5°C. The arrangement of the apparatus is shown in Figure 11.

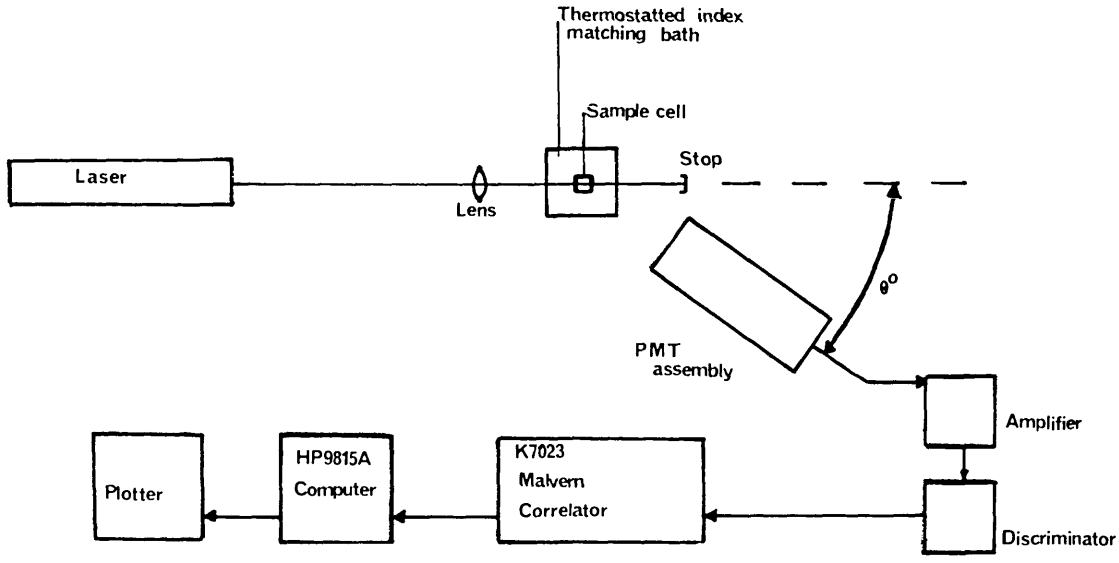


Figure 11: Photon correlation spectroscopy system.

(6) Data Analysis

The coherence time of the particle is related to the diffusion coefficient for that particle and from the autocorrelation function of the scattered intensity, the coherence time can be extracted. The autocorrelation function is a measure of the correlation between the value of a function and its value with a different value of the variable (in our case time τ). It is especially useful in characterising the properties of irregular functions.

The intensity of scattered light from any system is a continuous function. As the fluctuation in intensity is due to the motion of particles then its value cannot change infinitely quickly. If the intensity is measured at time t and $t + \tau$ then depending on the value of τ the intensity at $I(t + \tau)$ is related to the intensity at time t. At short delay time there is the greatest correlation while at long delay times the intensity becomes increasingly less correlated. By measuring the intensity at the correct sampling time then the autocorrelation function of that data has an exponential form.

The first-order autocorrelation function (also defined in equation 2[46]) at a point in space is given by

$$G^1(t,t+\tau) = \langle E(t)E^*(t+\tau)\rangle \qquad \text{Equation 4(5)}$$

While the second-order or intensity autocorrelation function is given by

$$G^2(t,t+\tau) = \langle I(t)I(t+\tau)\rangle \qquad \text{Equation 4(6)}$$

The correlation functions can be normalised (also defined in equation 2[47]) to

$$g^1(t,t+\tau) = \frac{\langle E(t)E^*(t+\tau)\rangle}{\langle I\rangle} \qquad \text{Equation 4(7)}$$

and

$$g^2(t,t+\tau) = \frac{\langle I(t)I(t+\tau)\rangle}{\langle I\rangle^2} \qquad \text{Equation 4(8)}$$

In homodyne experiments this expression may be related, for Gaussian light, to the normalised field autocorrelation function $|g^1(\tau)|$ using the Siegert (77) relationship.

$$g^2(\tau) = |g^1(\tau)|^2 + 1 \qquad \text{Equation 4(9)}$$

For monodisperse and noninteracting particles the electric field correlation function has an exponential time decay

$$|g^{(1)}(\tau)| = \exp(-\Gamma\tau) \qquad \text{Equation 4(10)}$$

where $\Gamma = D_T Q^2$, and through the Einstein and Stokes relationships the diffusion coefficient may be related to the hydrodynamic radius R_H,

$$D_T = \frac{k_B T}{6\pi\eta R_H}$$

If there is a distribution of particle sizes the correlation function is a sum of exponentials. If one has two particle sizes in the dispersion, the correlation function has a double exponential form which can under certain circumstances be separated. For relatively broad particle size distributions, various methods (77,78,79) for numerical inversion of equation 4(13) have been calculated.

$$|g^{(1)}(\tau)| = \int G(\Gamma) \exp(-\Gamma\tau)\, d\Gamma \qquad \text{Equation 4(11)}$$

where $G(\Gamma)$ is the normalised distribution of decay rates. For narrower distributions (81) the expontential factor in Equation 4(13) is expanded about its mean value exp $(-\Gamma\tau)$ where Γ is the mean value of the decay rate

$$\bar{\Gamma} = \int G(\Gamma)\Gamma\, d\Gamma \qquad \text{Equation 4(12)}$$

and it can be shown that

$$\ln C^{\frac{1}{2}}|g^{(1)}(\tau)| \equiv \frac{1}{2} \ln C - \Gamma\tau + \frac{1}{2!}\left(\frac{\mu^2}{\Gamma^2}\right)(\Gamma\tau)^2 - \frac{1}{3!}\left(\frac{\mu^3}{\Gamma^3}\right)(\Gamma\tau)^3 + \qquad \text{Equation 4(13)}$$

Where the μ's are moments of $G(\Gamma)$ about the mean

$$\mu^2 = \int(\Gamma - \bar{\Gamma})^2\, G(\Gamma)\, d\Gamma \qquad \text{Equation 4(14)}$$

If the distribution is narrow then the data can be fitted by the first two or three terms of equation 4(13). If the particles are identical then $\mu^2 = \mu^3 = o$ and the data is described by a linear function of τ.

CHAPTER 5: LIGHT SCATTERING AND NEUTRON SCATTERING FROM CONCENTRATED DISPERSIONS OF SMALL UNILAMELLAR VESICLES

(1) Introduction

In recent years a great deal of research has been done on the properties of phospholipid vesicles (liposomes), the main objective being to gain some insight into the structure and function of biological membranes.

Ultrasonic disruption of multilamellar liposomes results in the formation of small, spherical single-walled vesicles (85,86). The size and polydispersity of vesicles prepared in this way depends on a number of factors, such as the size and shape of the sonication vessel, intensity and duration of sonication, temperature and concentration of the dispersion, and on the molecular properties of the "surfactants" used. Prolonged sonication above the phase transition temperature yields vesicles which have a minimum size (usually ca. 200Å for phospholipids of natural origin) and a narrow size distribution.

We now report measurements on concentrated and kinetically stable vesicular dispersions. The phospholipids used in this study were 1,2-diacyl-sn-glycero-3-phosphocholine (phosphatidylcholine; PC), which is zwitterionic at pH 3-11 and 1,2-diacyl-sn-glycero-3-phosphoserine (phosphatidylserine; PS), which has ionisable carboxylate, phosphate and ammonium groups and carries a net negative charge at neutral pH. Both phospholipids were of natural origin, and therefore possessed a distribution of acyl chain lengths and levels of unsaturation, resulting in phase transition temperatures below 0°C. The following discussion therefore relates to vesicles in the fluid state whose stability was not affected by proximity to a phase transition.

Liposomes are by no means the exclusive domain of the bioscientist. Vesicular dispersions may be regarded in many respects as conventional colloids, and as such they are amenable to study by techniques such as static and dynamic light scattering (87,88), neutron scattering (89), x-ray scattering (90), particle electrophoresis (91) and analytical ultracentrifugation (92). The well known DLVO theory (54) of colloid stability has been applied with some success to explain the aggregation

of charged vesicles as a function of the ionic composition of the suspending medium (93,94). In particular, the role of Ca^{2+} ions in promoting aggregation and fusion of negatively charged vesicles has been studied extensively because of its proposed relationship to processes which may occur during biological membrane fusion (87, 93-97). These experiments, however, have tended to rely on determination of initial aggregation rates and are therefore normally restricted to unstable systems at low concentrations (<1% phase volume). Although small unilamellar vesicles are not thermodynamically stable, they are certainly metastable, being kinetically stabilised by strong repulsive forces in low-ionic-strength media, particularly when charged phospholipids are included.

The repulsive forces which give rise to the formation of lamellar phases in phospholipid + water mixtures and stabilise liposomes in colloidal dispersion have been studied extensively by Rand, Parsegian and co-workers (98-101). In all cases, a strong exponentially decaying repulsion appears to dominate the interaction at bilayer separations <30Å. This has been tentatively ascribed to a 'hydration force' originating from water structuring around the polar phospholipid headgroups (98-101). Repulsion at larger separations is due to overlap of electric double layers and the results are qualitatively consistent with DVLO theory, although quantitative fitting in some cases requires adjustment of parameters such as the surface charge density (99) or the Debye screening length (101).

Neutron and light scattering data were collected over a wide range of wavevector Q at various number concentration of vesicles. At low phase volume of particles the data at high and low Q were modelled by a single-particle form factor P(Q) (equation 2[36]) for a shell particle. At high phase volume data were collected over the same Q region, however, in the scattered intensity, information about P(Q) and the interparticle interference terms S(Q) was available (equation 2[7]). For spherical particles the intensity scattered into a given angle was given by

$$I(Q) = ACM^2P(Q).S(Q) \qquad \text{Equation 5(1)}$$

where C was related to the optical refractive indices or the scattering length densities for light or neutrons (equation 2[10]), respectively, ρ is the number density of particles of molecular mass, M_1 and A is an instrument constant.

In a scattering experiment the distance scale observed is governed by the wave vector change on scattering Q. The vesicles investigated here have a diameter of ca. 200Å. The use of light ($\lambda \sim 5 \times 10^3$Å) and neutrons ($\lambda \sim 10$Å) thus allows exploration of a wide range of correlations within the scattering system, including long-range interactions and overall particle dimensions. The relative stability of the vesicle particle allows the single-particle and interparticle scattering terms to be separately determined in a way not possible for micellar systems (38,65). Previous neutron-scattering studies on vesicles have, however, been concerned with the bilayer structure itself rather than with the interparticle potentials (89).

(2) Theory

The interactions between vesicles have been calculated by use of an extended form of the DLVO theory (54,65). Initially it was considered that the net interaction potential between a pair of particles was given by the sum of repulsive and attractive contributions (equation 3[1])

$$V = V_R + V_S - V_A \qquad \text{Equation 5(2)}$$

where V_R was calculated using a modified form of the equation suggested by McCartney and Levine (56) (equation 3[7]). The constants for the hydration force V_S (equation 3[9]) were 2.56Å for the decay length ξ and the value for P_o was 7.05×10^9 dyn cm^{-2} (58). The attractive potential V_A comes from the expression of Vincent (59) (see chapter 3, page 53) and the precise composition of the sheath was determined by the area per molecule (74Å^2) and the bilayer thickness (40Å). The Hamaker constants for hydrocarbon and water were taken as 14kT and 8.9kT, respectively (59).

For the range of interparticle separations considered in this study (up to 2000Å) and a typical surface charge density of 2μC cm^{-2} calculation shows that the interactions are dominated by the electrostatic repulsion V_R. The effective dispersed phase volume of such a system should therefore be much larger than its normal phase volume, and structuring was to be expected (35). Assuming that the dispersion was essentially monodisperse in the absence of added electrolyte, the condition of electrical neutrality permits

interpretation of the coherent scattering data in terms of a pseudo-two-component system (31). We adopt the notion of an effective hard-sphere diameter as suggested in a recent publication (102). In this case the authors use the Barker-Henderson pairwise hard-sphere approach, which yields

$$R_{eff} = r(x_c + \int_{x_c}^{\infty} \{1 - \exp[-V(x)/kT]\}dx) \qquad \text{Equation 5(3)}$$

where $V(x)$ was of the form of V_R in equation 5(2) and x_c was an arbitrary cut-off distance, in units of the particle radius r.

This equation 5(3) was of the same form as equation 3(24) in Chapter 3.

The DLVO theory used on this data has been dealt with in detail in Chapter 3. Although all the contributions to the net interaction potential were considered for the concentrated vesicle analysis, only the repulsive contribution was used. Justification for this was given, for a single sheath vesicle by Figures 12 and 13. Figure 12 represents the attractive contribution represented by the Hamaker relationship using the parameter indicated, and Figure 13 gives the full attractive and electrostatic repulsive contribution for the ionic strengths 0.1 and 0.001 mol dm^{-3} (curve b and a respectively). Since the nature of the attraction yields only a primary minimum for this dispersion, the systems are not at thermodynamic equilibrium. However, concern with the essential kinetic stability of the particle requires consideration of only that part of the potential accessible within the time scale of the experiment. The calculation in equation 5(3) was thus carried out only over the positive contribution of V(r). Further justification for the choice of potential will be seen later in the good fits with the theoretical model of Hayter and Penfold (12).

(3) Experimental

(a) Materials

Egg phosphatidylcholine (PC) Grade I and bovine spinal cord phosphatidylserine (PS), monosodium salt, Grade I were obtained from Lipid Products, South Nutfield, and the Sigma Chemical Co., Poole, and were subsequently used without further purification. Water was distilled from alkaline $KMnO_4$. D_2O was obtained from B.D.H. AnalaR-grade sodium chloride was obtained from Hopkin and Williams.

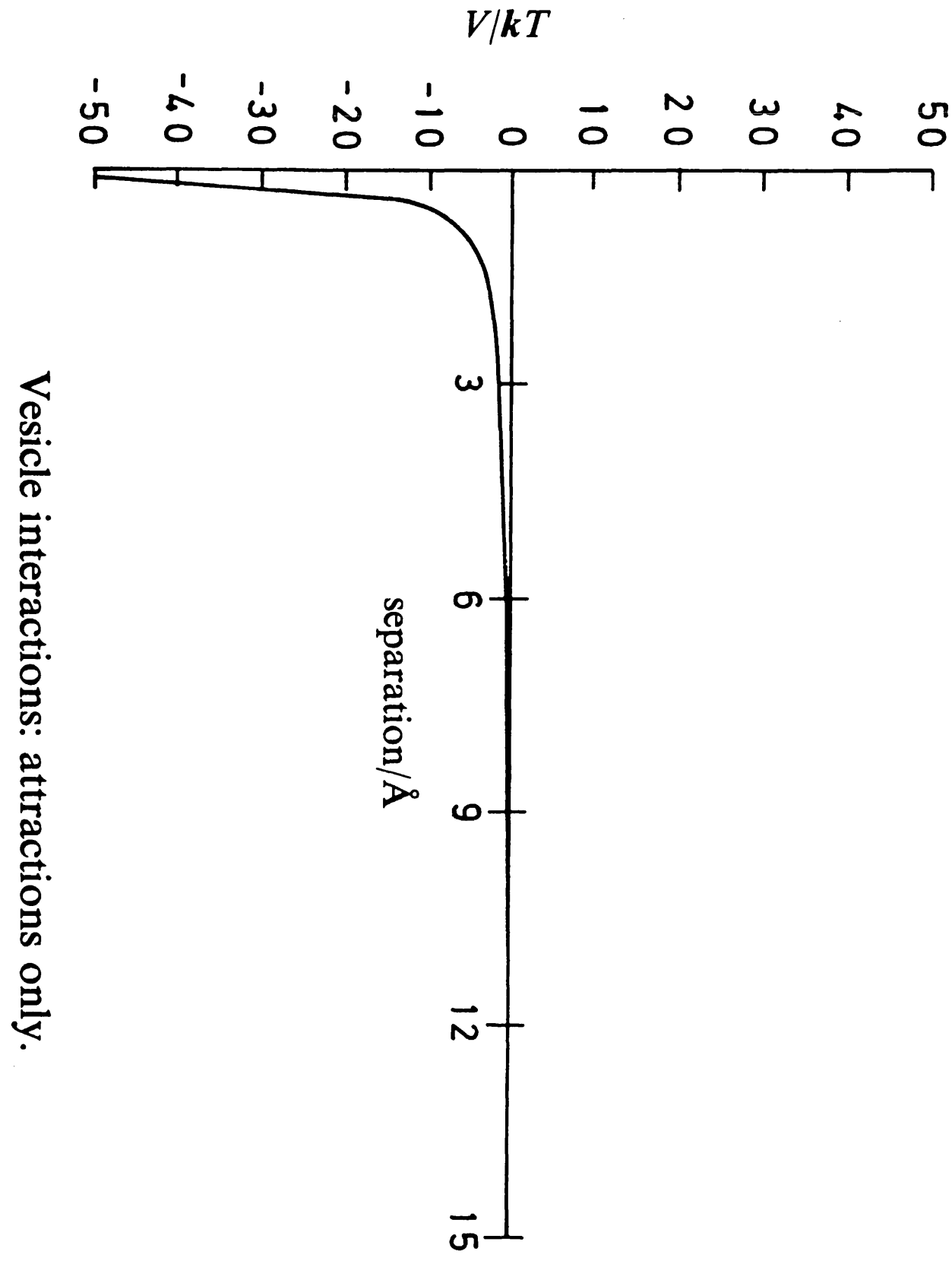


Figure 12: Vesicle interactions: attractions only.

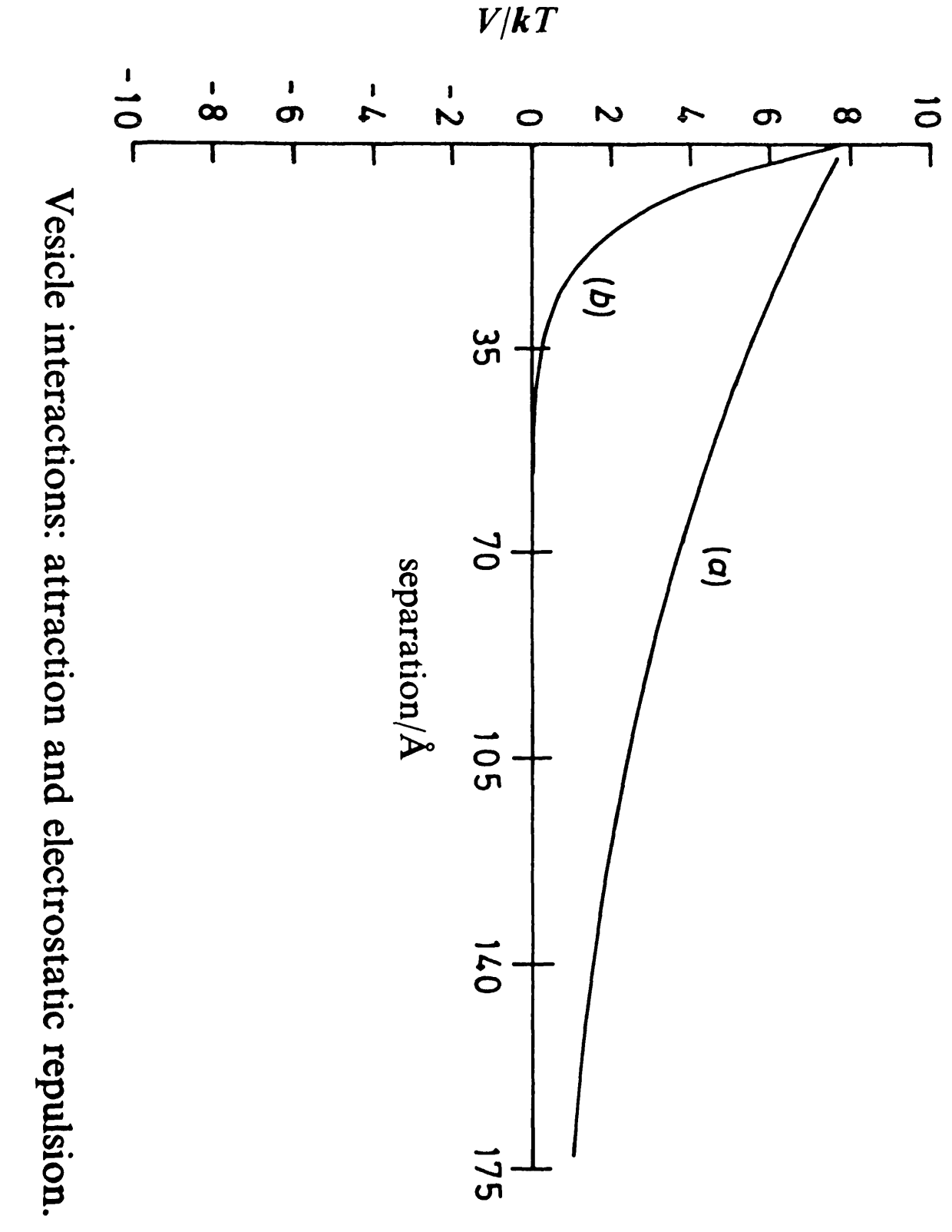


Figure 13: Vesicle interactions: attraction and electrostatic repulsion. (a) 0.001, (b) 0.1 mol dm^{-3} electrolyte.

(b) Preparation of Vesicle Dispersions

Vesicles were prepared from pure PC and from mixtures of PC with PS containing 5%, 10% and 50% by weight of the charged component, PS. Ca. 500mg of the required lipid mixture was dissolved in ca. 10cm^3 of a 2:1 mixture of chloroform and methanol. The solution was placed in a 250 cm^3 round-bottomed flask and the solvent removed by rotary evaporation: residual traces of solvent were removed by overnight storage under vacuum in a desiccator. 10 cm^3 of water (or D_2O) was then added and the flask swirled to wash the lipid film from the walls. The resulting turbid suspension of multilamellar liposomes was transferred to a small glass beaker which was covered over with Nescofilm and flushed with nitrogen for 15 min. The sample vessel was immersed in an ice bath and kept under nitrogen during sonication, which was carried out using a Dawe soniprobe tuned for maximum cavitation. Sonication was continued in 5 min bursts, to prevent overheating of the sample, until the suspension clarified. Normally 15-20 min total sonication time was adequate; slightly longer was required for the pure PC. which did not disperse so easily. The sample was centrifuged at 120,000g for 2.5 h to remove titanium fragments (released from the sonicator tip) and remaining large liposomes. The upper fraction from the centrifuge tube was used in the case of dispersions in water; for those in D_2O the lower fraction was taken.

When experiments were to be done in the presence of salt, an appropriate volume of concentrated NaCl solution was added to the dispersion. After preparation the vesicle dispersions were stored at 4°C and were used as soon as possible. This stock dispersion (nominally 4% wt/vol concentration) was diluted in simple ratios as required.

Quantitative determination of phospholipid concentrations (PC + PS) were made by colourimetric phosphate analysis following the method of Morrison or by direct weighing of the dried samples.

(4) Results and Discussion

(a) Neutron Scattering

Sample details are given in table 1 for uncharged (pure PC) and charged (PC with 50, 10 and 5% by weight PS) vesicles. Experiments were carried out at concentrations within the range 0.05-4.0% wt/vol and with the addition of NaCl up to 0.1 mol dm^{-3}.

Figure 14 shows data for uncharged vesicles for which we expect little structure in S(Q) especially at high Q. The residual structure at high Q in figure 14(a) was therefore to be associated with the single particle form factor, P(Q). We can discard an explanation in terms of interlamellar interference from multilamellar superstructures both because of the invariance of the structure with added salt and because the high Q Kratky plots (in $I(Q)Q^2$ against Q^2) show a positive slope, expected for unilamellar particles as opposed to the negative slope observed for polydisperse multilamellar particles (89).

Table 1. Determined concentrations (mg cm^{-3}) and lipid ratios

Technique	Neutron Scattering				Light Scattering	
Sample	PC	95:5	90:10	50:50	90:10[a]	90:10[b]
Concentration of nominal 4% material	25.2±0.5	21.6±4	41.1±4	30.0±2	48±3	43±3
Ratio PC:PS	100:0	96:4	91:9	50:50	90:10	91:9

[a]Diffusion measurements; [b]absolute intensity measurements

The high -Q data in figure 14(a) are therefore fitted by the single-particle form factor in equation (2[36]). Using a mean radius of 95Å and a bilayer thickness of 40Å, a Gaussian distribution of radii(104) (half width at half maximum, h.w.h.m., 18Å) has been convoluted with equation (2[36]) to give the solid line in the figure.

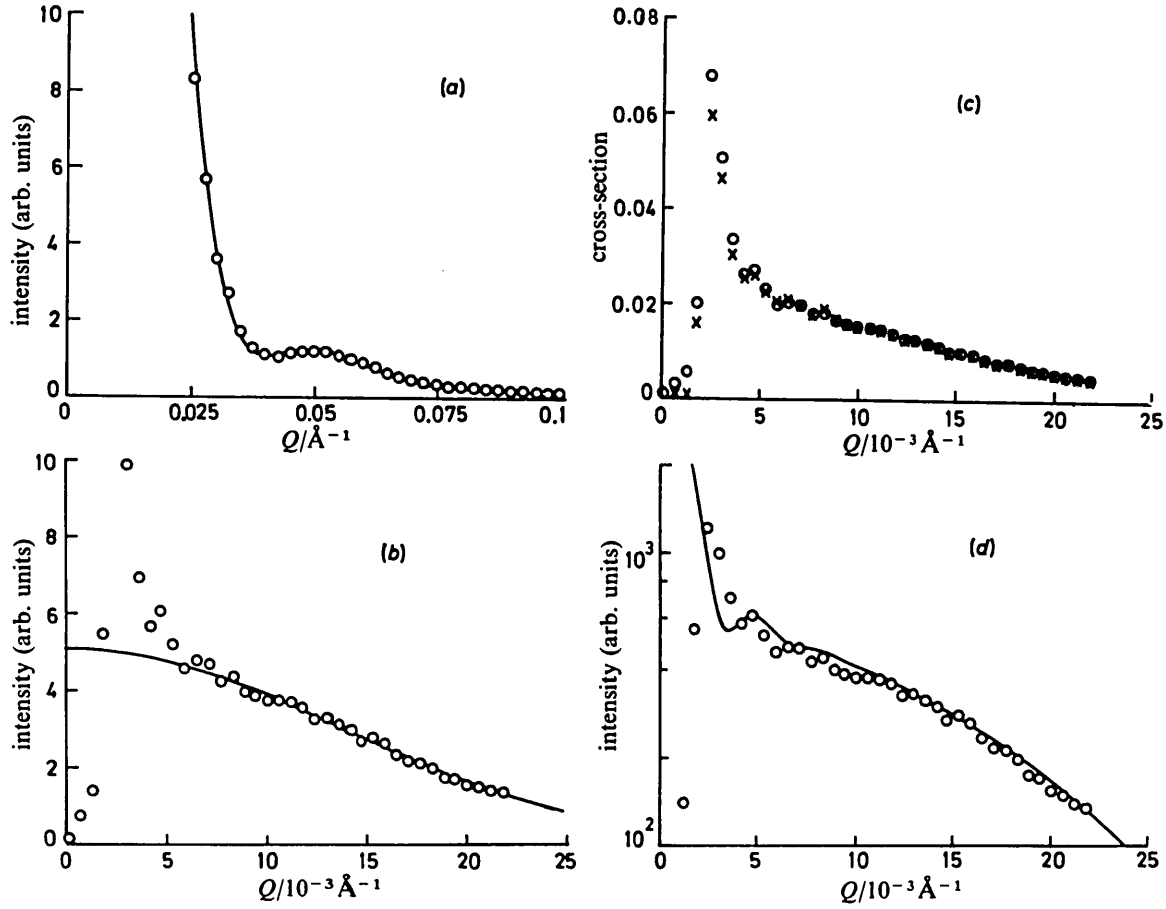


Figure 14: Neutron-scattering data for uncharged PC vesicles. (a) nominal 1% high Q. (b) nominal 1% low Q. The solid line is the calculated P(Q) for a fit using the following parameters: mean radius 95Å, thickness 40Å and h.w.h.m. 18Å. (c) comparison of low-Q data for nominal concentrations as shown (x, 0.05%; 0, 1.0%). (d) as (b) with bimodel size distribution shown as solid line.

At low Q the data deviate from this theoretical curve, as shown in Figure 14(b). The high intensity at very low Q indicates the presence of very large particles, and closer examination of the data in figure 14(b) and (c) shows several oscillations which could arise from the Bessel function in the form factor of such large particles. Figure 14(c) also shows that a change in concentration by a factor of 20 produces negligible change in the scattering curve, confirming the absence of interparticle interactions and the integrity of both types of particles. If the oscillations in the scattering curves are associated with Bessel functions then this indicates that any large particles must be highly monodisperse. Indeed, figure 14(d) shows that the data could be approximately fitted by a biomodal double Gaussian size distribution, comprising small particles as fitted for high-Q data and large particles with radius 900Å, membrane thickness 40Å, and a half width at high maximum of 130Å.

With this assumption of a vesicle form factor, in order to fit the data, the large particles must have a relative number concentration of 1:1200. Such trace contaminants have been observed previously (105)and, while their origin may remain obscure, their integrity allows us to handle the scattering in the same way as for the small particles.

Figure 15(a) and (b) show high-Q data for PC:PS 90:10 and 95:5 charged vesicle solutions, respectively. In this Q range S(Q) was expected to have reached its limiting value of unity and indeed figure 15(b) shows little effect on the scattering curves when electrostatic interactions are screened by addition of 0.1 mol dm^{-3} salt. The single particle form factor in equation (2[36]) again fits the data reasonably well, as shown by the solid lines in figure 14(a) and (b). On the other hand, the values of the radii obtained (71Å for 90:10 and 77Å for 95:5) are unreasonably small compared with the other neutron results which all give values > 90Å, and it seems possible that S(Q) is still contributing to the scattering curves. A negative slope in S(Q) would shift the Bessel function peaks to the right and cause equation (2[36]) to fit for an apparently diminished radius of the vesicles. Slight differences in the data for the 90:10 sample could be observed after addition of salt (data not shown) and this would be consistent with a residual contribution of S(Q), incompletely screened by the salt. The effect cannot be seen for the 95:5 data in figure 15(b) however.

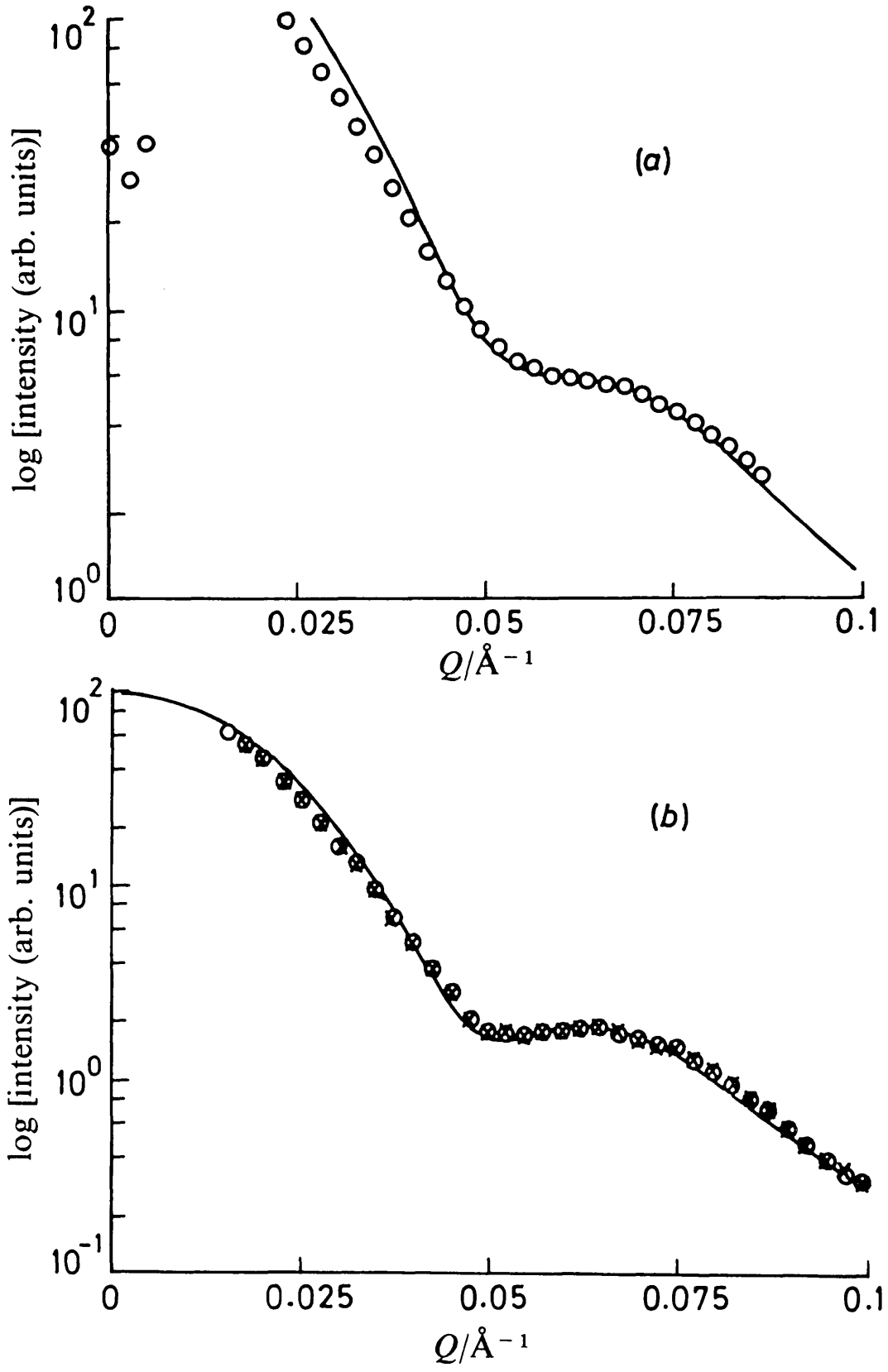


Figure 15: Neutron scattering data at high Q for charged vesicles. (a) 90:10 PC:PS nominal concentration 4%. (b) 95:5 PC:PS nominal concentration 1%; 0,in the presence of 0.1 mol dm^{-3} salt; x, no added salt. The solid lines are the calculated P(Q) for a fit using the following parameters: (a) mean radius 77Å, thickness 40Å and h.w.h.m. 13Å; (b) mean radius 71Å, thickness 40Å and h.w.h.m. 15Å.

The effect of concentration on S(Q) was clearly seen in the low-Q data for 90:10 charged vesicles shown in figure 16(a). On addition of 0.1 mol dm^{-3} salt the structure (except at low Q) disappears and data for a 1% solution become closely similar to that for 0.05% as shown in figure 16(b). The oscillations at low Q in figure 16(a) and (b) again indicate the presence of large particles. A relatively crude fit to the data in figure 16(b) (better at high Q) using the method described for figure 14(d) again indicated a bi-modal distribution of particles with diameters of 180 and 2000Å.

Figure 17(a) and (b) show the effect on the data of progressively screening out the interactions by addition of salt to 1% and 4% solutions of 90:10 charged vesicles. Although the effect of salt on the data for the 1% solution [figure 17(a)] is minimal above $Q = 1.2 \times 10^{-2}$ $Å^{-1}$, this is not the case for the 4% solution [figure 17(b)] indicating again (as suggested above in explaining the small particle sizes obtained from figure 15) that at high concentration S(Q) does not reach its limiting value of unity until rather high Q values are reached. The suppression in intensity at low Q at low ionic strength may be understood as an apparent reduction in the compressibility of the system arising from the increased effective diameter of the particles. A real increase in particle size is ruled out, in view of the invariance of the scattering at high Q shown in figure 16(b).

The effect of concentration on I(Q) may also be seen in the other ratios of PC:PS (95:5 and 50:50) charged vesicles [Figure 18(a) and Figure 18(b)]. The peak position is related to the particle concentration in the dispersions. As seen in the table 1 the concentration of each stock dispersion varied depending on the preparation. The preparation of the 95:5 and 90:10 samples gave higher concentrations than the 50:50 sample. These concentration differences account for the difference in the peak positions.

Suppression of the interactions by addition of screening electrolyte has the same effect on the 95:5 and 50:50 charged vesicles (not shown) as on 90:10 vesicles. As the percentage of charged PS increased from 5 to 50%, one would expect the amount of electrolyte needed to remove interactions to increase. However, more detailed experiments would be needed to correlate the different systems with the electrolyte suppression levels.

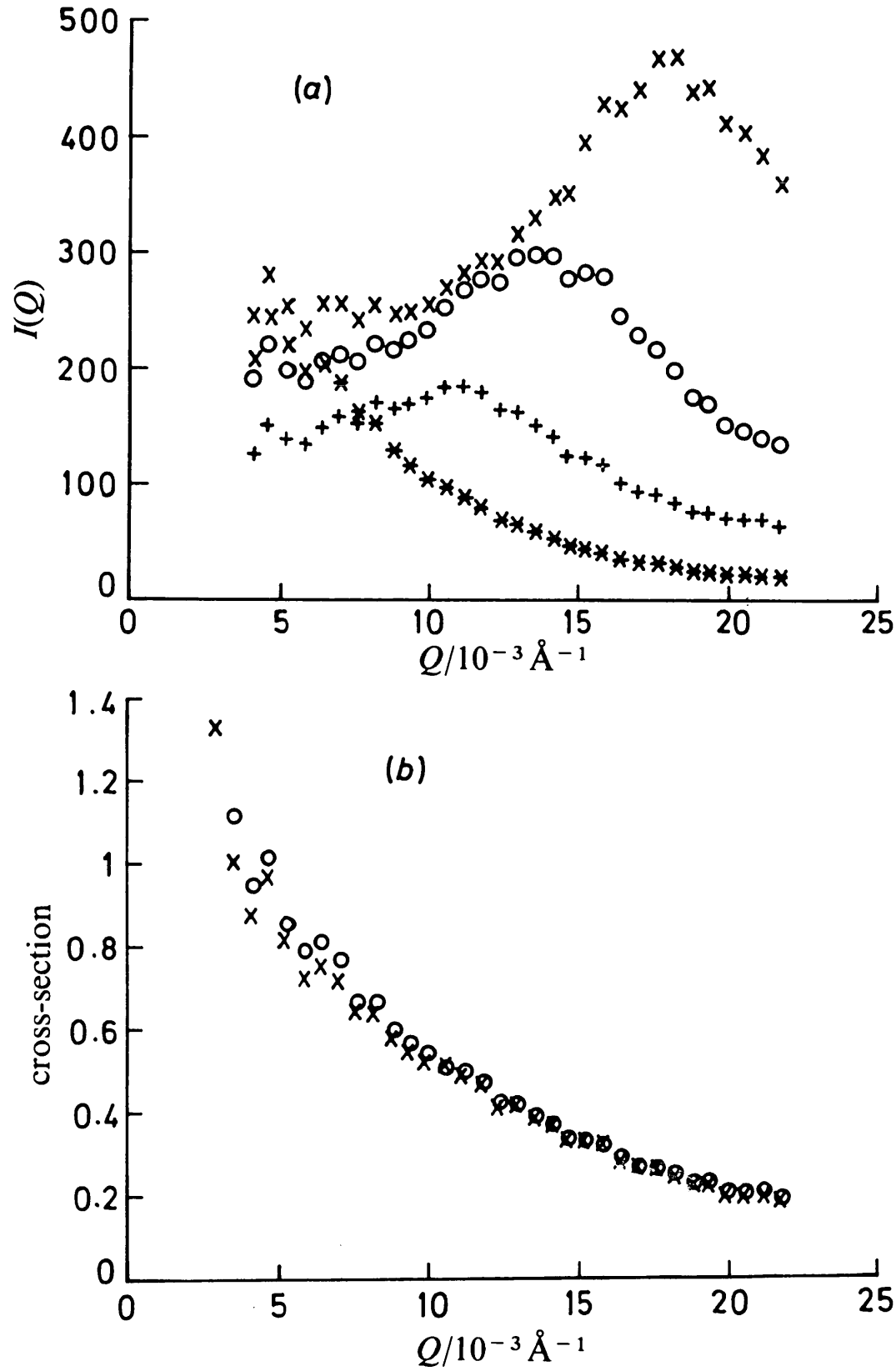


Figure 16: Neutron scattering data at low Q of 90:10 PC:PS vesicles. (a) intensity plotted against Q at various nominal concentrations: *0.5; +, 1; 0, 2; x, 4%. (b) comparison of (o) nominal 0.05% and (x) nominal 1% in the presence of 0.1 mol dm^{-3} salt.

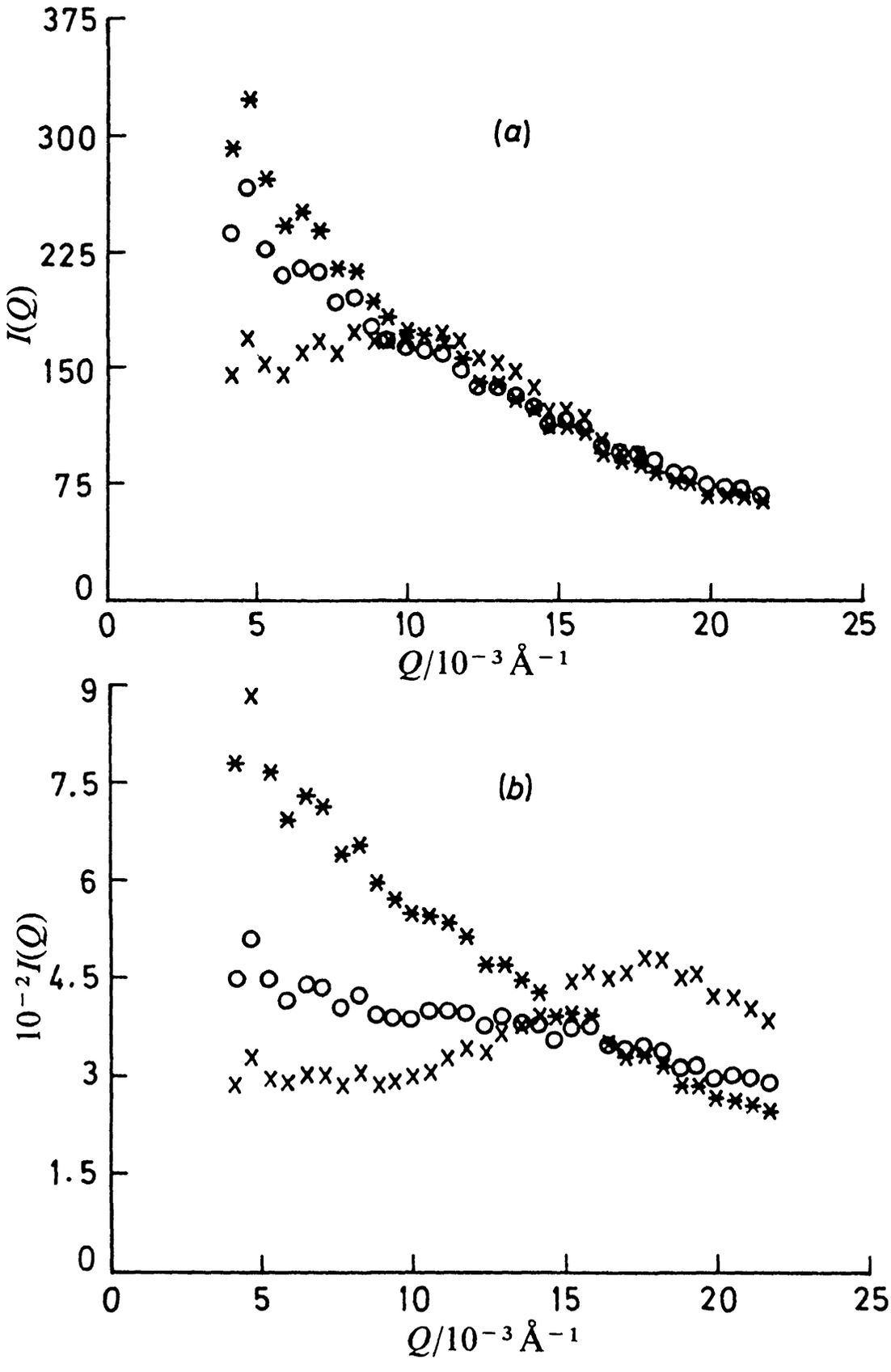


Figure 17: Neutron scattering data at low Q for 90:10 PC:PS vesicles in the presence of salt. (a) nominal 1%. (b) nominal 4%. x, 0.001; 0, 0.01; *, 0.1 mol dm^{-3} NaCl.

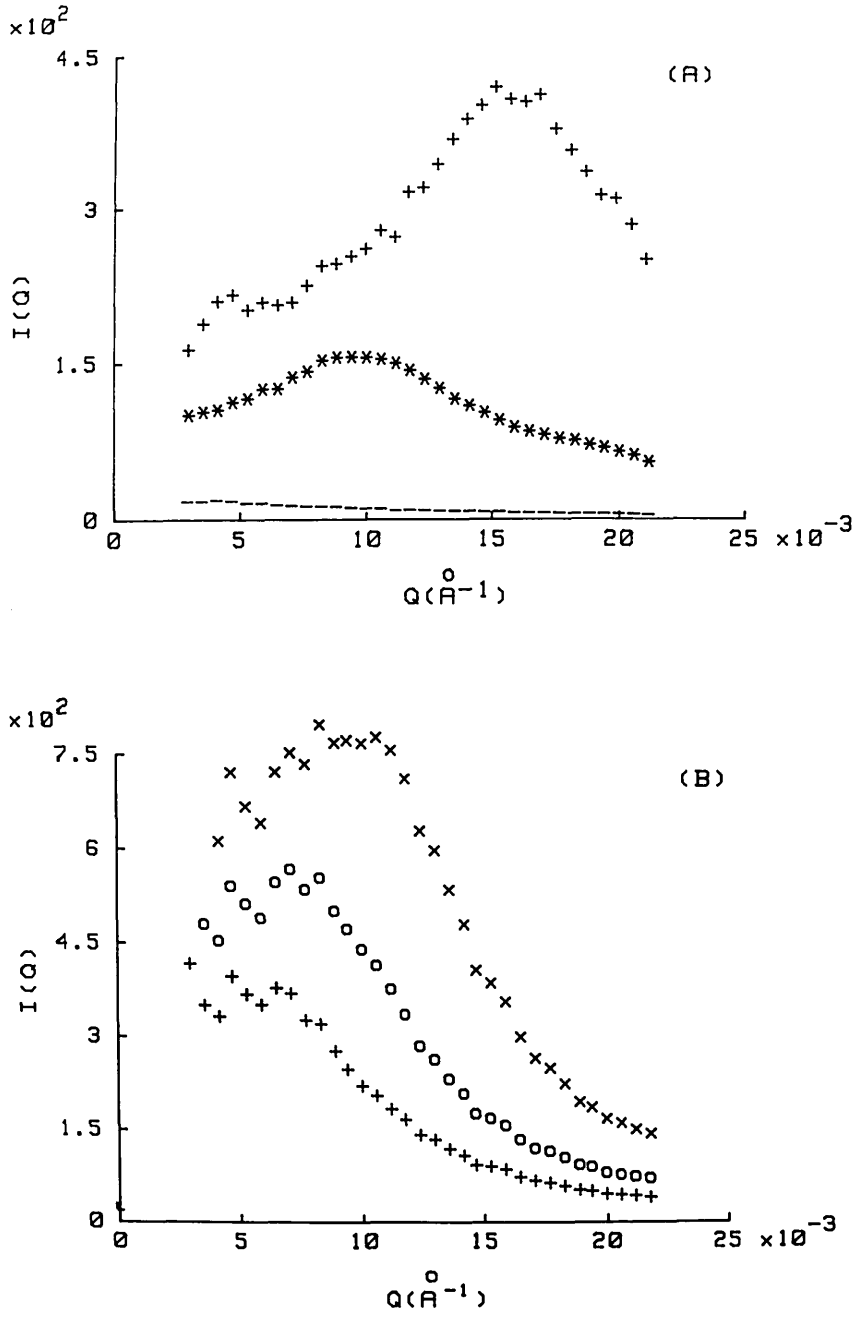


Figure 18: Low Q neutron scattering data of 95:5 and 50:50 PC:PS vesicles. Intensity plotted against Q at various nominal concentrations (a) 95:5 PC:PS vesicles: + 4; *1; - 0.05%. (b) 50:50 PC:PS vesicles: x 4; 0 2; + 1%.

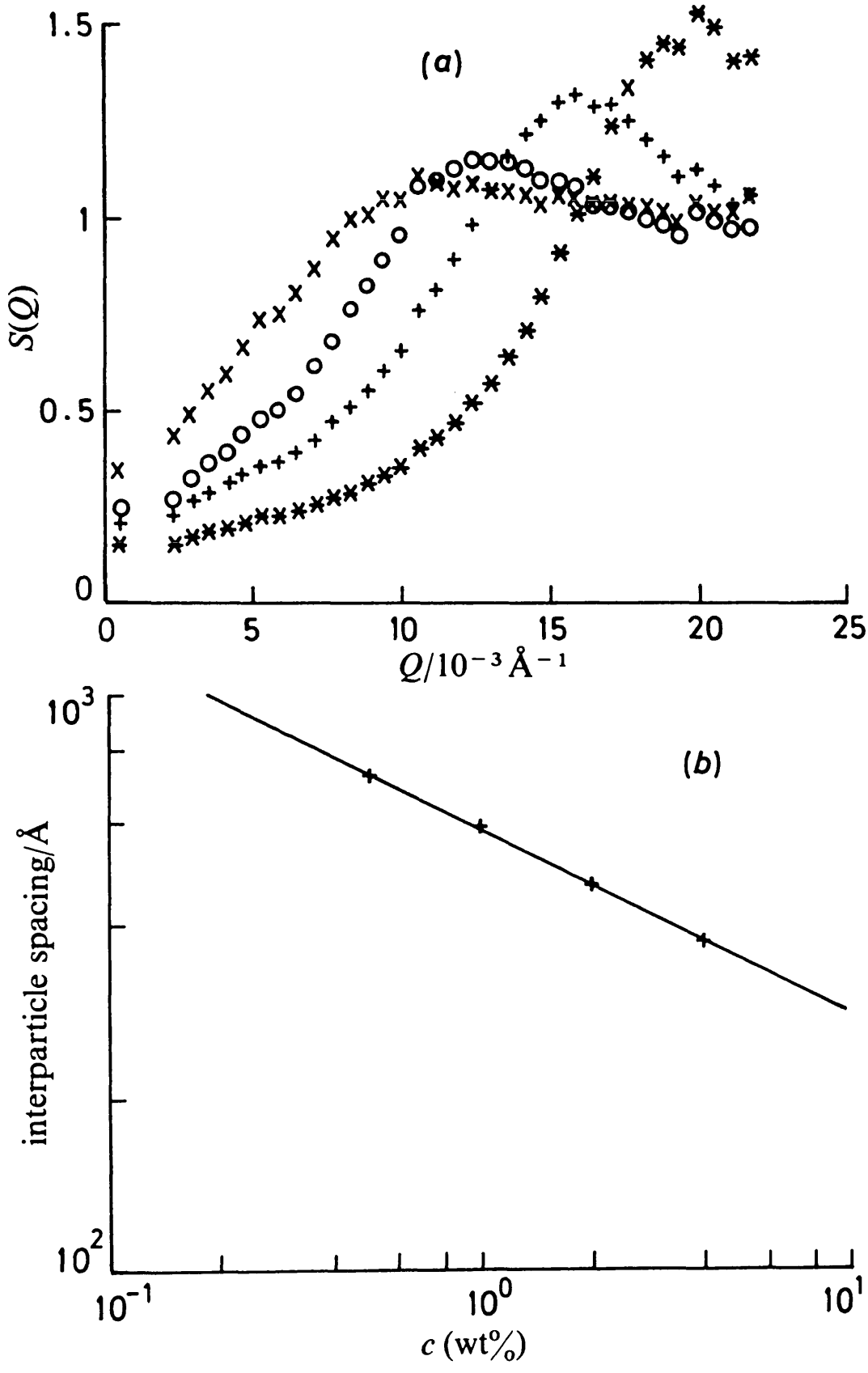


Figure 19: (a) structure factor S(Q) plotted against Q for 90:10 PC:PS vesicles for various nominal concentrations: x, 0.5; 0, 1; +, 2; *, 4%. (b) obtained from peak position in (a) plotted against nominal concentration; gradient = -0.321.

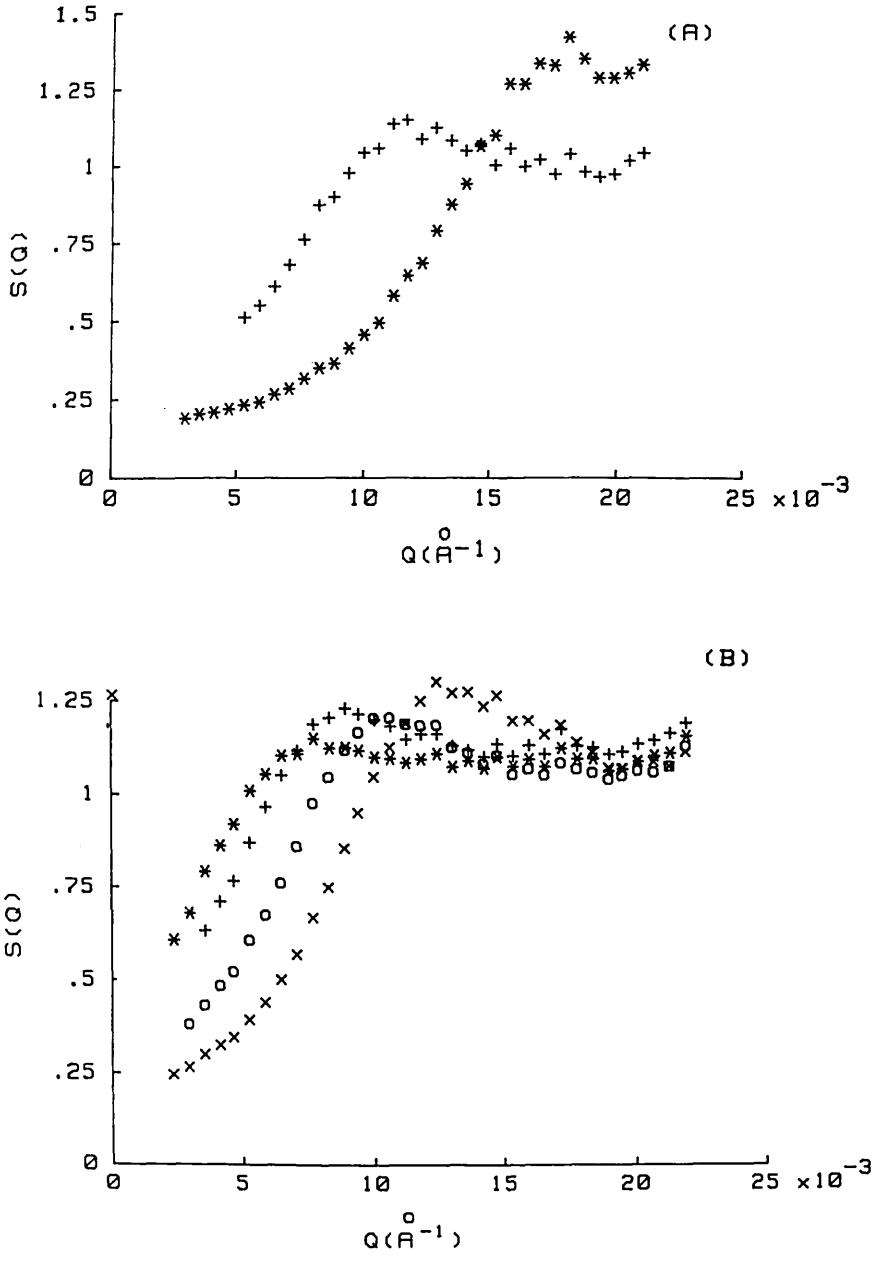


Figure 20: Structure factor S(Q) plotted against Q for 95:5 and 50:50 PC:PS vesicles for various nominal concentrations. (a) 95:5 PC:PS vesicles: + 4; * 1%. (b) 50:50 PC:PS vesicles: x 4; 0 2; + 1; * 0.5%.

Relying on the evidence presented that both large and small particles retain their integrity with changing concentration, the structure factor S(Q) was obtained following equation 5(1) by dividing the high-concentration data by the whole curve for the lowest concentration (0.05% unstructured system). This assumes that the large particles behave coherently with respect to the structuring and was formally justified if there was no correlation between size or orientation and position. Figure 19(a) shows the results of the procedure for the 90:10 system. The data follow the general predictions of the models described in Chapter 3, normalising correctly to unity. The reliability of the low-Q, data (and hence of our division involving the large particles) was confirmed by the light-scattering values of S(0) which are included in the figure (see light scattering results section).

The 95:5 and 50:50 PC:PS charged vesicles show similar experimental S(Q) data, Figure 20(a) and 20(b). One would expect that as a percentage of charged lipid was increased from 5→50 the peak should sharpen as surface potential increases and the system orders, however, this was not the case. This was probably to do with polydispersity problems or that only a certain percentage of counter ions can dissociate and at concentration of PS >5% the remaining PS added has its counter ion bound to the surface.

Riley and Oster (106) have shown that for a close-packed array

$$\frac{Q_{max}\, d_{max}}{2\pi} = 1.22 \qquad \text{Equation 5(4)}$$

However, Pusey (47) has obtained an experimental value of 1.18 which we used here since our arrays may not be closed-packed but are certainly similar in organisation to those discussed by Pusey. Table 2 lists the interparticle spacings calculated from figure 19(a), together with the particle number density ρ_N calculated assuming cubic packing. Figure 19(b) shows that d_{max} scales closely with (concentration)$^{1/3}$ as was necessary for any three-dimensional arrangement of particles.

A value of the number density can also be obtained from the exact concentrations given in table 2. For a vesicle of radius 90Å, molecular volume 1480Å^3, surface area per molecule ca. 74Å^2 and lipid density

1.019g cm^{-3}, (107) values of 1345 and 359 molecules on the outer and inner layers of the bilayer, respectively, (92,107) are calculated. The number densities ρ'_N calculated on this basis are shown in table 2 and are in good agreement with those calculated from the interparticle spacing.

Table 2. Interparticle spacing and number density for 90:10 vesicles

Nominal Concentration c(wt%)	Actual Concentration c(wt%)	Interparticle spacing, d/Å	No. density (d)$\rho_N/10^{16}$ particle cm^{-3}	No. density (c)$\rho'_N/10^{16}$ particle cm^{-3}
0.5	0.51	741	0.24	0.25
1	1.03	591	0.48	0.49
2	2.06	469	0.97	0.98
4	4.11	378	1.85	1.96

(b) Comparison of Hayter and Penfold and Hard Sphere Theoretical Models

In attempting to analyse the data both the hard sphere model (108-115) based on the Ashcroft and Lekner modified Percus-Yevick and the mean spherical approximation (MSA) Hayter-Penfold (37, 65-68) models have been used.

Dispersions with a nominal concentration less than and approximately equal to 2% of 90:10 charged vesicles show good agreement with both models [figure 21] as do concentrated samples [Figure 22] with a high level of electrolyte present. At the higher-phase volumes the peak in S(Q), and the compressibility limit S(0) may not be simultaneously modelled [Figure 23a-d]. The discrepancy between the model S(0) and the lightscattering S(0), whilst maintaining a good quality fit for the peak, increases with concentration. One explanation for such a deviation could arise from the incoherence/diffuse scattering associated with the

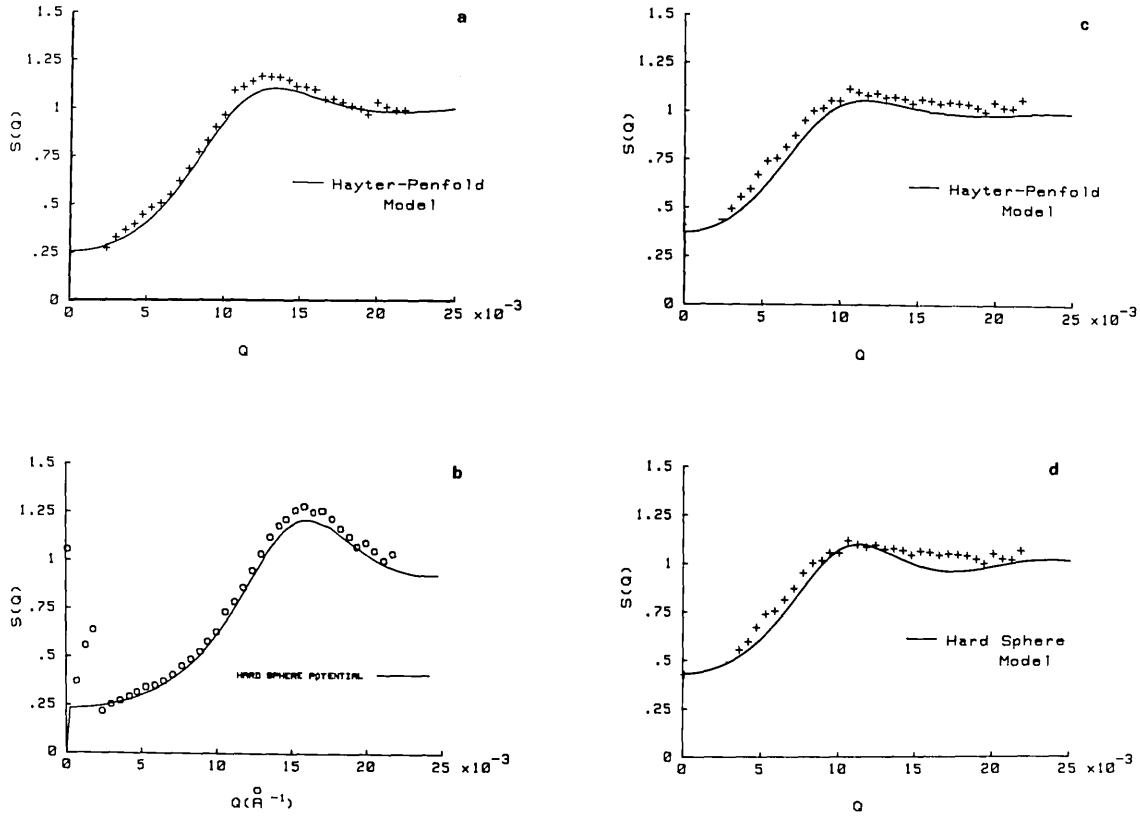
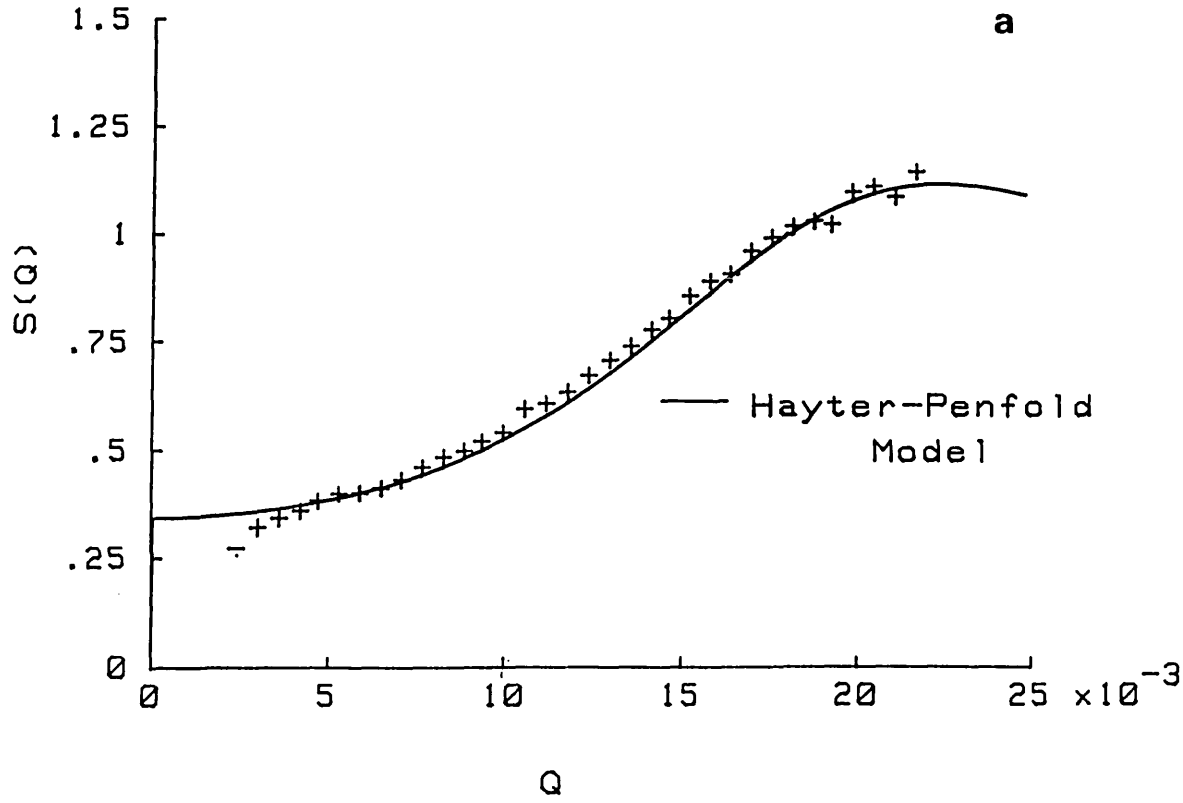


Figure 21: Structure factor S(Q) against Q for 90:10 PC:PS vesicles for various nominal concentrations (a) 1%, (b) 2%, (c) and (d) 0.5%. The solid line in the figures was the theoretical model, either hard-sphere or Hayter-Penfold. With the parameters (a) ϕ = 0.013, diameter = 197Å, 1/K = 106, V = 42 mV, (b) ϕ = 0.025, diameter = 500Å, (c) ϕ = 0.0066, diameter = 198Å, 1/K = 125, V = 42 mV, (d) ϕ = 0.0107, diameter = 525Å.



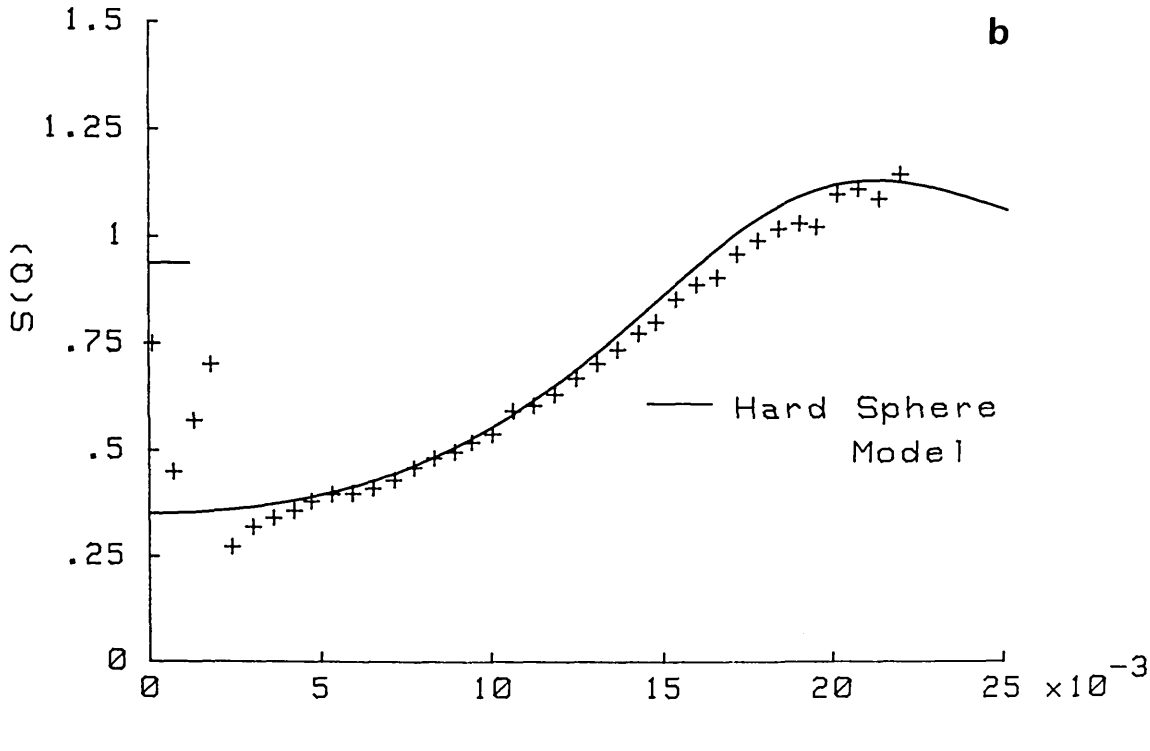
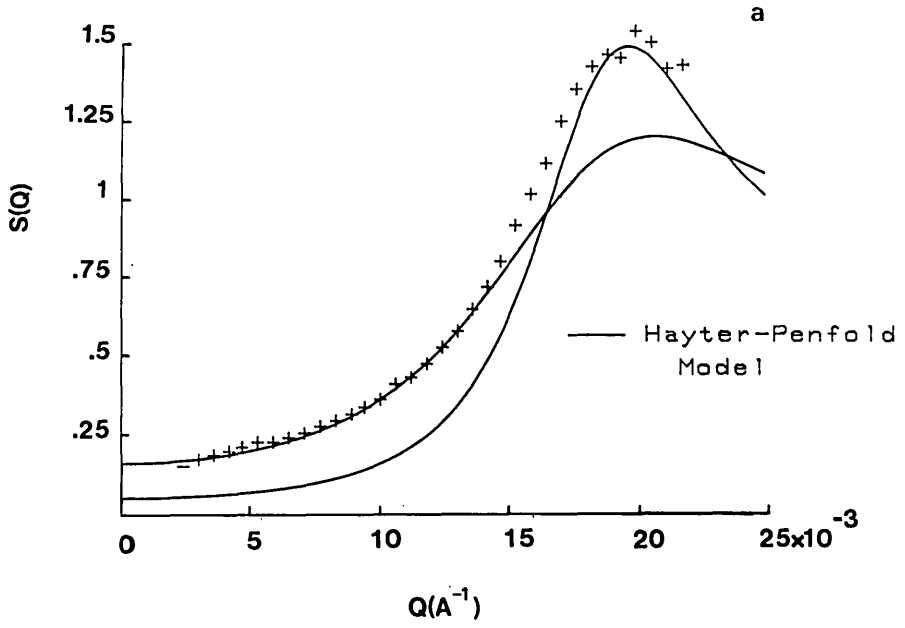
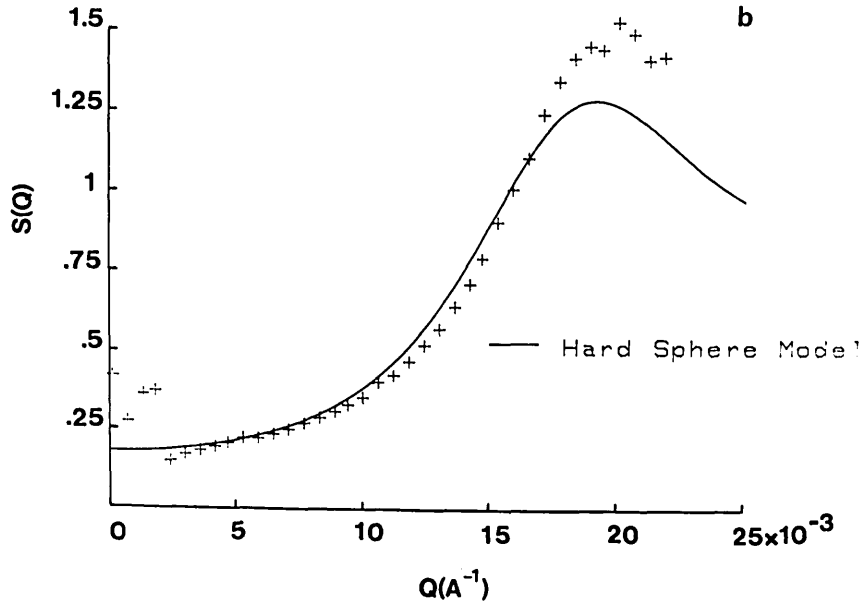


Figure 22: Plot of S(Q) against Q for PC:PS = 90:10, 4% vesicles in 0.01 mol dm^{-3} salt. (a) Hayter-Penfold model; ϕ = 0.053, diameter = 193Å, 1/K = 24, V = 38 mV, (b) hard sphere model: ϕ = 0.13, diameter = 280Å.


a
1.5
1.25
1
.75
.5
.25
S(Q)
Hayter-Penfold
Model
0
5
10
15
20
25x10-3
Q(A-1)


b
1.5
1.25
1
.75
.5
.25
S(Q)
Hard Sphere Model
0
5
10
15
20
25x10-3
Q(A-1)

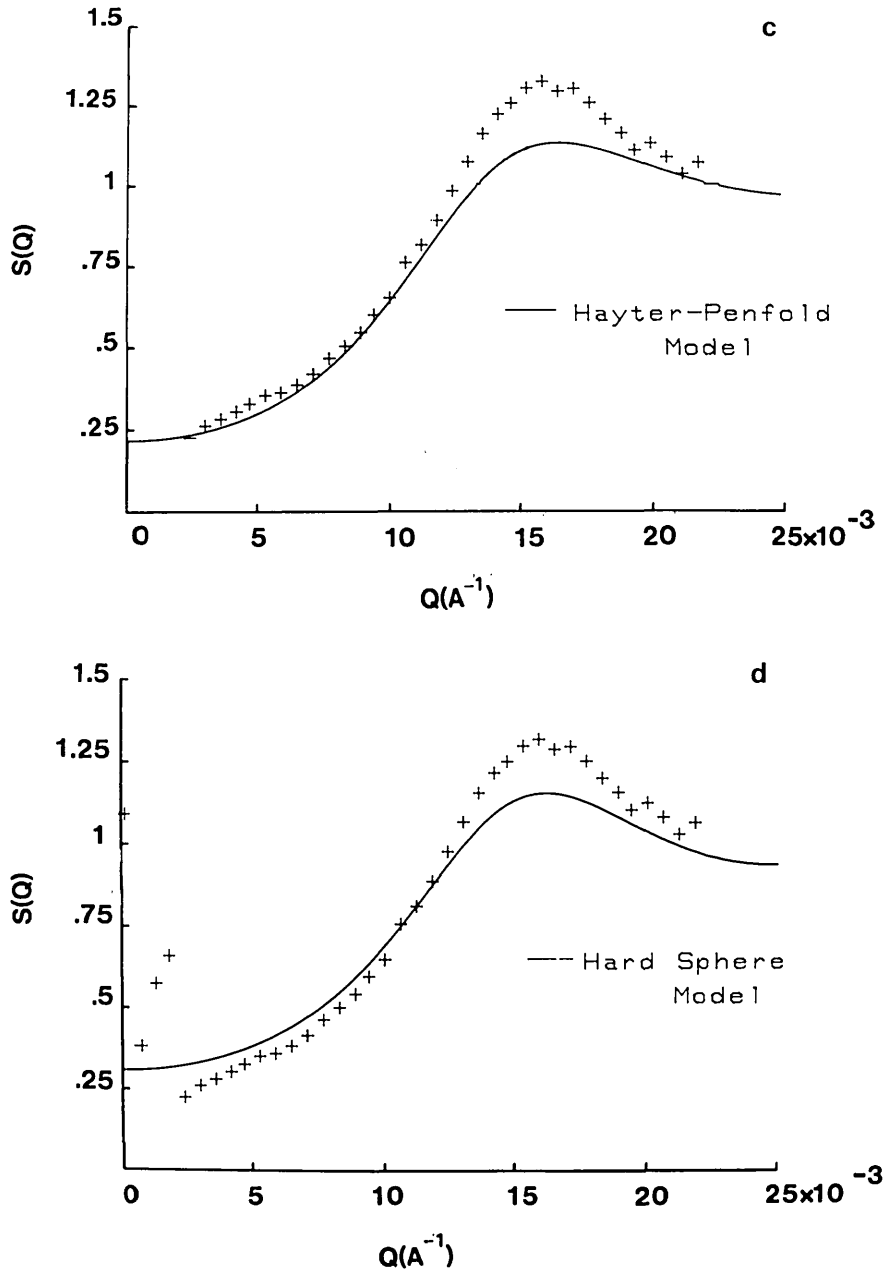


Figure 23: Plot of S(Q) against Q for PC:PS 90:10 vesicles, (a) 4% data modelled by Hayter-Penfold model fitted at Imax and S(0), (b) 4% data modelled with hard sphere model ϕ = 0.018, diameter = 320Å, (c) 2% data modelled with Hayter-Penfold model ϕ = 0.0265, diameter = 192Å, 1/K = 77 and V = 37 mV, (d) 2% data modelled with hard sphere model ϕ = 0.015, diameter = 370Å.

polydispersity of the materials. An immediate candidate for such a contribution is the trace amounts of large particles present in the sample. Many other works (116-120) investigating the size distribution of vesicles have observed this type of distribution.

The scattering intensity from these large particles would have a linear dependence on the concentration in opposition to the coherent contribution which yields the compressibility limit S(0). As a result, provided there was no correlation between position and scattering amplitude, this incoherent contribution (i.e. the P(Q) of the large particles) should increase linearly with concentration. Within this simplistic model, the difference between the model S(0) and the light-scattering S(0) should generate an incoherent/diffuse intensity linear with concentration. Figure 24 shows such a plot for the data presented.

For a further increase in the diffuse scattering one would expect the P(Q) function for the large particles to become identifiable as an upturn in S(Q) at low Q. This feature does not appear to be present, however, and the overall profile of S(Q) in relation to the theoretical model will also reflect a contribution from the polydispersity in the size distribution of the small species.

Since the S(Q) are very structured and available in numerical form up to very large Q values, it is possible to Fourier transform them accurately to obtain g(r) according to equation 3(15). In figure 25 the g(r) are shown which were obtained from the Fourier transformation of the S(Q) fit (hard sphere and Hayter-Penfold models). In figure 25, the g(r) corresponds to the S(Q) Hayter-Penfold fits in Figure 23a. In both cases the probability of finding another vesicle at the distance of two diameters was extremely high as evident by the peak position for g(r) and another equally high probability occurs at four diameters. This repeat distance about the central vesicles tells the order in the 4% dispersion was fairly high. Fitting the S(Q) model to the peak in the S(Q) data would imply that the system is more ordered than if the fit was preformed in the light-scattering S(0) region. From the discussion above we can conclude that the system was of the higher order and should be described closer by the more structured S(Q). In Figure 25(c) the probability of finding a vesicle was higher at about 3* diameter which

was expected as the dispersion was dilute and vesicles will be further apart. However, this peak in g(r) was only slight and the function rapidly equilibrates to a probability of one at higher distance. That was to say there was an equal probability of encounter of vesicles at these distance scales. There was only slight order in the system of 1% concentration.

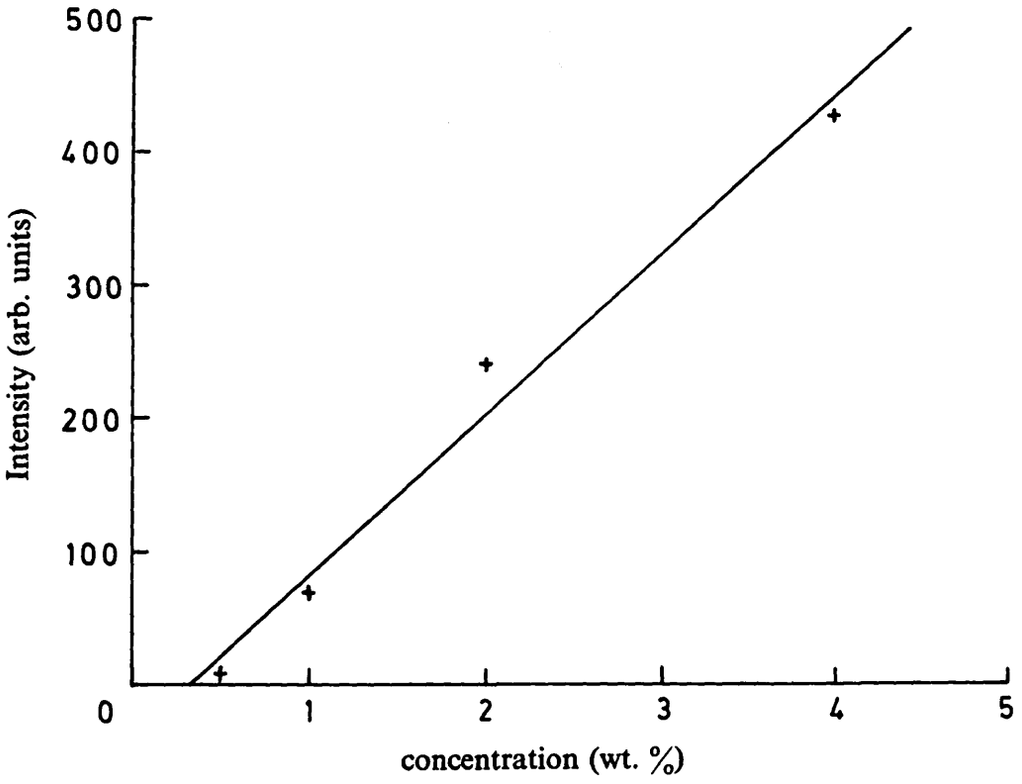


Figure 24: Plot of incoherent scattering intensity as a function of concentration. PC:PS = 90:10.

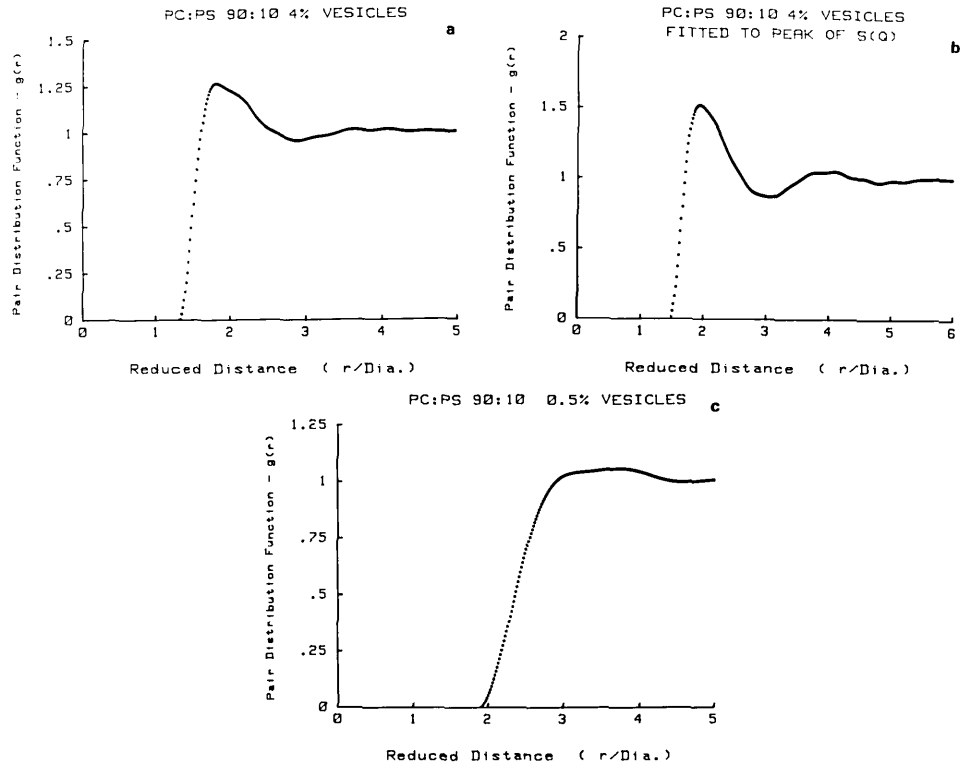


Figure 25: Pair distribution function obtained by Fourier transforming the model fit to the data in figures 23(a) and 21(c).

(c) Light Scattering

Light scattering experiments fall in the Q range $<2 \times 10^{-3}$ $Å^{-1}$ and are hence at the $Q \rightarrow 0$ limit of the neutron scattering results. P.C.S. experiments were carried out on freshly prepared D_2O dispersions of PC:PS 90:10 and 95:5 charged vesicles. The sample details in table 1 show reasonable consistency with the neutron samples.

The effective Stokes diameters (2R) obtained via eqn 4(10)-4(13) are shown as a function of concentration in figure 26(a) and (b) for 90:10 and 95:5 samples. (The viscosity of the D_2O was determined separately using a polystyrene latex of well characterised size). In both cases, there was a rapid increase at low concentrations to the infinite-dilution result. Addition of salt to the 4% samples increased the effective diameter back to the infinite-dilution result. No similar effect of salt or concentration was observed for uncharged PC vesicles (not shown). The data are summarised in table 3, where it was notable that the particle dimensions are larger than the neutron results. The logarithmic plots of correlation functions (equation 4[13]) were distinctly non-linear at high concentration and this was reflected in the values of the variances included in table 3. No phase volume correction has been made to these values in table 3, but since $\phi < 0.07$ this was not a large source of error and cannot explain the effect of concentration on the diameters.

Table 3: Effective diameters (Å) and second cumulant (in brackets)

Sample	Nominal 0.05%	Nominal 4%	4%+electrolyte
PC	270 (0.1)		
95:5	240 (0.2)	128 (0.7)	250 (0.1)
95:10	245 (0.3)	175 (0.8)	238 (0.1)

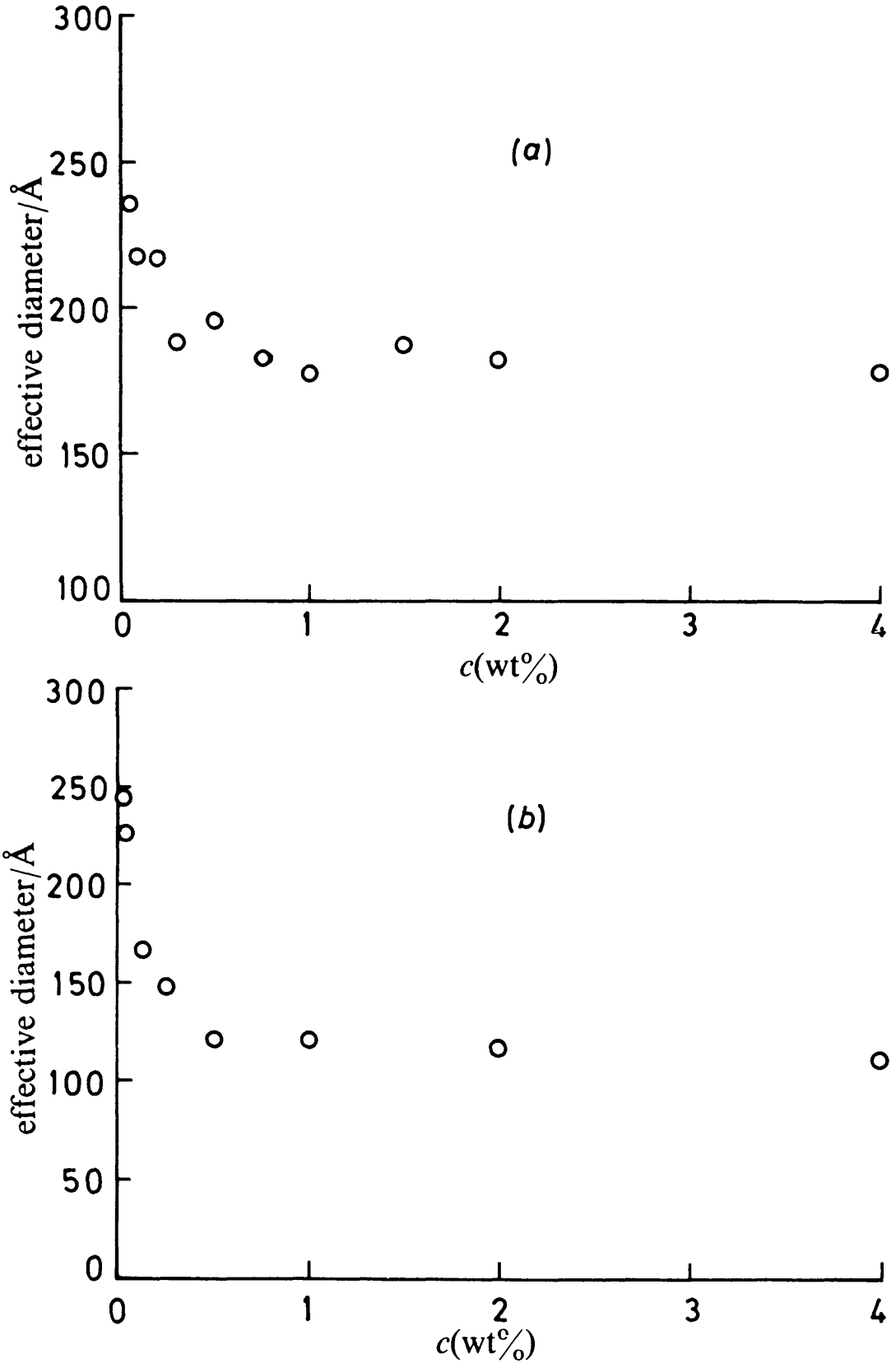


Figure 26: Diffusion data for charged vesicles. Effective Stokes diameter against nominal concentration, (a) 90:10 PC:PS vesicles; (b) 95:5 PC:PS vesicles.

The intensity of scattered light followed the same reduction with increasing concentration as the low-Q neutron data [figure 17(a)] and again addition of salt to the concentrated dispersions restored the intensity. However, the addition of small amounts of electrolyte (resulting concentration $< 5 \times 10^{-4}$ mol dm $^{-3}$) produced little change in the compressibility of a 2% dispersion of 95:5 vesicles. This suggests an equivalent ionic strength for the dispersion of ca. 5×10^{-4} mol dm^{-3} an admittedly crude estimate which is consistent with a 50% dissociation of the PS. The addition of electrolyte to the charged vesicle solution should rigorously be treated in terms of a multicomponent solution (31,122). The low-concentration intensity light scattering results in figure 27(a), however, indicate that the infinite-dilution limit was invariant with electrolyte concentration. Thus the intrinsic scattering cross-section of the particle remains unaltered despite the multicomponent nature of the disperion.

Figure 27(b) shows intensity light scattering data for 90:10 vesicles over a wide concentration range, and at various concentrations of electrolyte. At these very low Q values where P(Q) tends to unity c/I was proportional to $S(0)^{-1}$ [equation 5(1)] and hence may be related to the phase volume of the sample. The data in figure 27(b) have therefore been normalised to unity at infinite dilution using the intercept in figure 27(a). We have then applied a semi-empirical extension of the Percus-Yevick equation introduced by Carnahan and Starling (121,122)to relate $S(0)^{-1}$ to the phase volume

$$S(0)^{-1} = \frac{1 + 4\phi + 4\phi^2 + \phi^4 - 4\phi^3}{(1 - \phi)^4} \qquad \text{Equation 5(5)}$$

where ϕ was the effective hard-sphere phase volume, related to the hard-sphere radius R_{eff} and the number density ρ by $\phi = 4/3\pi\rho R_{eff}^3$. Curves (i) and (ii) in figure 27(b) have been fitted to the data using an effective phase volume as a simple multiple of the nominal phase volume, calculated using a particle model and the packing constraints for the lipid molecules outlined in section 3.2. The data at high salt concentration are fitted with a radius that maps to the effective phase volumes (curve ii). In the absence of salt the ratio was 26:1 [curve (1)]. It was, moreover, clear that equation 5(5) cannot fit these data with a simple multiple of the phase volume.

The dissociated Na^+ counter-ion contributions in the solution will, in the absence of a salt reservoir, increase the effective ionic strength with increasing concentration. This in turn affects V_R [equation 3(7)] through the contribution of κ [equation 3(3)] and hence changes the effective hard- sphere radius in equation 5(3). Curve (iii) in figure 27(b) was obtained from equation 5(4) using an effective phase volume calculated from equation 5(3) for each nominal phase volume, assuming arbitrarily that the PS species was 50% dissociated and that a surface potential of 30 mV persists. Adjusting the degree of dissociation and the surface potential produced fits of similar quality to curve (iii).

This alternative description of the low Q (light scattering) data does not include any polydispersity especially the important contribution from large particles. However, this latter process must be occurring so that the actual truth must be a hybrid of both explanations.

A common factor in all the calculations was a divergence from the data at high concentration indicating that the sample was more compressible at these concentrations than the model suggests. Deformation of the particles themselves was partly ruled out by the invariance of the particle scattering factor in the high-Q (neutron) data as electrolyte was added. Consideration of only pairwise interactions appears justified as κ^{-1} was typically <0.25 times the intersurface spacing. Three possible reasons for the discrepancy are suggested: (a) reduction in surface potential (consistent with reducing the interparticle interaction); (b) the inadequacy of an equivalent hard-sphere approach for describing very soft potentials; (c) the sensitivity at high concentration of this approach to the assumed particle size.

In the absence of hydrodynamic effects the apparent diffusion coefficient at finite concentration D_{eff} (and hence the effective Stokes diameters in figure 26) was directly related to the infinite dilution D_o value via S(0) (65,124). $D_{eff} = D_o S(0)^{-1}$ and thus the effective diameter should directly follow S(0) as concentration increases. Comparison of figure 26 and 27 shows that this was clearly not the case. The differences in behaviour may be attributed to hydrodynamic effects in the diffusion data associated with frictional drag. These effects have been calculated for hard spheres, and such corrections certainly improve the aggreement between data in figure 26 and 27.

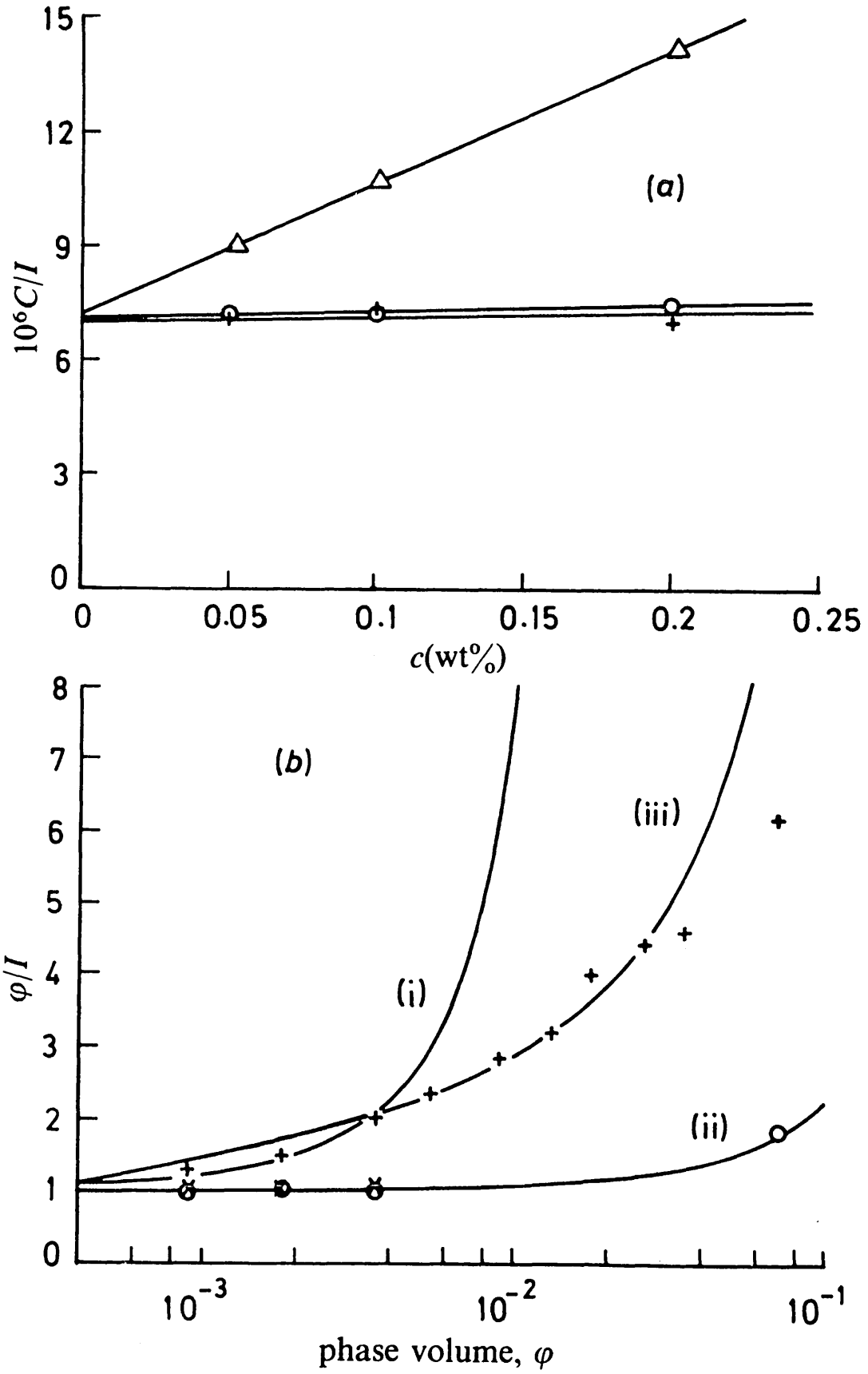


Figure 27: Absolute intensity light scattering data for 90:10 PC:PS vesicles. (a) inverse density as a function of low nominal concentration: Δ = no added electrolyte; 0, 0.01 mol dm^{-3} NaCl; +, 0.1 mol dm^{-3} NaCl; λ = 632.8 nm. (b) normalised inverse intensity against phase volume; +, no added electrolyte: x, 0.01 mol dm^{-3} NaCl; 0, 0.1 mol dm^{-3} NaCl. The solid lines are calculated curves as described in the text.

However, the corrections cannot explain the rapid change in apparent particle size at very low concentration, and until the exact form of the static behaviour has been clarified it was not fruitful to speculate on the details of the hydrodynamic interactions.

(5) CONCLUSIONS

(1) Both light and neutron scattering data confirm the integrity of the vesicles with changing concentration.

(2) The extraction of S(Q) by simple division using the whole P(Q) curve including the large particles was well justified by the overall shape of the curves, which normalise correctly to unity at high Q, by the variation in position of Q_{max} with concentration and by the agreement of the S(0) values with independent light scattering results. The detailed shape of the curves may be explained by one or both of the two mechanisms: the existence of large particles of low number density, of the change of surface and bulk ionic properties when an ionic reservoir was not present.

(3) Differences in the concentration dependence of S(0) and the effective diameters obtained from diffusion data may indicate the importance of hydrodynamic effects in the latter. The very low concentration behaviour of D_{eff} remains to be explained.

CHAPTER 6 - POLYMERISED VESICLES

(1) Introduction

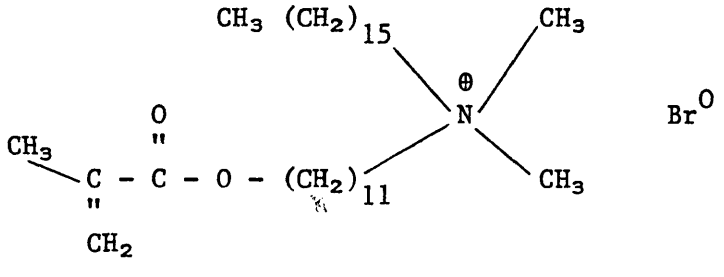
In recent years the interest in vesicles has been stimulated by the hope that these systems would provide interesting applications, either technologically or as drug carrier system (125-135).

Phospholipid vesicles and liposomes have been studied extensively as potential drug carriers but their usefulness in this role has been questioned due to the instability of liposomes in the presence of proteins and lytic agents in the body fluids, which can cause premature rupture of the particle. Recently the preparation of polymerisable lipids has opened up the possibility of preparing more stable vesicles.

All polymerised vesicles that have been reported thus far fall into five classes of polymerisation as shown in figure 29.

(a) through the centre of the lipid bilayer;
(b) through a monolayer lipid membrane;
(c) through the lipid chains of inner and outer monolayers;
(d) through the polar head groups of each monolayer;
(e) Finally the rather new type where the lipid bilayer is not covalently linked together, but is, instead, ionically encased with two concentric poly(methacrylate) monolayers (136).

Using the well characterised ammonium salt in Figure 28, vesicles were formed and polymerised as in Class (a).



Ammonium Salt

Figure 28

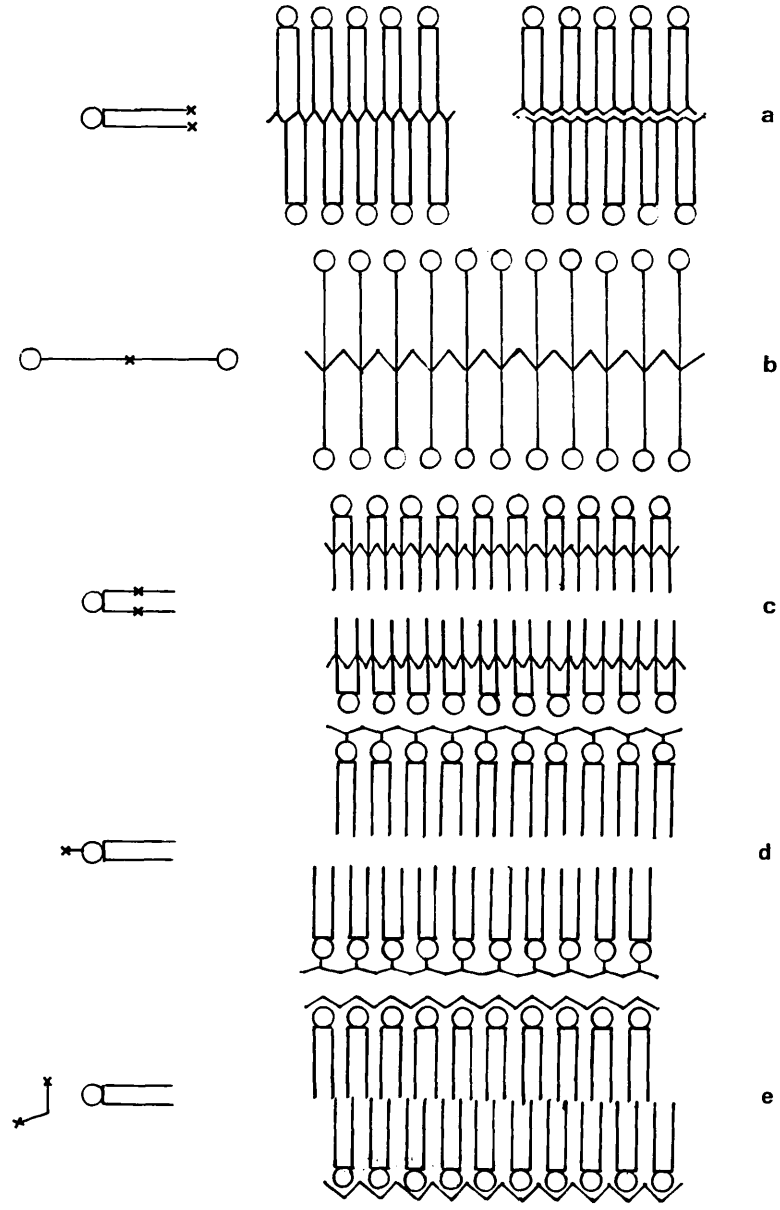


Figure 29: Method of polymerisation of surfactant bilayer. Five possible schematic monomers and mechanism for polymerisation are shown (x = polymerisable group). (a)-(c) and (e) polymerisation preserving head group properties. (d) and (e) polymerisation preserving chain mobility. Please also refer to text.

These particles have been studied as a colloidal dispersion using neutron and light scattering. Measuring their hydrodynamic radius, particle size distribution and stability (aggregation) properties in the presence of electrolyte.

(2) Experimental

(a) Experimental Materials - polymerisable methylarcyl monomer was obtained from R.J. Clark, Unilever Organic Section, and was subsequently used without further purification. Two stocks of monomer were available (IL and PS) which looked distinctly different in texture but were used in separate preparations. D_2O was obtained from Hopkin and Williams.

(b) Preparation of Polymerised Vesicle Dispersions - approximately 100mg of the monomer was dissolved in chloroform in a 250ml round-bottomed flask and the solvent removed by rotary evaporation. Also added was the free radical initiator azoisobutyronitrile (AIBN), 0.5 mg pre-dissolved in ethanol. This thin film of monomer on the bottom of the flask was stored for eight to ten hours in a desiccator under vacuum to remove residual traces of solvent. 10ml of water (D_2O) was then added and the flask swirled to wash the lipid film from the walls. The dispersion was transferred to a glass sonication tube which was covered with a rubber Suba-seal and flushed with nitrogen for approximately 20 minutes. The nitrogen inlet and outlet were removed and the sealed tube was then exposed to sonic energy from a water bath sonicator. This was done for a period of 20 minutes at maximim power at a temperature of 50°C. After the sonication period the "unilamellar" vesicles were transferred to a water bath at 80°C for 8 hours to complete the polymerisation of the reactive groups. The samples were centrifuged at 120,000g for 1-2 hours to remove large liposomes and semi-soluble polymer. On inspection of the centrifuge tubes the dispersion had separated into two distinct layers: a lower, clear, newtonian-like fraction and an upper fraction of viscous gel. These two fractions were separated and the gel was stored on the side of a sealed tube with a small amount of D_2O at the bottom to minimise evaporation. The lower fraction, which henceforth we shall refer to as the disperse phase, was used directly in scattering experiment while the upper fraction, the gel, was re-dispersed in D_2O for light scattering and used without dilution in neutron scattering (both D11 and D17) experiments.

(3) Results

A. Electrolyte Effects

(a) Neutron Scattering

Due to the limited momentum transfer (Q) of the instrument, D17, at Grenoble, prior to the experiment we recognised that for any estimation of particle size (i.e. P(Q)) a vesicle size of approximately 200-400Å diameter would be required. Initial uses of the preparation had given particle diameters in this range. The first preparation was exactly as described above and gave a particle size of un-centrifuged vesicles of approximately 1000Å. Six stock dispersions of "unilamellar" vesicles were prepared in turn with the aim to produce pseudo-small size vesicles. Each of these stock dispersions were prepared under different experimental conditions (i.e. sonication vessel, sonication time, sonication temperature, change of monomer and different method of sonication, i.e. probe rather than bath) (See Table 4). The earlier preparation were not centrifuged, however after failure to obtain small particle sizes, the samples were centrifuged in an attempt to remove a proportion of the larger particles. Examination of the gel and dispersed phase by light scattering indicated that the distribution of the vesicles was not a simple function and could be bimodal or log normal in nature. Both re-dispersed gel and the disperse phase had a fairly small ($v = 0.05 \rightarrow 0.1$) second cumulant indicating that the particles were fairly monodisperse. The dozen or so samples were all sized with PCS and particle diameters were in the range 400-1800Å (Table 4). Although the description of the preparation of the polymerised vesicles seems uncomplicated and well documented the procedure does not produce reproducible vesicle sizes.

Early workers on polymerised vesicles had sonicated the dispersions at 50°C. It was assumed the reason for this choice was a high gel-crystalline transition temperature (~45°C). As a result unilamellar vesicles would not form below this value. However, DSC work (J. Cahill) and optical microscopy (Dr. G. Tiddy) techniques ensured that the monomer transition was below room temperature.

In an effort to establish the significance of sonication (time and power), on the formation of vesicles a light scattering procedure was adopted. A multilamellar suspension was placed in a light scattering

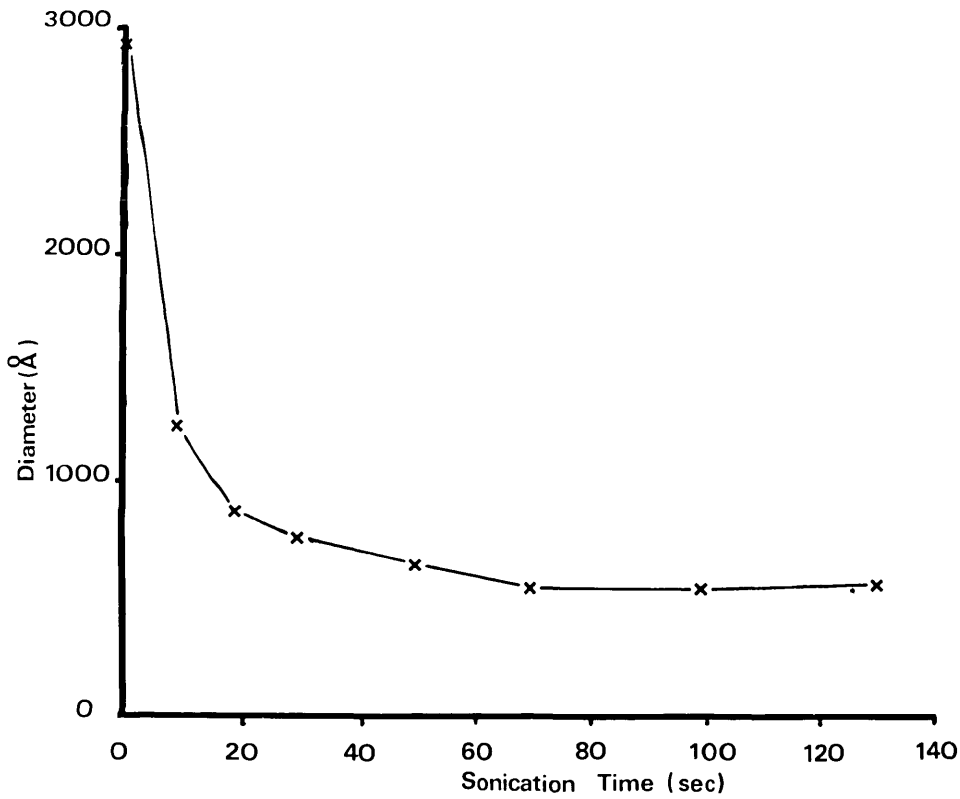


Figure 30: The effect of sonication time in a preparation of polymerised unilamellar vesicles. PCS data obtained during the probe directly in the scattering cell.

Table 4: Preparation of Polymerised Vesicles

Preparation	Conditions	Monomer	Polymerised initial diameter (Å)	Diameter after 1st centri. (Å)	Diameter gel phase (Å)
1	Normal (D_2O)	IL	1150	518	-
2	Normal (H_2O)	PJ	850-900	650	-
3	Normal (D_2O)	PJ	1800	400	2100
4a	55°C sonibath (D_2O)	PJ	1100	480	1100
b	Added 2% $C_{12}E0_8$	PJ	900	465	1060
5a	Sonibath (D_2O)	IL	1500	1020	-
b	Soniprobed	IL	530	480	-
6a	Soniprobe 635Å→ 550Å overnight (D_2O)	IL	520	514	-
b	Normal	IL	750	-	-
G2	Normal (D_2O)	IL	940	-	-

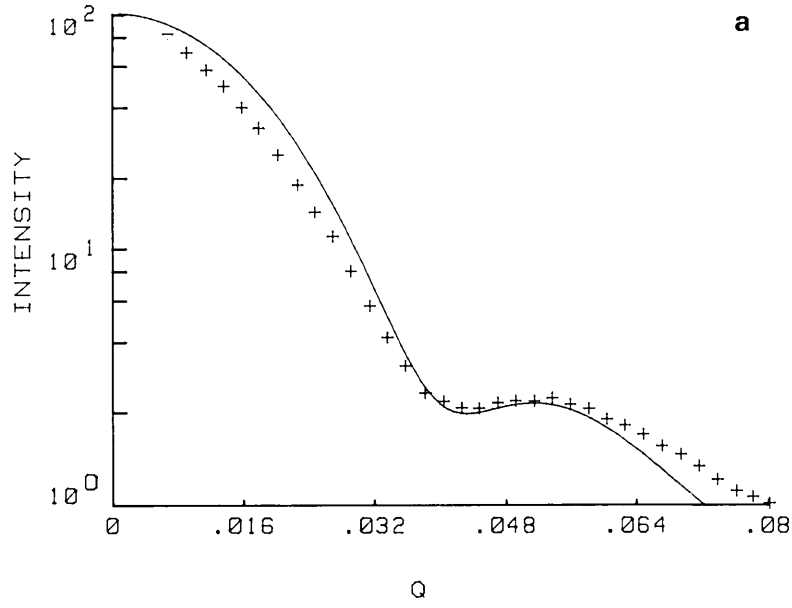
cell and the soniprobe microtip immersed in the suspension so as not to effect the scattering volume. The cell was then sealed with parafilm to prevent contamination. The index matching bath was at 50°C. The particle size of the multilamellar suspension was measured (time zero) and then the suspension was given bursts of sonic energy of approximately 1-5 sec. duration. Adequate time was allowed between the ultrasonic bursts and the scattering experiment so that the sample was bubble-free and at thermal equilibrium. Several experiments on each sample ensured this to be the case.

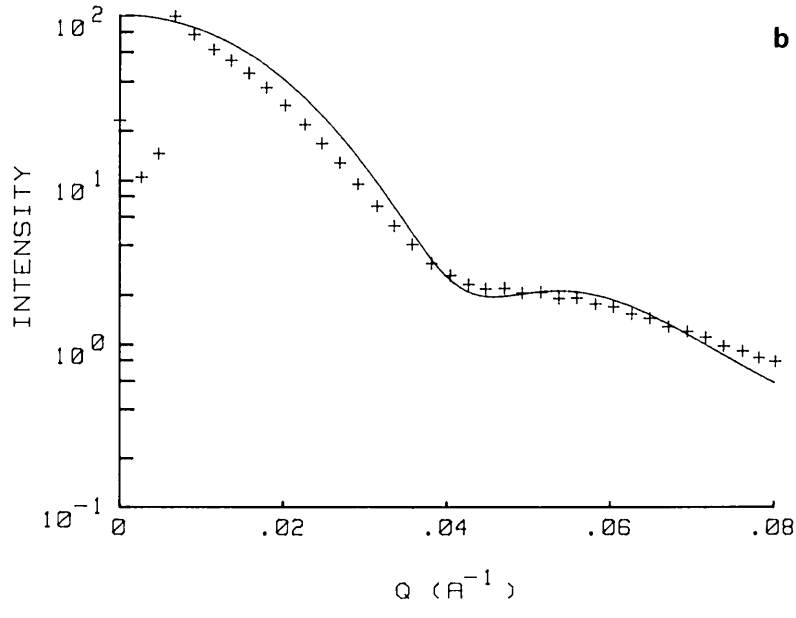
Figure 30 shows the sonication time versus particle diameter. No apparent effect was seen on tuning the power to match the cavitation properties of the cell. This could be a property of the scattering cell as the volumes used were small and the amount of energy needed was proportional to the volume of sample. The particle size obtained from the dynamic light scattering experiment indicated a small limiting size irrespective of sonication time or power.

The neutron scattering on the polymerised vesicles was exploratory, the aim being to find a sample having form factor oscillations indicating a monodisperse sample and then to observe the effect on the size and intensity with various additives. The first samples were chosen as they had the higher scattering intensity. The spectra were identical, a simple exponential type decay with no intra-particle structure. This indicates that the samples were polydisperse. The intensity falls off with a Q^4 dependence. This final slope was dependent on the fine structure of the particle rather than (and not on) the characteristic "integral" parameters volume, radius and correlation length which give the overall dimension of the particle.

This fourth power law was derived independently by Debye et al (137) and by Porod (138). In the derivation, even if there exists a well defined internal surface, only the outer surface was responsible for the final slope. The results should not be influenced by the large scale properties of the particles or their mutual arrangement. Any shaped particle, as long as it has these surface characteristics, will scatter with fourth power dependence.

Figure 31 shows sample 3 which has structure at high Q associated with the single particle form factor, P(Q). These data can be fitted reasonably by the single particle form factor in equation 2(36), using a mean radius of 90Å and a bilayer thickness of 40Å. A Gaussian distribution of radii (half width half maximum HWHM 18Å) has been convoluted with equation 2(36) to give the solid line in the figure. The effect of salt on the polymerised vesicles is shown in Figure 31 (b,c,d). Figure 31b shows the result of adding 0.01M sodium chloride to sample 3. Fitting a P(Q) (solid line) (mean radius 86Å, bilayer thickness 40Å, HWHM 18Å) gives a better curve fit to the data than in the absence of salt, although the effect was not marked. On increasing the electrolyte level to 0.05M and 0.1M, a marked effect in the scattering profile was observed. Fits to the data were attempted and mean radii of 112Å and 195Å with HWHM 28Å and 60Å respectively were obtained. This could be the result of an osmotic effect forcing the inner liquid out of the vesicles and flattening them to disc-like particles. The increase in polydispersity (as seen in HWHM values) would substantiate this hypothesis since a range of shapes from flat to circular particle could occur. Aggregation of vesicles would show the same effects, however.


a
INTENSITY
10^2
10^1
10^0
0
.016
.032
.048
.064
.08
Q


b
INTENSITY
10^2
10^1
10^0
10^{-1}
0
.02
.04
.06
.08
Q (A^{-1})

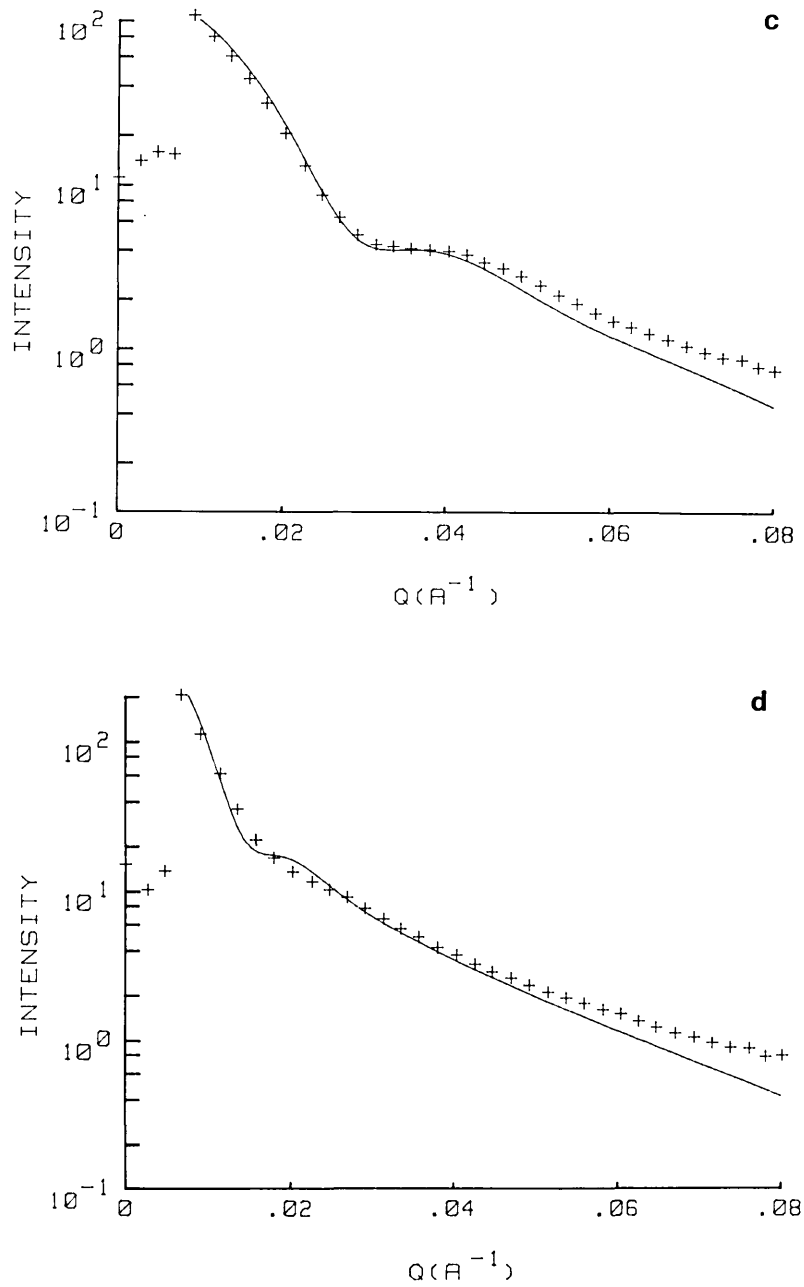


Figure 31: Neutron scattering data at high Q for polymerised vesicles, sample (3) in the presence of various salt concentrations. (a) no salt, (b) 0.01M NaCl, (c) 0.05M NaCl, (d) 0.1M NaCl. The P(Q) fits to the data using the following parameters: (a) radius 90Å, thickness 40Å, h.w.h.m. 18Å, (b) radius 86Å, thickness 40Å, h.w.h.m. 17Å, (c) radius 112Å, thickness 40Å, h.w.h.m. 28Å, (d) radius 195Å, thickness 40Å and h.w.h.m. 60Å.

The zero scattered intensity [I(0)] would be unaffected by a change in shape, whereas it would be highly sensitive to aggregation [I(0) would increase as aggregation increases]. Consequently, the difference between no salt and 0.01M NaCl may be a true decrease in size due to osmosis, whereas at higher ionic strength an aggregation process could be beginning. Both a shape change and an aggregation process could be occurring simultaneously.

In this Q range S(Q) was expected to have reached its limiting value of unity and indeed figure 32 shows little or no effect on the scattering curves when the sample was diluted by a factor of two. Sample 3 did show aggregation after a period of three months. This was seen in the turbidity of the solution and in the scattering curves (figure 34).

In this chapter we suggest that it was the larger species within the distribution that are susceptible to aggregation and that any aggregation process will lead to a bimodal distribution, with the lower mode possessing less intrinsic polydispersity, i.e. a smaller mean radius. Using the available theoretical single-particle form factor models it was extremely easy to show this effect. The particles have a distribution which was not precisely known, however, it will probably be a skewed (log normal or Schulzien) type. In our model, a Gaussian distribution was used which has a range of ±3 times the radius. It was assumed that the aggregates form another distribution and that the old distribution was simply truncated at the large limit to mimic this aggregation. In figure 33 (curve 1) the P(Q) of a 90Å radius vesicle (bilayer 40Å, HWHM 15Å) convoluted with an isotropic (normal) Gaussian distribution was compared with the sample P(Q) convoluted with an anisotropic Gaussian distribution with the imposed limits of -3 to + 0.5 times radius (curve 2). Using a Gaussian distribution to show this effect the higher limit had to be cut radically before any observable effect was noticeable. One observes that the mean was effectively smaller and the distribution effectively less polydisperse. However, if a skewed type distribution was used then because of the large number of larger particles, a less extreme truncation sufficed to show the same effect.

In the experiment the first peak in the structure P(Q) factor has moved to higher Q (figure 34) indicating that a percentage of the larger particles may have fused and are scattering out of this Q range (lower Q). A fit to the data was attempted (figure 34) using the theoretical

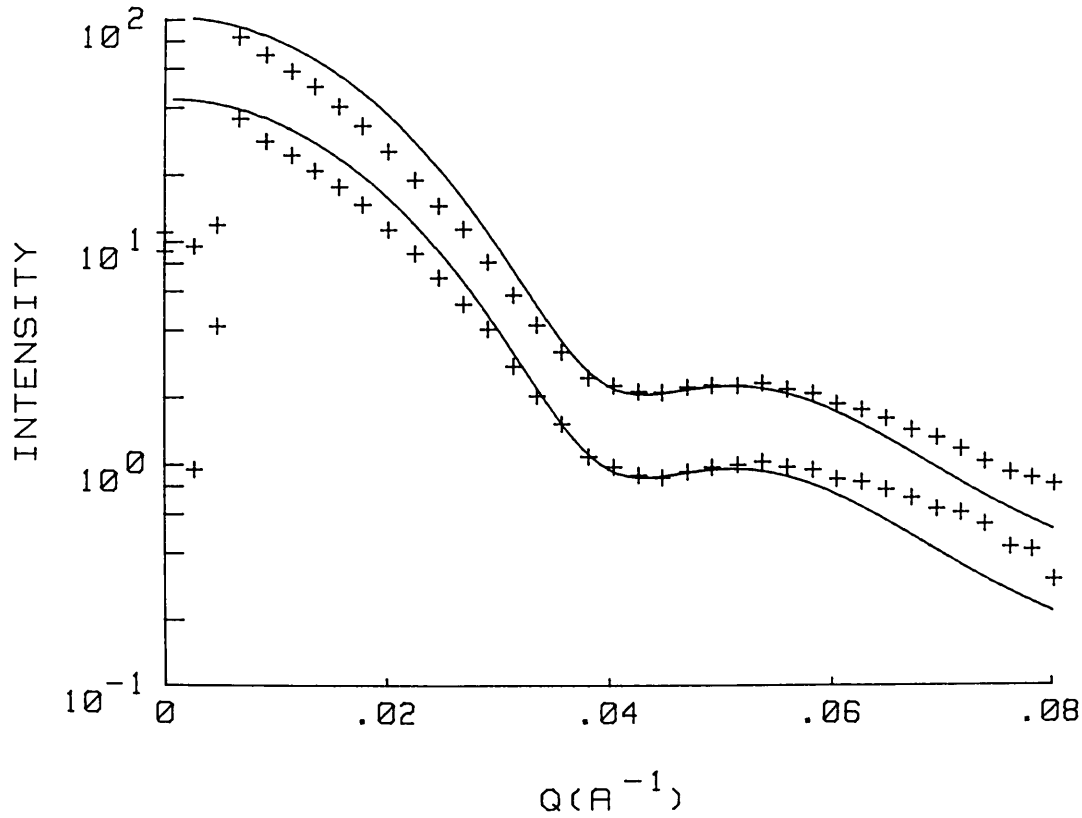


Figure 32: Neutron scattering data at high Q for polymerised vesicles, sample (3) at two concentrations (∿1% and ∿0.5%). The solid line fitted to both lines is P(Q) with the parameters; radius 90Å, thickness 40Å and h.w.h.m. 18Å in both cases.

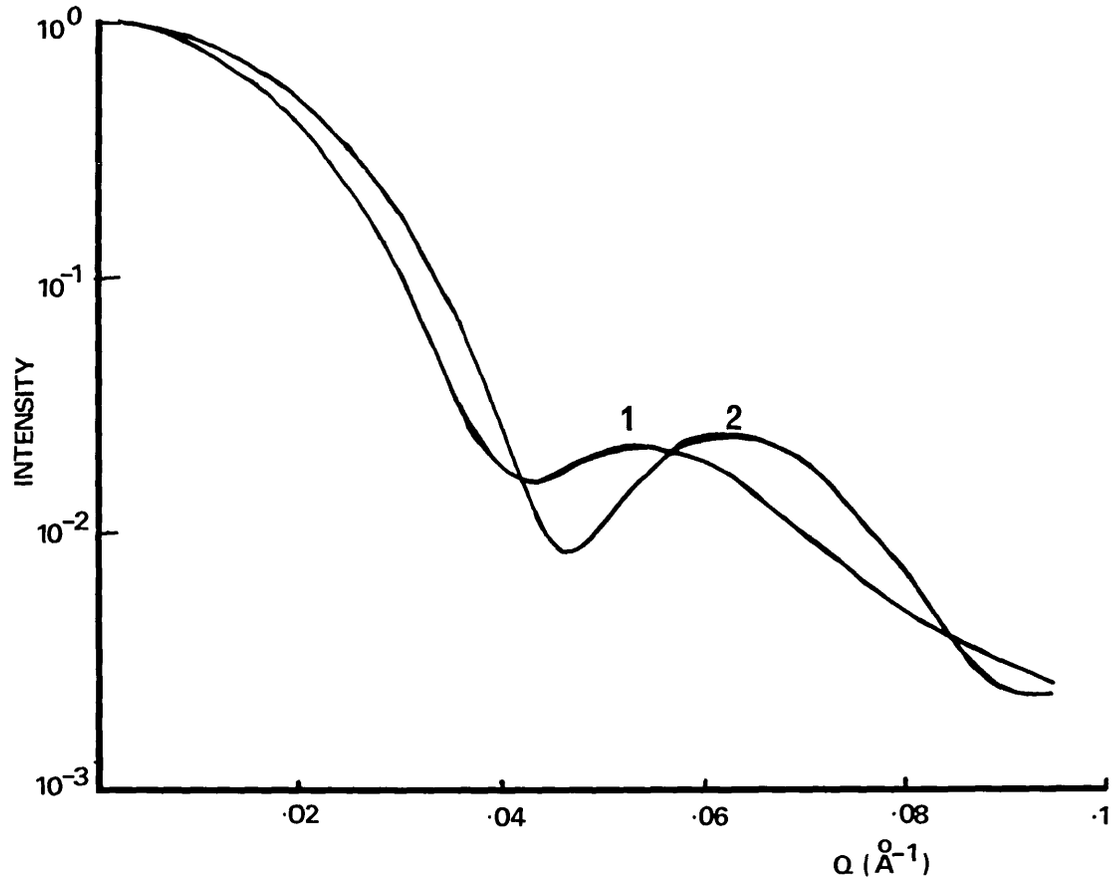


Figure 33: Theoretical model for aggregation over a long time period. The fitting parameters are in text.

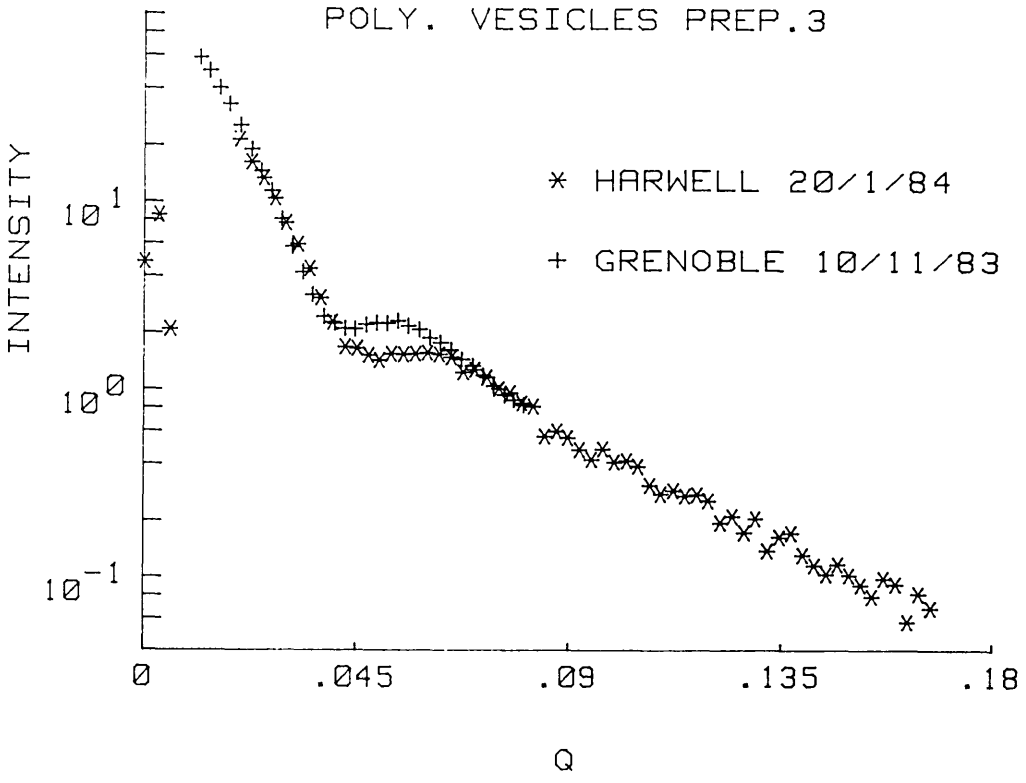


Figure 34: Neutron scattering data at high Q for polymerised vesicles, sample (3) at two time periods. The data collected at Harwell has been fitted using P(Q) with the following parameters: mean radius 85Å, thickness 40Å and h.w.h.m. 16Å (not shown).

curve with a mean radius of 85Å with HWHM of 16Å and bilayer thickness of 40Å. The change in size was due to the change in the distribution function as seen in the theoretical example.

At the Q values above $0.09Å^{-1}$ the theoretical curve deviates dramatically from the data. The high intensity in this region may be due to scattering from individual monomer chains or segments and has a Q dependence rather than the Q^4 dependence of a vesicle.

Further studies on the osmotic effects of adding aqueous soluble polymer to the vesicle dispersion were inconclusive. This may be due to the fact that the concentration of the polymer was too low or that the polymer (PEG 700) molecular weight was too small. Surfactant (C12E8) was also added to the polymerised vesicles to test their integrity, however, no change in the scattering profile was observed. We can deduce from this that the bilayer is unaffected by surfactant concentration of these levels (5%).

A sample of the gel phase (figure 35) was observed at high and low Q. At the high Q the intensity falls with Q, however, this spectra was not smooth and appears to have two inflexions, perhaps resulting from intra-particle structure. These inflexions are unusual for intra-particle structure, as, examination of the first minimum would indicate a high level of polydispersity due to an observed damped minimum. We would, however, expect no second minimum at the P(Q) to be observed at such a degree of polydispersity. As the system was highly ordered and has a potential approaching a hard sphere it is expected that the S(Q) function will have a second peak at high Q. The inflexions therefore may originate from this function. Alternatively, a combination of a peak in S(Q) and a minimum in P(Q) may have affected the first minimum in P(Q) so as to reduce its magnitude.

Earlier work on the gel phase dispersed in water using light gave particle diameters in the order of 1000-2000Å. The theoretical curve for that size particle would not fit the scattering at all well. To fit the inflexions with a P(Q) a small particle diameter (~200Å) would be required. The light scattering was dominated by large particles while the neutron scattering observes a different part of the distribution. This may account for the vastly different particle sizes obtained from PCS and neutron scattering on sample 3.

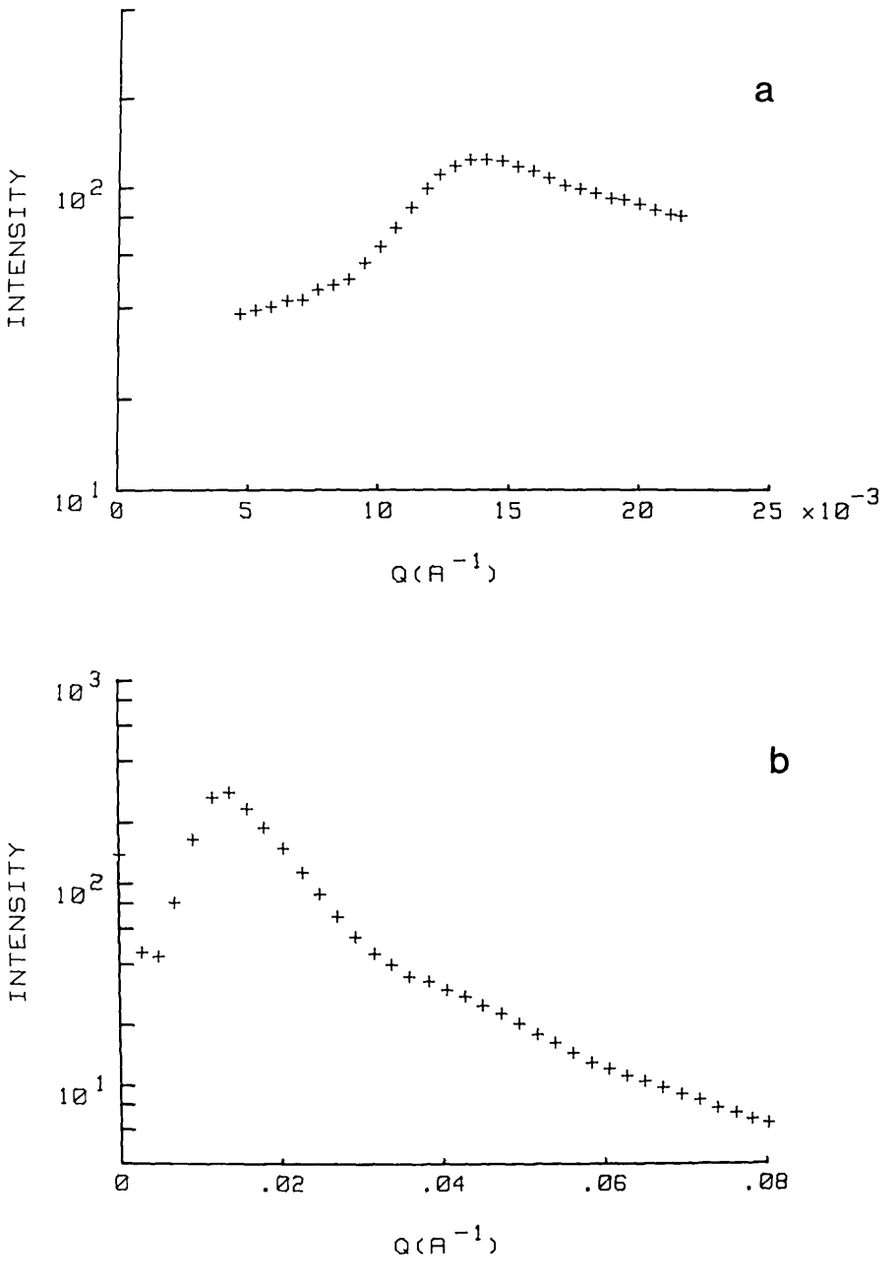


Figure 35: Neutron scattering data for the gel phase, (a) low Q, (b) high Q.

At the lower Q the spectrum is dominated by the structure factor S(Q) which relates to the inter-particle spacing of the gel. Using equation 5(4) the experimental inter-particle spacing dmax. is approximately ~550Å from the I(Q) versus Q data. This value would seem far too small for a close packed array of vesicles of diameter 1000Å. The expected peak would be at ~7 x 10^{-3}Å^{-1}. If the gel contained small particles of order ~160-200Å together with large particles of approximately ~1000-1500Å then if they packed in a regular pattern the dmax. would be of order 600Å. Calculating the Qmax gave a Q value of approximately 13 x 10^{-3}Å$^{-\pm}$ in agreement with the experimental peak. This implies that there are far more small particles than large ones and they are packed around the surface of the larger species. The unit cell associated with this geometry means that three large and eighteen small particles combine together to form the unit cell. However, the system was far too disorganised to have this sort of ordered unit cell. If the low Q range from light scattering was not available all the data could be explained in terms of small particles. Two further experiments (high and low Q) on the redispersed (dilute) gel would have solved most of the problems as the P(Q) for the dispersion could possibly have been modelled over this widest Q range.

(b) Light Scattering

Initially the polymerised vesicle samples showed similar effects to the phospholipid vesicles (chapter 5, figure 26). The effective diameter as a function of concentration, obtained by PCS, was studied over a wide range of concentration. At the high concentration (neat stock dispersion ~1%) an effective particle diameter was measured. Due to structuring at these phase volumes, this was in the order of 450Å. This order and size remained until the sample concentration was approximately 0.2%. At this concentration the effective diameter began to alter noticeably. On dilution of the original stock dispersion by a factor of 10 or 20 the actual diameter associated with the particle diffusion coefficient was measured to be 550Å. The percentage change was not so extreme with the polymerised vesicles compared to the phospholipid systems. From the absolute intensity, Zimm plots showed the typical positive slope.

In the presence of electrolyte long and short time effects were surprisingly present in the form of slow aggregation. On a short time scale, in the presence of 0.05M NaCl the effective diameter was observed simultaneously with the absolute intensity.

The effective diameter increased as if true linear aggregates were formed, i.e. a lnI against ln (effective diameter) plot had a gradient of two. Using Smoluchowski kinetics, if small particles were aggregating then an equilibrium system should occur within approximately 15 minutes. A dilute dispersion (5 x dilution of the stock dispersion) in 5 x 10^{-2}M NaCl was sampled over an extended period of approximately 48 hours. The vesicles appeared monodispersed even when observed at several available Q values. At these long time scales the lnI versus ln (effective diameter) gave a gradient of 2 initially and 6 finally. No equilibrium was reached. For a true equilibrium aggregation process the gradient should finally reach a gradient of 1. Subsequently, the sample was found to have creamed and when redispersed the system had very high multiple scattering.

Subtle changes in the electrolyte used had a marked effect on the gradient of the lnI versus ln (effective diameter). One particular sample was prepared in the presence of 0.05M NaBr. The gradient of the lnI vs ln effective plot was three which was consistent with coalesence.

(c) Discussion

From these scattering studies on the polymerised vesicles a knowledge has been acquired of the electrostatic and attractive forces between these particles and the particles integrity.

It was worth at this moment comparing the physical properties of the polymerised vesicles described in this Chapter and the phospholipid vesicles in Chapter 5. One of the striking differences was in the two systems properties on addition of electrolyte. In Chapter 5 Figure 15 it was observed at high Q that addition of electrolyte to a dilute dispersion of phospholipid vesicles had no effect on the particle integrity and the system did not aggregate over the time scale of the experiment. Whilst the addition of electrolyte to a dilute dispersion of polymerised vesicles considerably altered the particles instantaneously. The reason for these vastly different properties was probably due to the differing internal bilayer structure and different interactions between particles that these systems possess.

The second distinction between the systems was seen in the measurement of the effective diffusion coefficient. In both cases the effective diameter obtained from the diffusion coefficient was smaller than the actual diameter (dilute experiment). With these systems, as the Coulombic electrostatic forces present are not interacting over large distances, information about S(Q) cannot be obtained in this Q range (one must go to higher Q range). However, S(0) will be reflected in the effective diffusion coefficient. The larger the percentage change between the diffusion coefficient and effective diffusion coefficient the stronger the interactions in the system. The phospholipid systems (Chapter 5, figure 26) 90:10 and 95:5 reduced the effective diameter by 25% and 50% respectively on increasing the phase volume, while the reduction with the polymerised vesicles was only 20%. Therefore, the phospholipid systems are more repulsive than the polymerised vesicles system.

As with the phospholipid vesicles, the polymerised vesicle particle sizes from neutron and light scattering do not agree.

The polymerised vesicles prepared have an extended shelf life compared with phospholipid vesicles and were stable over periods tested (months). The potential forces between the particles were weak and this potential energy profile could easily be altered by the addition of electrolyte or other additives as seen in the results. Particles could then enter the primary or secondary minimum associated with irreversible or reversible aggregation respectively.

In observing the aggregation process the particles in the scattering volume remain fairly monodisperse. This was unexpected as the addition of larger aggregates should affect the diffusion coefficient. If, however, as in the long time scale experiment, creaming was occurring then in the scattering volume the particle size distribution would remain constant throughout the duration of experimental observation.

The subtlety of the potential energy barrier was illustrated by the addition of chloride co-ions. The synthetic lipid molecules had Br^- counter ions. On addition of the sodium chloride electrolyte an equilibrium was set up between the original Br^- ions and the Cl^- ions as counter ions in the diffuse double layer. For overall electroneutrality the particle could not distinguish between the two ions. The change in

the dissociation constant would cause variation in the surface charge and the area per head group which could generate the subtle slope changes that have been observed.

From the deduced shapes of the aggregates the addition of the chloride co-ions has increased the dissociation. As in the presence of chloride ions the aggregates formed were rod-like - the particles still maintained some repulsion as the particles are only in contact at one point. The electrostatic force for the dispersion in NaBr was neglible. As in the aggregates the particles were in contact with several particles. At the points of contact the surface must be neutral therefore the bromide ions are adsorbed. The reason for this counter ion effect on the aggregation was due to the size of the bromide ion compared to the chloride ion, the ion's ability to hydrate and the ions dissociation properties.

B. Osmotic Shock on Polymerised Vesicles

(a) General Background

Vesicles derived from naturally occurring phospholipids and synthetic surfactants may be prepared in the laboratory by sonicating an aqueous dispersion of the relevant molecule. It has been demonstrated that the resulting apparently spherical structures encapsulate small molecules. As a result these biologically compatible vesicles, whose overall diameters are of the order of 300-600Å, offer a potential mechanism for the delivery of drugs. Fundamental to this carrier function was the residence time of the foreign material within the membrane structure either as a bound species attached to the membrane directly or as a "free" hydrophilic molecule within the water core. These entrapped molecules may escape from the vesicle by several mechanisms including vesicle fusion, stimulated release and passive permeation. The rate of release of the molecules and ions provides a sensitive measure of the membrane permeabilities in a well-defined system. Thus the interest in these systems as model membranes.

The basic encapsulating principle simply involves the preparation of vesicles in the presence of the desired encapsulated molecules. Subsequently the solute molecules in the surrounding medium of the vesicular system are exchanged for an isotonic solution using a gel filtration technique. On exchanging the extra vesicular solution the leakage from the particle will commence.

In a neutron scattering experiment it was proposed to study the passive leakage of encapsulated "core molecules" as a function of the physical state of the lipid membrane. This state was altered by addition of structure-disrupting molecules such as detergent or protein into the membrane or in some cases, simply by varying the temperature. The rate of release of a given molecule from a specific liposome would depend on several factors, such as the size and charge of the molecule and its water/oil partition coefficient. With these factors and the requirement for scattering contrast to use deuterium labelled materials, i.e. the observed diffusing species were deuterium labelled, the study of tetramethylammonium chloride encapsulated in phosphatidylcholine-phosphatidylserine vesicles was chosen.

The deuterated material was encapsulated within the vesicle and the extra vesicular deuterated molecules exchanged for hydrogenous molecules by gel filtration. The vesicle system contained deuterated molecules inside and hydrogenous salt outside to levels of concentration such that osmotic pressure difference did not lead to membrane disruption. The time scale for D/H exchange between water and the deuterated solutes was assumed to be slow (a matter of many hours to days for the tetramethylammonium chloride when in pH >>7) so it was not envisaged that this would give rise to problems in interpretation of experimental results.

The use of deuterated included molecules and normal H_2O solvent offered a clear method of following the leakage since the signal would start as essentially that of a spherical particle from the deuterated solute in water core and would decay to virtually zero as the deuterated and hydrogenous salt concentration equilibrated.

The alternative experiment using D_2O solvent and the same salts would be more complex as a change in P(Q) from a solid to hollow spherical particle must be followed, but the intensity will not change as rapidly as in the first case.

The leakage rates would have been observed as the change in scattering cross-section I(Q) resulting from the falling contrast of the vesicle core with respect to the surrounding solvent.

This experiment was attempted with little success. However, a number of important practical problems should be noted as they have consequence in the choice of the polymeric vesicle experiment.

(b) Disadvantages

(i) Preparation of Vesicles

In the preparation of the vesicle dispersion (at the highest possible concentration of entrapped material) problems arise due to the viscosity of the dispersion.

(a) The size of unilamellar vesicles formed by sonication of aqueous dispersions of lipid was limited by the viscosity of the medium. It was found that the mean of the particle size distribution of the vesicle dispersion in a concentrated medium was larger than the mean size in a pure water solvent.

(b) Application of these viscous dispersions to gel filtration columns produced an extremely slow separation process.

(ii) Electrolyte effects

If the entrapped species was an electrolyte then at high concentration (<0.1M) the electrical double layer would be rapidly diminished. The fusion or aggregation of vesicles would occur (even with a high surface charge) during the time scale of the experiment.

(iii) Isotope effects

The hydrogenous tetramethylammonium chloride was extremely soluble in water, however, the fully deuterated isotope was poorly soluble in water. The maximum concentration of electrolyte was 0.5M which greatly reduced the inner core's contrast to neutrons.

(iv) Column Dilution

On passing through the column the concentration of the dispersion was reduced by a factor of 2. To concentrate up the dispersion would take a considerable time which would hinder the initial part of the experiment.

Mainly due to these four disadvantages and the high level of incoherent scattering from the water, measurement of initial leakage from the phospholipid vesicles was not successful.

Due to the combination of problems encountered with the early phospholipid vesicle leakage experiment it was decided that only a crude leakage experiment was possible with polymerised vesicles. Polymerised vesicles were prepared in the usual manner in deuterium oxide for the largest neutron contrast. To the dispersion concentrated hydrogenous glucose or sucrose solution was added. At this moment the vesicular system has contrast between the internal D_2O and the external sugar/D_2O solution plus an osmotic gradient between the inside and outside. This pressure will increase the rate of diffusion through the bilayer compared to a passive permeation type experiment and may force the vesicle to contract. As the system equilibrates both these factors will decrease to zero.

The question was would the polymerised vesicle be strong enough to withstand the osmotic pressures. If this was the case then the change in contrast could be observed with time. However, if the vesicle was not strong enough the particle would distort during the experiment and at the extreme it would rupture.

It must be realised that if the particle were to distort due to the osmotic gradient there would still be a contrast between inner and outer layer, but it remains to be seen if these factors are separable or whether one would dominate the scattering.

On addition of the concentrated sugar solution to the vesicular system the specimen was sampled with time and the spectra compared with the spectrum of the vesicle in the absence of added sugar. In some cases methanol was added; this incorporates into the bilayer and should affect the permeability.

(c) Neutron Scattering

(i) Characterisation of the dispersion

Using sample G2, (ca 1% wt) which NMR measurements had confirmed as polymerised, the initial experiment was performed on the system without additives but at an eight times dilution. This dilution ensured that the vesicles were non-interacting. In Figure 36 the spectrum (plot lnI versus Q) was fitted with two Gaussian distributions close together, which simulates a Schulzian type distribution, the fitting parameters were, smaller radius 190Å, HWHM 50Å and larger radius 330Å, HWHM 100Å. In both distributions the bilayer thickness was assumed to be 40Å. The intercept I(0) was 150 and the ratio of large particles to small particles was 1100. The number distribution associated with these parameters was shown in Figure 37.

The resulting pseudo-bimodal distribution was only a means of producing a distribution that was broad and slightly skewed towards the larger particles. Variation of the radius and half width of half maximum of these two Gaussian distributions and their ratio was inconsequential to the quality of the actual fit. The distribution could easily be a continuous function as indicated by the dotted line joining the peaks in Figure 37.

The particle size distribution obtained from the modelling of the scattering data was the first time a broad complex distribution has been resolved in this manner. However, if additional data were collected and fitted over a wider Q range this would have further substantiated the model particle size distribution used. This spectrum was extremely important as all the further osmotic shock and subsequent leakage experiments described were compared to this spectrum as it was at equilibrium.

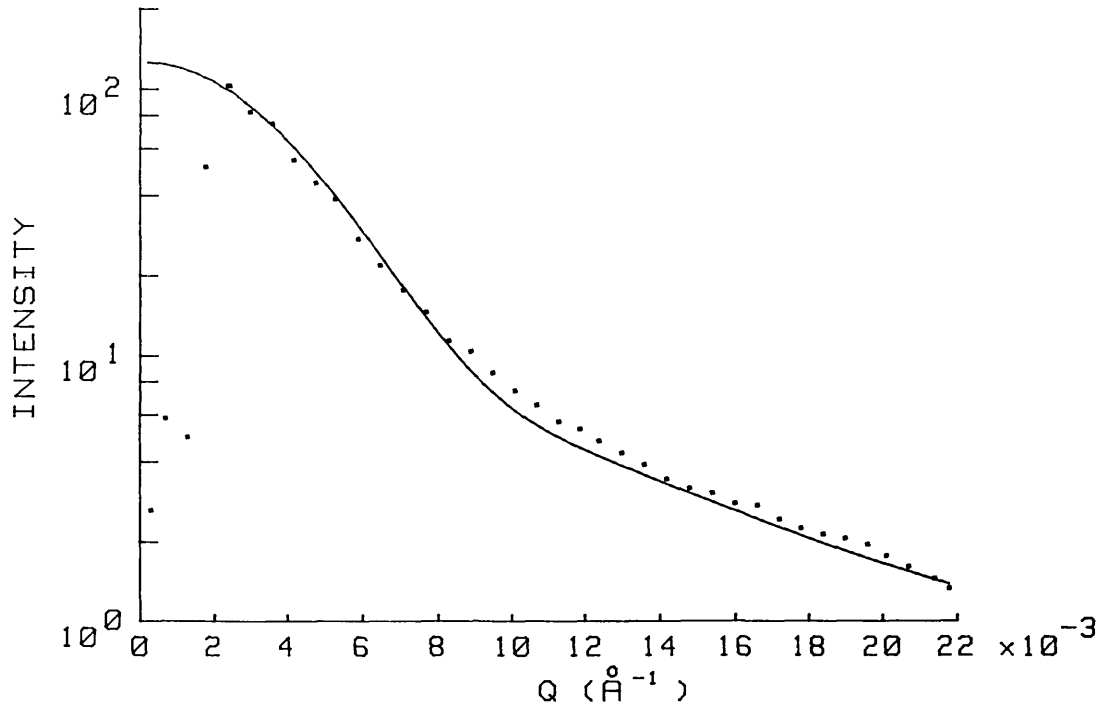


Figure 36: Neutron scattering data for sample G2 polymerised vesicles modelled by P(Q) with parameters described in text.

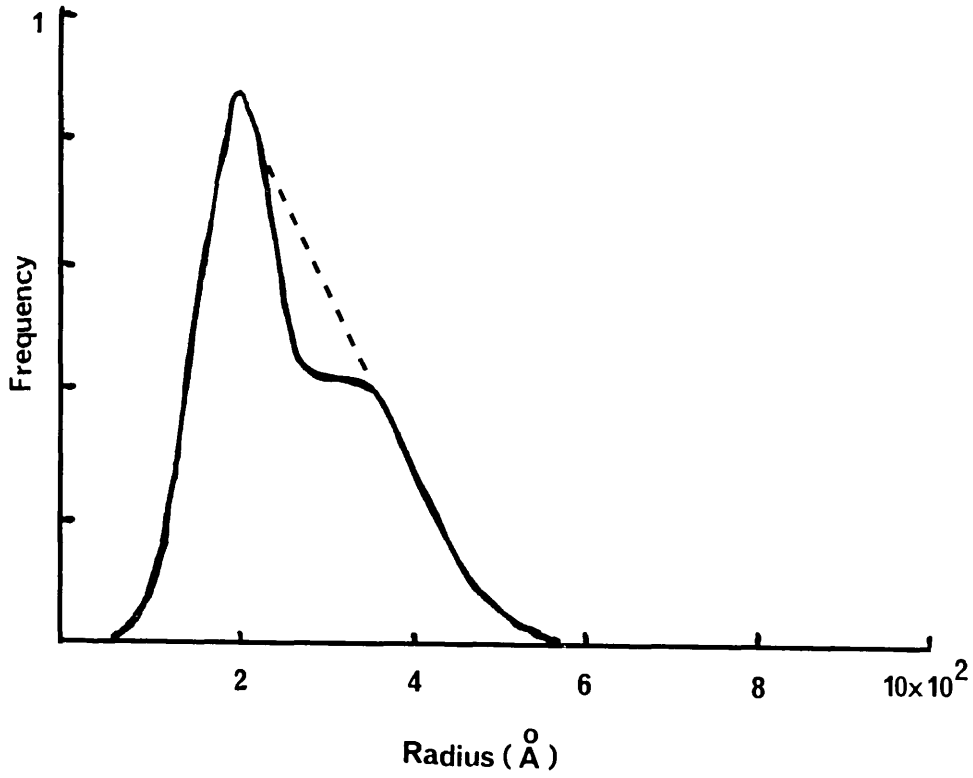


Figure 37: Particle size distribution for sample G2 obtained from the model P(Q) used to fit the data in figure 36.

(ii) Sucrose

10% Sucrose (0.3M)

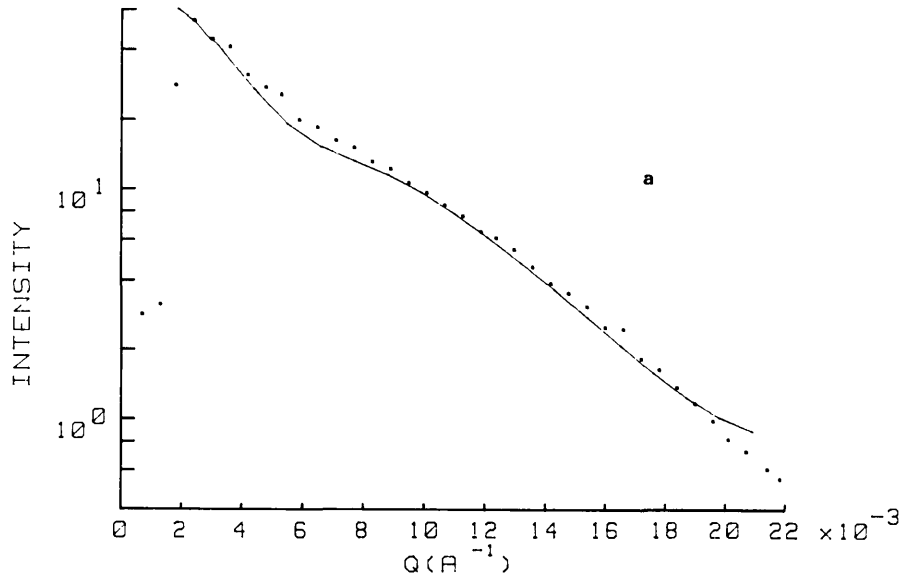
On addition of 10% sucrose the scattering curve changed shape dramatically (as seen in Figure 38). From this dramatic change in scattering profile the idea of only the contrast change affecting the scattering profile can be ruled out. It can be assumed that the vesicles have contracted or distorted to an average smaller radius and that this distortion dominates the scattering spectra. An attempt to fit the data collected within the first few minutes of the experiment with the same double Gaussian distribution as figure 38a gave a reasonable fit with the parameters small radius 154Å, HWHM 40Å and larger radius 400Å, HWHM 130Å the I(0) intercept was 77 and ratio of large particle to small particles was now 100.

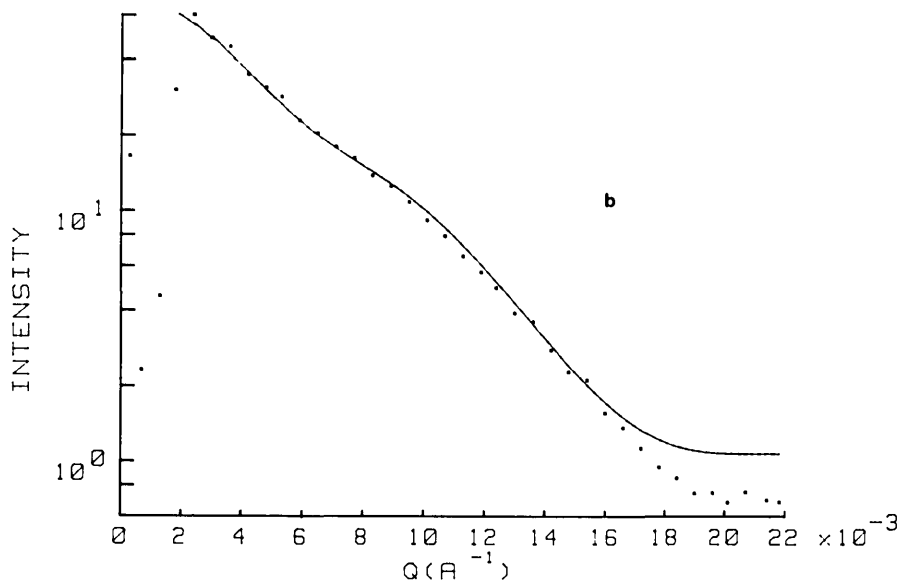
Table 5: Fitting parameters used to model the data over the time course: 10% sucrose addition to G2 polymerised vesicles.

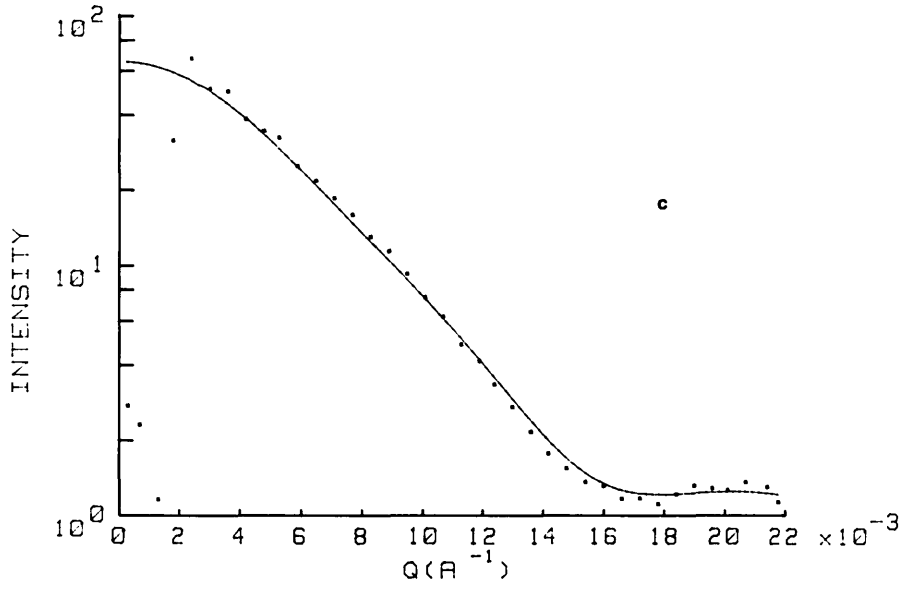
		Fitting Parameters					
Run No.	Time	Rad_1(Å)	HW	Rad_2(Å)	HW	Ratio 1/2 (a)	*Factor (b)
7490	4 mins	154	40	400	130	100	77.4
7492	15 mins	170	44	400	100	100	70.4
7494	26 mins	185	43	350	100	100	55.6
7496	37 mins	195	44	300	100	100	50.0
7498	49 mins	200	45	300	57	150	50.5
7468	9½ hrs	170	50	300	69	4000	81.8
7447	48 hrs	175	50	300	100	1500	112.0

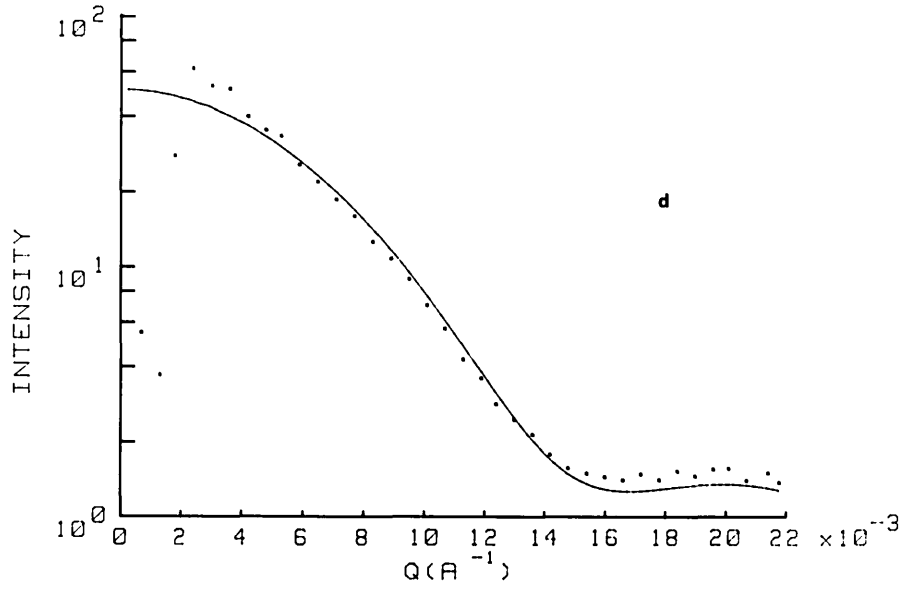
(a) The ratio 1/2 was the ratio of material in the two distributions
(b) *Factor was the factor the model had to be multiplied by the fit the data.

It can be assumed that the vesicles have contracted or distorted to an average smaller radius. The early stages of the leakage were observed in detail at approximately eleven minute intervals. As time progressed the fitted distribution moved to a high mean radius as the data moved to


a
INTENSITY
10^1
10^0
0 2 4 6 8 10 12 14 16 18 20 22 $\times 10^{-3}$
Q(Å $^{-1}$)


b
INTENSITY
10^1
10^0
0 2 4 6 8 10 12 14 16 18 20 22 $\times 10^{-3}$
Q(Å $^{-1}$)


INTENSITY
10^2
10^1
10^0
0 2 4 6 8 10 12 14 16 18 20 22 $\times 10^{-3}$
Q(A $^{-1}$)
c


INTENSITY
10^2
10^1
10^0
0 2 4 6 8 10 12 14 16 18 20 22 $\times 10^{-3}$
Q(A $^{-1}$)
d

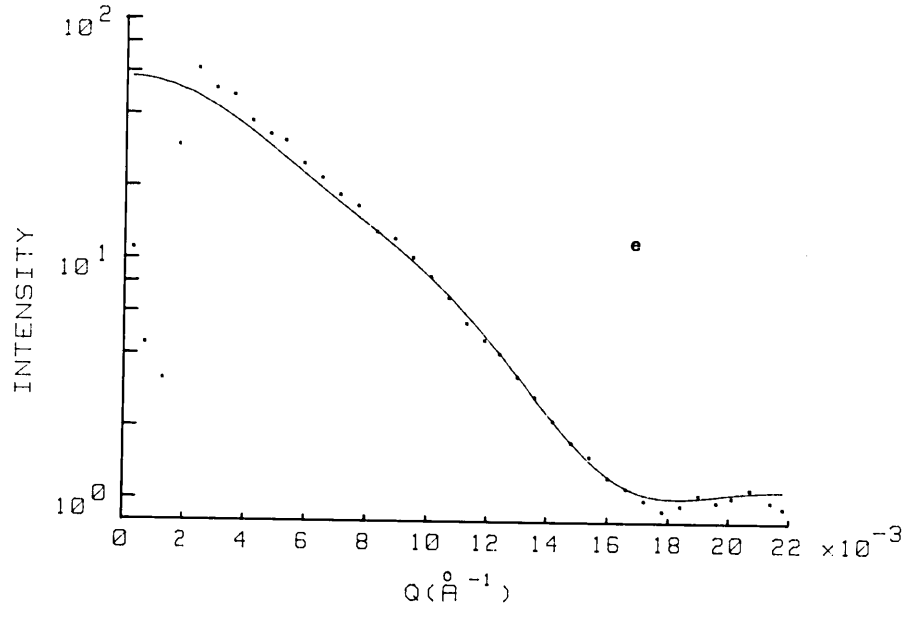


Figure 38: Neutron scattering data for sample G2 on addition of 10% sucrose over a time course. The fitting parameters are described in table 5. (a) 4 mins, (b) 15 mins, (c) 26 mins, (d) 37 mins, (e) 49 mins.

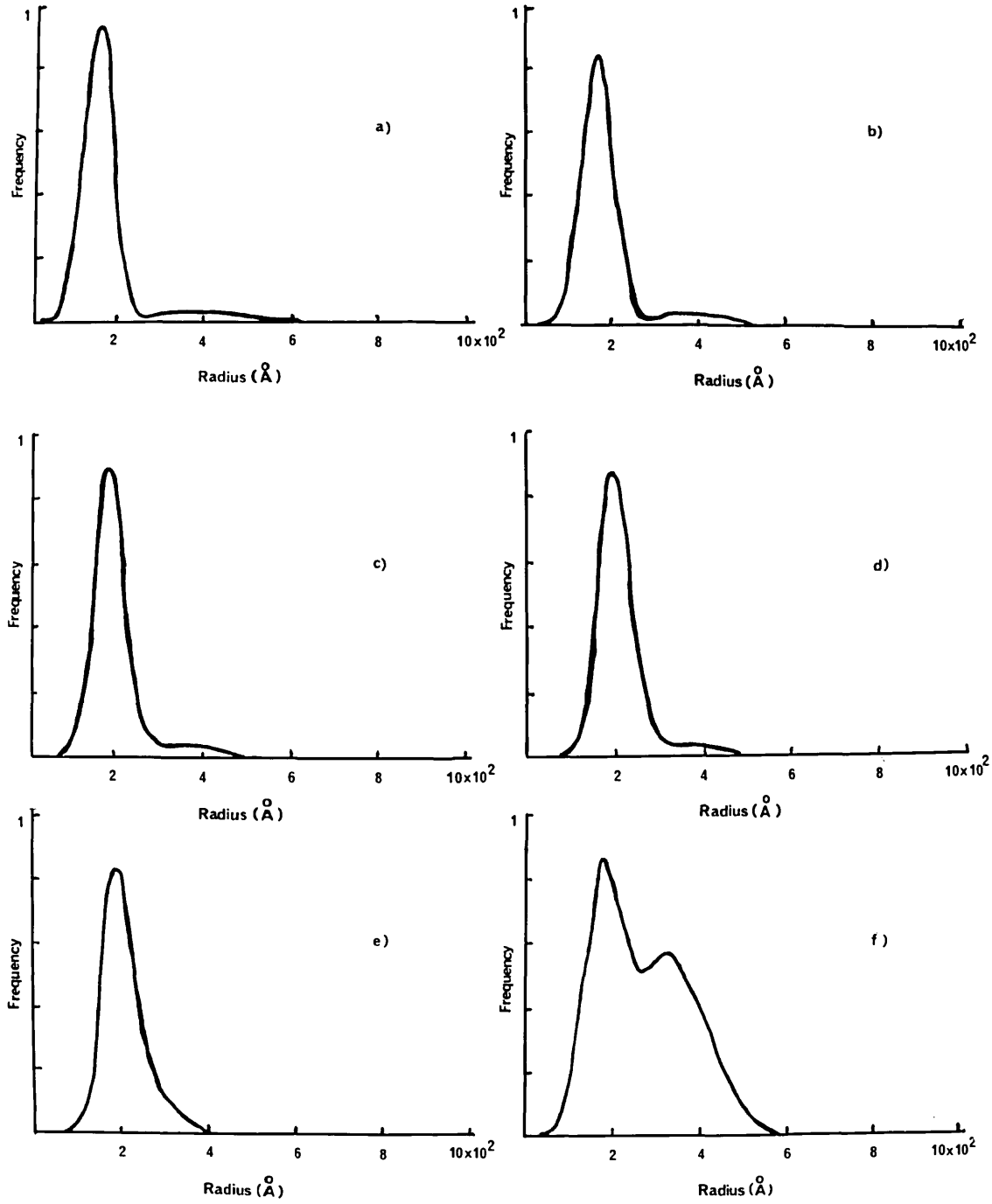


Figure 39: Particle size distribution for sample G2 in the presence of 10% sucrose obtained from the fits to the data in figure 38. (a) 4 mins, (b) 15 mins, (c) 26 mins, (d) 37 mins, (4) 49 mins, (f) 48 hours.

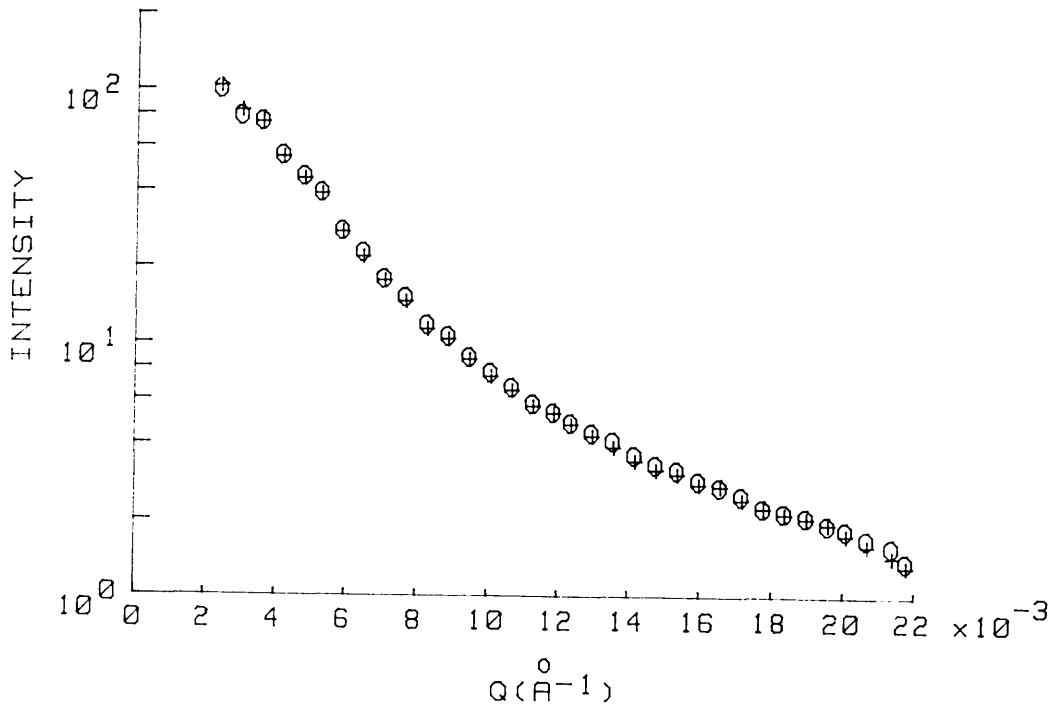


Figure 40: Comparison of the sample G2 (+) and the 10% sucrose at equilibrium after 48 hours (o). The spectra were normalised together at the tenth data point.

lower Q. After two hours the system had not reached equilibrium. Table 5 indicates the apparent shift in the fitting parameter to the data while figure 38 shows the quality of the fits. A further means of representing the shift was to actually produce the distributions (Figure 39) associated with the fits. It must be recognised that the table of the fitting parameters and reconstruction of the distribution are the only ways of explaining and displaying the data at the present time. After 9½ hours the scattering curve was identical within experimental error to that for a 48 hour old sample. Comparison of both these spectra with that for the standard vesicle (G2) without additive showed them to be almost identical in shape. In figure 40 sample G2 and 7447 (the 48 hour sample) are compared, the spectra has been normalised at the tenth point by multiplying the sucrose data by 1.23 to take into account the scattering length density of 10% sucrose. One can assume from this that the leakage has reached equilibrium and the vesicles have survived radical distortion and returned to the original distribution. As expected the I(0) for the two equilibrated systems was not identical, as scattering length density of 10% sucrose solution (D_2O) is very different from that of pure D_2O.

30% Sucrose (0.88M)

In the vesicular system with 30% sucrose the scattering profile dramatically changes on addition of the concentrated stock sucrose. The scattering curve collected at 4 minutes was modelled with a P(Q) convoluted with a distribution of 140Å smaller radius and 300Å large radius with HWHM of 50Å and 100Å respectively. The ratio of the number of particles in these Gaussian distribution was 120. Due to the higher osmotic pressure applied on the vesicles the initial mean particle diameter was approximately 14Å smaller than the initial mean diameter in the vesicular disperion in 10% sucrose. Table 6 shows the fit parameters data (not shown). As the 30% sucrose experiment did not extend through the long time scales, equilibrium was not observed.

However, it would seem logical to assume that the 30% sucrose would take longer to equilibrate than the 10% sucrose system. At 2½ hours the specimen was observed and fitting the scattering spectrum with the same model indicated that a shift to a larger mean radius was still occurring similar to the 10% sucrose sample at this time scale.

Table 6: Fitting parameter used to model the data over the time course: 30% sucrose addition to G2 polymerised vesicles.

Run No.	Time	Fitting Parameter Rad_1(Å)	HW	Rad_2(Å)	HW	Ratio 1/2 (a)	* (b)
7491	4 mins	140	30	350	112	120	43
7493	15 mins	150	38	350	87	130	37
7495	26 mins	170	40	300	90	100	32
7497	37 mins	170	30	300	96	250	37
7499	49 mins	175	48	350	83	100	35
7513	2 hrs, 16 mins	200	60	350	86	75	40

(a) and (b) as in table 5.

(iii) Glucose

The osmotic pressure in the system was increased by changing the diffusing species. Glucose was chosen because of its similar chemical nature to sucrose. However, the molecule was very much smaller. Identical experiments were performed by addition of concentrated stock solution of glucose to the vesicle dispersion.

Glucose 10% (0.56M)

After addition of the glucose stock solution the specimen was sampled with time. The first spectrum which was completed 4-5 minutes after addition of glucose. The data was fitted to the P(Q) model with the parameters smaller radius 195Å and larger radius 300Å and the ratio of big to small was 200. The size distribution was unexpected as the osmotic pressure on the vesicles was greater than the osmotic pressure on the 10% sucrose therefore it was expected to contract to a smaller size. The implication from this result was that the particles do contract very much smaller than the measured value, but the time lag between addition of the glucose and measurement, enables the vesicle to recover slightly from the osmotic shock. As the higher the osmotic pressure the diffusion of molecules through the membrane would be enhanced. Within half an hour the sample had reached equilibrium. In table 7 the details of the particle size distribution convoluted with the P(Q) model used to fit the data are displayed.

Table 7: Fitting parameters used to model the data over the time course: 10% glucose addition to G2 polymerised vesicles.

Run No.	Time	Rad_1(Å)	HW	Rad_2(Å)	HW	Ratio 1/2 (a)	* (b)
7519	4 mins	195	53	300	96	200	61
7521	15 mins	200	60	250	67	2000	75
7523	26 mins	220	56	280	80	500	70
7525	37 mins	150	37	300	60	2000	85
7527	49 mins	150	40	300	60	2000	75
7557	251 mins	280	62	330	100	500	85

(a) and (b) as in table 5.

Table 8: Fitting parameters used to model the data over the time course: 30% glucose addition to G2 polymerised vesicles.

Run No.	Time	Rad_1(Å)	HW	Rad_2(Å)	HW	Ratio 1/2 (a)	* (b)
7520	4 mins	170	45	400	150	150	56
7522	15 mins	190	54	400	130	100	50
7524	26 mins	200	60	400	130	100	55
7526	37 mins	210	50	350	114	200	31
7528	49 mins	220	70	350	120	120	55
7558	250 mins	160	45	290	73	2000	55

(a) and (b) as in table 5.

30% Glucose

The first scattering profile was fitted to the P(Q) model with the parameters smaller radius 170Å and larger radius 400Å with the ratio big to small of 150 (as in all the bimodal fits the thickness was assumed to be 40Å and HWHM of both gaussian distribution were broad).

This concentration of added glucose has imposed the largest osmotic pressure on the vesicles and it would be expected to contract the vesicle the most, which would be seen in the scattering profile. However, as in the 10% glucose experiment, a leakage of exponential nature had to some extent occurred and the sample was well on the way to returning to the original distribution by the time data of sufficient statistical significance had been collected on the first sample.

Due to the size of the diffusing species (glucose) and the high osmotic pressure the leakage in the glucose experiment occurred extremely rapidly. There was only a small change in the fitting parameters with the first four to five experiments (see table 8) and the spectra were almost identical. There was a detectable difference between the first five spectra and the data collected at 7 hours. This set of data should have been better collected over longer time intervals, as the leakage (if exponential) had mainly occurred after the first few minutes and the particle was compressed to its minimum then relaxed back to the observed diameter after 4 minutes. From 4 minutes to equilibrium the leakage would have been slow. The equilibrium was reached within 7 hours as the curve was then identical to that of G2.

(iv) Incorporation of methanol in bilayer

The effect of methanol or ethanol on unpolymersied vesicles was studied in a simple and easy additional experiment. The co-solvent acts as a disrupting agent. The effect on the scattering profile of an unpolymerised dispersion (G4) on addition of the alcohol (methanol-deutrated) was that instantaneously the intensity was strikingly reduced in the Q range observed. Methanol disrupts the membrane and vesicle. Methanol had no effect on the polymerised vesicles, however, as demonstrated by an experiment in which the polymerised vesicles had 10% methanol added as co-solvent and then a similar leakage experiment observed the vesicles reach an equilibrium exceedingly fast (within minutes). The methanol molecule incorporation into the membrane affects the permeability of the vesicle.

Table 9: Fitting parameters used to model the data over the time course: 10% sucrose addition to G2 polymerised vesicles in the presence of 10% methanol.

		Fitting Parameters					
Run No.	Time	Rad_1(Å)	HW	Rad_2(Å)	HW	Ratio 1/2 (a)	* (b)
7502	4 mins	200	62	270	82	2500	70
7504	15 mins	175	48	320	75	1000	81
7506	26 mins	175	48	310	100	900	78
7508	37 mins	175	48	310	100	1000	78
7510	49 mins	200	58	360	100	600	115

(a) and (b) as in table 5.

Table 10: Fitting parameters used to model the data over the time course: 30% sucrose addition to G2 polymerised vesicles in the presence of 10% methanol.

		Fitting Parameters					
Run No.	Time	Rad_1(Å)	HW	Rad_2(Å)	HW	Ratio 1/2 (a)	* (b)
7503	4 mins	150	41	310	70	1000	50
7505	15 mins	170	50	320	100	1000	57
7507	26 mins	170	50	320	100	1000	59
7509	37 mins	170	50	320	100	1000	59
7511	49 mins	170	50	320	100	1000	59
7530	145 mins	190	55	330	100	800	60

(a) and (b) as in table 5.

Tables 9 and 10 show the fitting parameters used to model the data collected with 10% methanol added, with 10% and 30% sucrose respectively. The systems reach equilibrium extremely fast. For 10% sucrose, the vesicles had probably reached equilibrium in 15-20 minutes, while the 30% sucrose system definitely reached equilibrium at 15 minutes.

(v) Conclusions

For all the leakage experiments on sucrose and glucose at various concentrations the overall results were similar, i.e. a dramatic change in the observed scattering profile. If the profile was followed over a period of time there was found to be good agreement between the modelled distribution and the static sample (G2) at equilibrium.

The incorporation of methanol into the 10% and 30% sucrose system leads to equilibrium being rapidly achieved compared to the situations where methanol was absent. It may be assumed that methanol makes the membrane more permeable, by its incorporation into the membrane or by some other means.

The trends in the leakage rates are as follows:-

Methanol incorporated systems > 10% Glucose > 30% Glucose > 10% Sucrose > 30% Sucrose

It was originally assumed that the glucose systems, which had the largest applied osmotic gradient, would contract to the smallest diameter. This was not observed. Although the initial information on these systems was inaccessible the overall time to equilibrate was most important. This lack of information on the lag time between the addition of the sucrose or glucose and the measurement will apply to all of the systems studied, but was most extreme and detectable in the systems with the greatest osmotic pressure or the most permeable membranes (methanol added).

The particle size distributions which are convoluted with the shell particle-form factor are complex and model the data quite closely. In the modelling of the static G2 sample it was found that the distribution used could be altered fairly harshly but still gave a reasonable fit. If one assumes that the G2 particle size distribution was correct, then on applying the osmotic pressure to the system the vesicle will contract probably to non-spherical shaped vesicles. However, the data were still modelled with the same P(Q). Further, one would assume if vesicles remain intact then the dispersion would become more polydisperse on contraction. This was not the case - the dispersion became more monodisperse on contraction.

Finally, the most important unresolved problem was the fact that if the vesicles do contract, then the mass of lipid needed to produce a vesicle of 140nm diameter was far less than the amount of material in a 300nm diameter vesicle. Where did this material go? As the vesicles were polymerised the lipid cannot transfer or form another particle. These two problems will remain unresolved until a different rationale to describe these data is hypothesised.

CHAPTER 7 - VISCOELASTIC MICELLAR SOLUTION: A STUDY OF THE TRANSITION FROM ROD-LIKE TO SPHERICAL MICELLE

(1) Introduction

As the composition of a micellar solution approaches the liquid crystal phase boundary a significant change in the viscosity is often observed. It is thought that this property can be assigned to long range order or a network structure since in some cases the solution can become viscoelastic. It may be that at these concentrations the micelles change shape and convert to rod-like structures, however, it is not always true that elastic properties are a consequence of the existence of such rod-like particles. Conversely, it has been shown that some rod-like micelles do not have the property of viscoelasticity (139). At much higher concentrations these rod-like micelles may be arranged in a hexagonal array forming the hexagonal liquid crystalline phase.

The transition between viscoelastic and Newtonian behaviour (sphere-rod transition) has been measured in numerous ways. These include conductivity, electric binefringence, pressure jump, shock wave techniques, T-jump, static and dynamic light scattering and finally rheological measurements (140-147).

In this chapter small angle neutron scattering was used to study this transition in a mixed micellar system of sodium dodecyl sulphate (SDS) and tetradecyl-dimethyl ammonio propane sulphonate (TDPS) (148-150). A simplified three dimensional phase diagram of the system is seen in Figure 41. The micellar (M), viscoelastic (VE), liquid and liquid crystalline (L + LC) and the liquid crystalline (LC) phases are indicated. The phase boundaries of these regions are marked as lines A, B and C.

The two main structural parameters associated with a rod-like micelle are the radius of the rod end and its length (L). The L-values can be determined from elastic binefringence and viscosity measurements (142, 144). In both cases the L-values obtained are only strictly valid for stiff non-interacting rods. Calculation of the Debye screening lengths for the types of systems studied here gave values in the order of 100Å or more. So, on top of the structural parameters is an electrostatic interaction which extends considerable distances. The size of the rods is dependent on the concentration of surfactant and salt concentration so it is not possible to suppress the interactions.

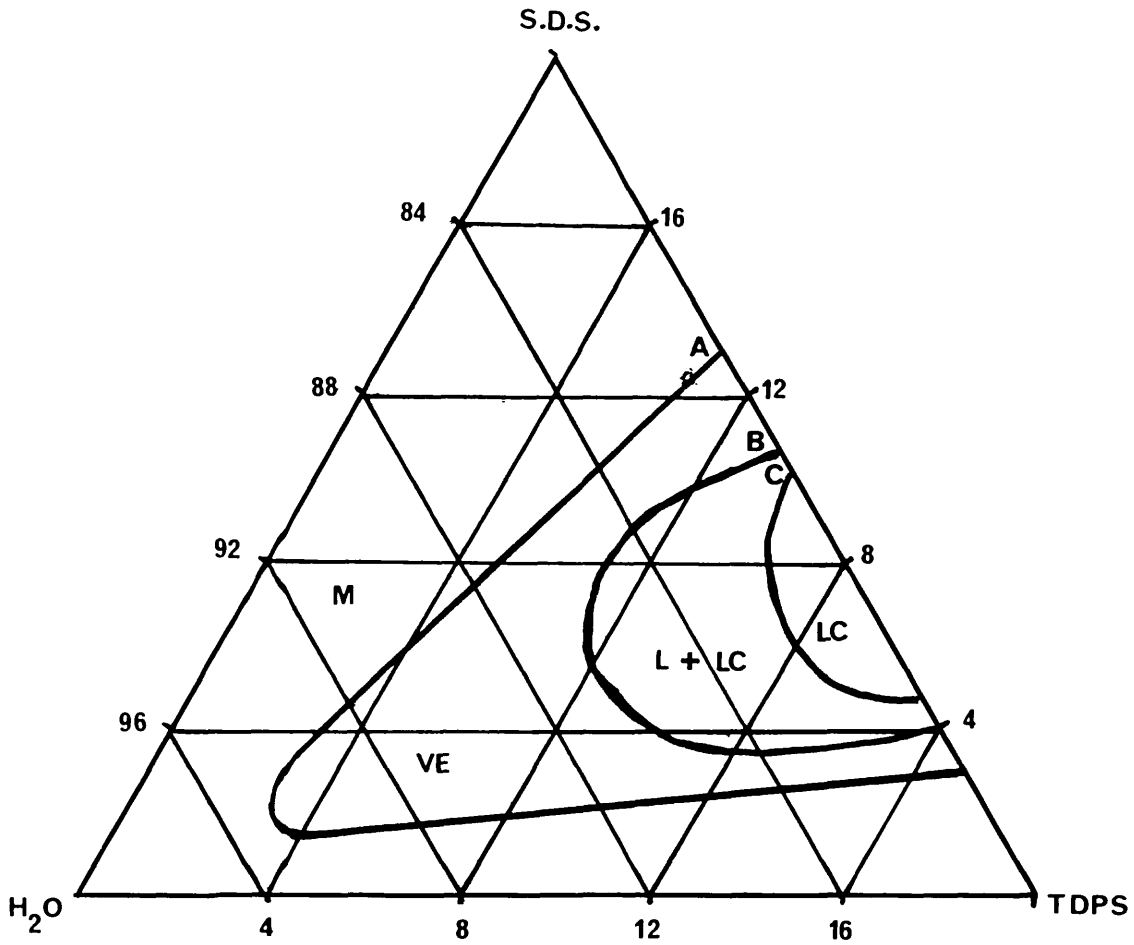
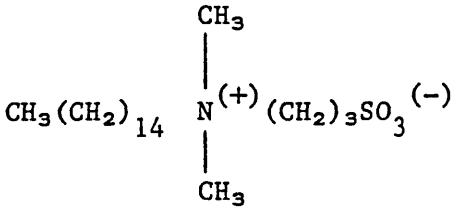


Figure 41: The three dimensional phase diagram for SDS/TDPS/H_2O system: Micellar (M), viscoelastic (VE), liquid and liquid crystalline (L + LC) and liquid crystalline (LC). A,B and C are phase boundaries.

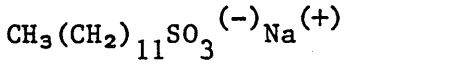
(2) Experimental

The mixed micellar solution consisted of two surfactants; tetradecyl dimethyl ammonio propane sulphonate (TDPS) I



I

and sodium dodecyl sulphate (SDS) II



II

The solutions were prepared by dissolving TDPS in D_2O then adding SDS to this solution. Finally, a remaining volume of D_2O was added to make up the correct weight percentage. This was done to eliminate any order of mixing disparities. The solution was equilibriated at 60°C for approximately 30 minutes and then at room temperature for generally a period of about 2 days.

Samples were prepared with one of the components at constant weight percentage. Five lines of interest were investigated. The samples numbering system and lines along which the actual weight percentage of the components were tabulated in table 11 and shown in the phase diagram in figure 42.

Table 11: Sample Preparations

Samples	Line No.	TDPS	wt % SDS	H_2O*
1	1	5.73	0.48	93.8
2		5.74	0.95	93.3
3		5.75	1.90	92.3
4		5.75	2.38	91.9
11	3	5.23	0.48	94.3
12		4.80	0.90	94.3
13		4.30	1.40	94.3
14		3.80	1.90	94.2
15		3.30	2.50	94.2
16		2.90	3.00	94.1
17		2.40	3.40	94.2
18		1.90	3.80	94.2
32	2	-	5.99	94.0
19		3.8	0.48	95.7
20		3.8	0.99	95.2
21		3.8	1.50	94.7
(14)		-	-	-
22	4	7.40	0.50	92.10
23		7.00	1.05	92.0
24		6.50	1.50	92.0
25(3)		6.00	2.00	92.0
26		5.50	2.50	92.0
27		5.03	2.90	92.1
28		4.01	3.96	92.0
29		2.89	5.11	92.0
30		1.99	5.97	92.0
40		1.50	6.7	91.9
39		0.92	6.9	92.2
38		0.49	7.7	91.8
31		-	8.00	92.0
42	5	0.5	-	99.5
41		1.0	-	99.0
36		2.0	-	98.0
35		4.0	-	96.0
33		5.9	-	94.1
34		8.0	-	92.0
37		9.9	-	90.1

*equivalent % H_2O of the quantity of D_2O added.

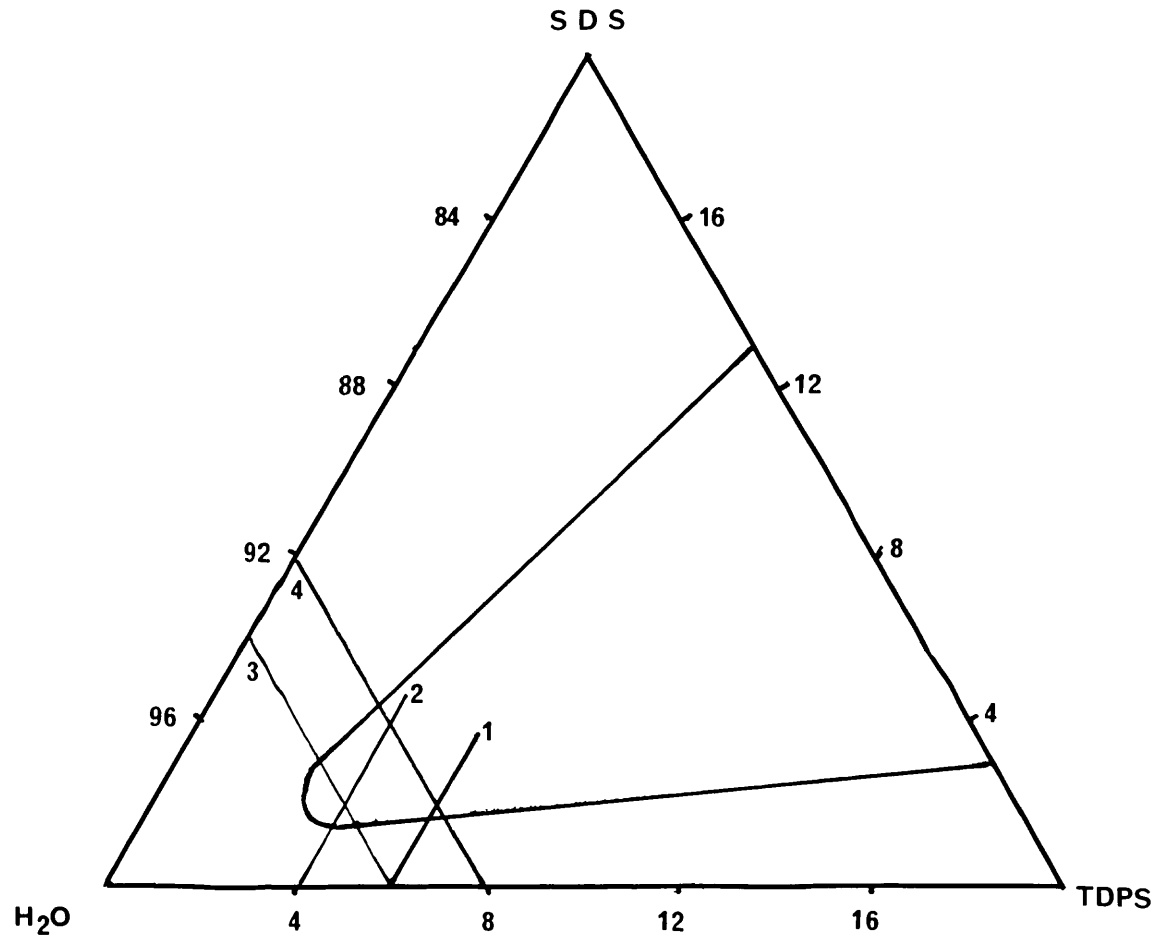


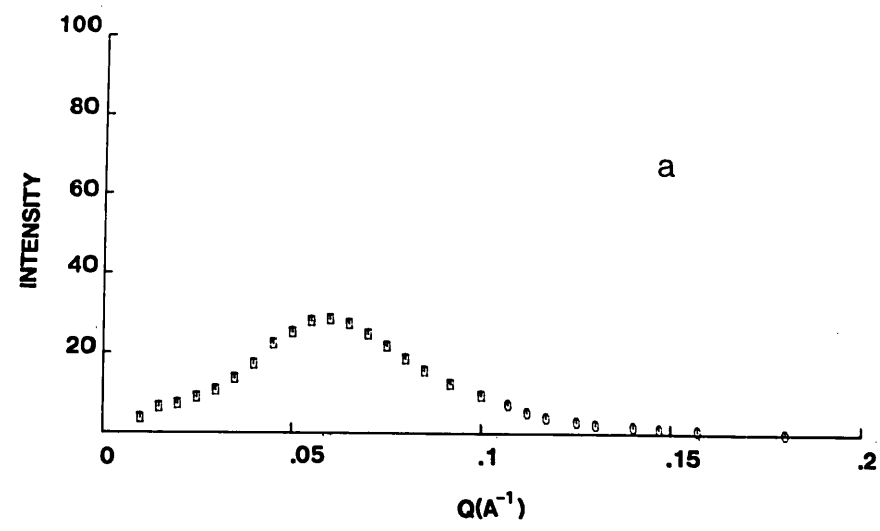
Figure 42: Phase diagram showing where data had been collected on lines 1-4.

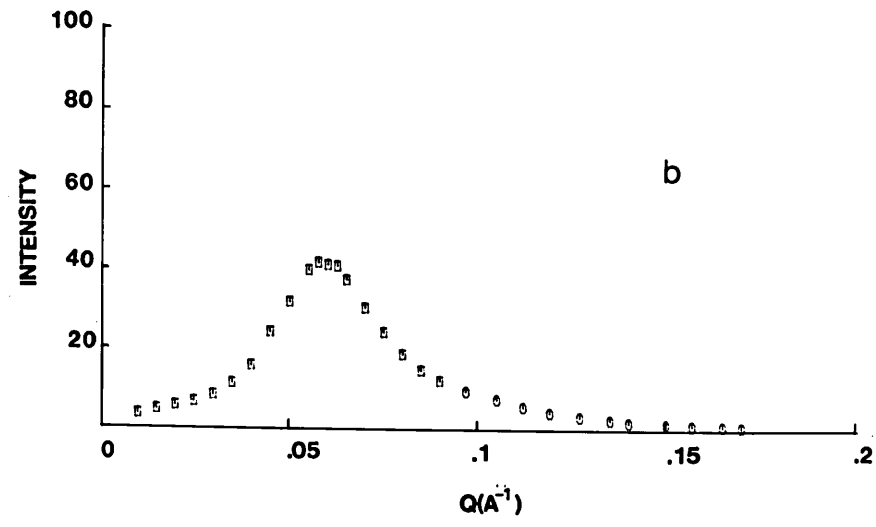
(3) Results

The samples were prepared with constant weight percentage of one of the three components (2 surfactants and water). Samples prepared on lines 1 and 2 had constant weight percentages of TDPS of 6% and 4% respectively, where the ratio of the other two components were varied (figure 41). Samples on lines 3 and 4 respectively had a constant 94 and 92 weight percentage of water and again the ratio of the other two components was varied.

In the description only the spectra on lines 1 and 3 will be discussed in depth as the other two lines 2 and 4 show exactly the same trends. The spectra and spectral parameters of these lines will be shown in graphical form. Along line 1, constant 6% (wt%) TDPS composition, four samples were examined. The SDS composition in these samples increased from 0.5% to 2.5%. The scattering spectra compared as a set are readily described and are shown in Figure 43. At low SDS concentration the spectrum was broad with low intensity at the peak position (Figure 42a). As the SDS concentration increases the peak sharpens and moves to lower Q values while the intensity at the peak position increases (figures 42b, c and d). The spectral parameters were separated into four measurable quantities, the intensity at the position of the peak, the value of Q associated with the interparticle spacing (Qmax), the area under the scattering curve and the half width at half maximum of the peak. Figure 44 shows all these features graphically. Theoretically the area under the curve should be constant if the scattering mass remains constant and the number of particles remains the same. This was not the case. Due to the limited Q range observed, power was moving into this region from outside the spectral limits.

As the system enters the viscoelastic region the solution appeared to become more "crystalline" or "ordered" and was readily observed in the neutron scattering data. Although the parameters from each spectra show the trend to a more ordered solution the main evidence was in the shape of the intensity against wave vector plot where apart from the sharp first peak, which represents the first nearest neighbour distance (~126Å), there was a shoulder which may be the second peak in the S(Q) function.


100
80
60
40
20
INTENSITY
a
0
.05
.1
.15
.2
Q(A^{-1})


100
80
60
40
20
INTENSITY
b
0
.05
.1
.15
.2
Q(A^{-1})

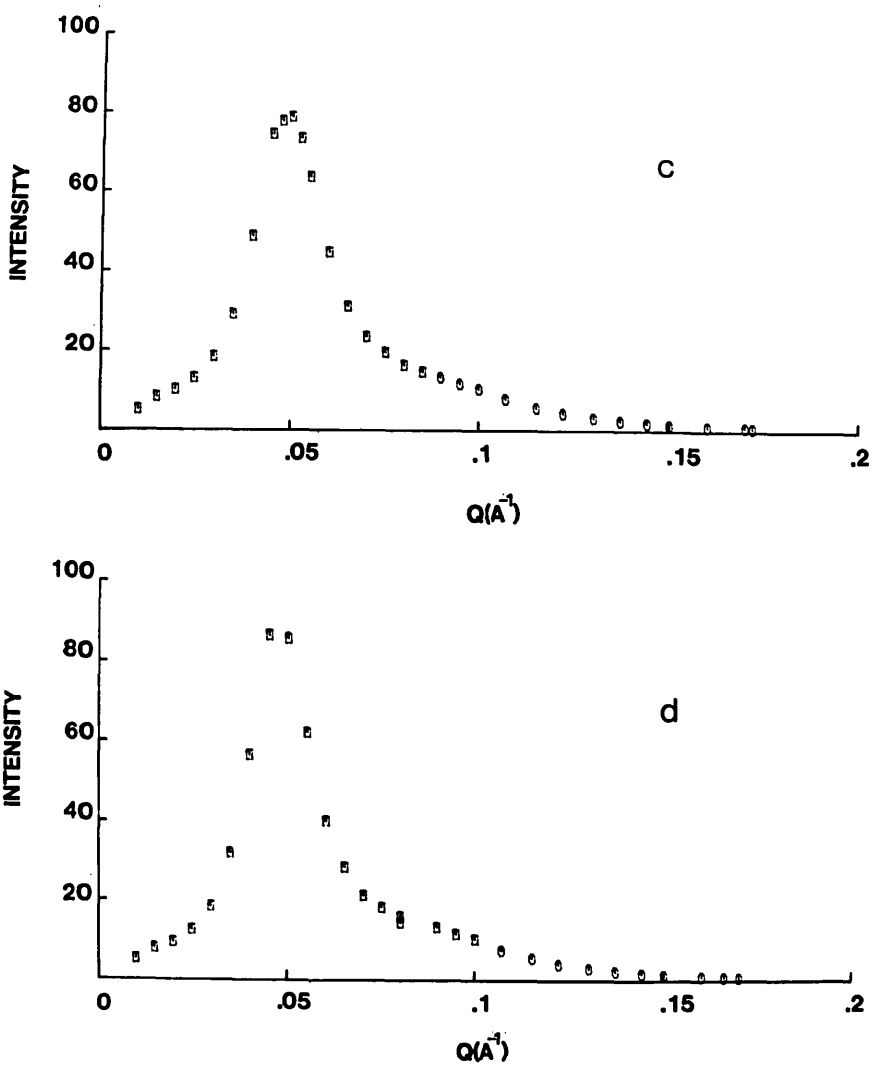
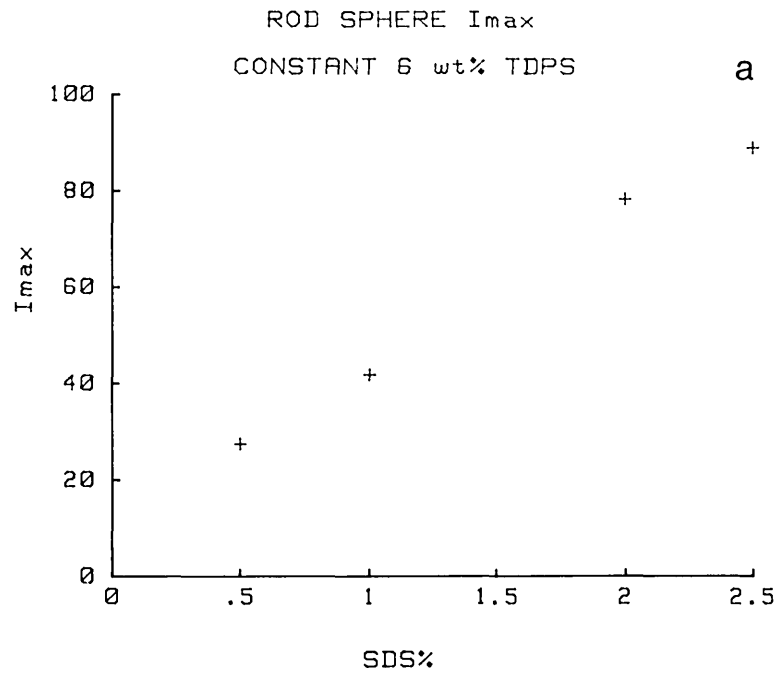
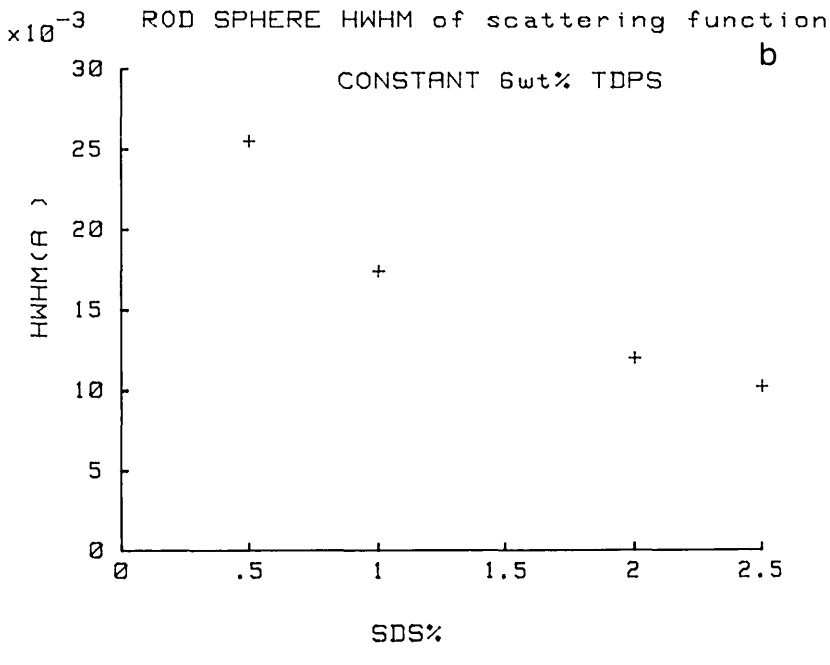


Figure 43: Neutron scattering data at high Q for SDS/TDPS mixed micelles along line 1, (a) sample 1, (b) sample 2, (c) sample 3, (d) sample 4 (from table 11).


ROD SPHERE Imax
CONSTANT 6 wt% TDPS
a
100
80
60
40
20
0
Imax
0
.5
1
1.5
2
2.5
SDS%


x10-3
ROD SPHERE HWHM of scattering function
b
CONSTANT 6wt% TDPS
30
25
20
15
10
5
0
HWHM(A)
0
.5
1
1.5
2
2.5
SDS%

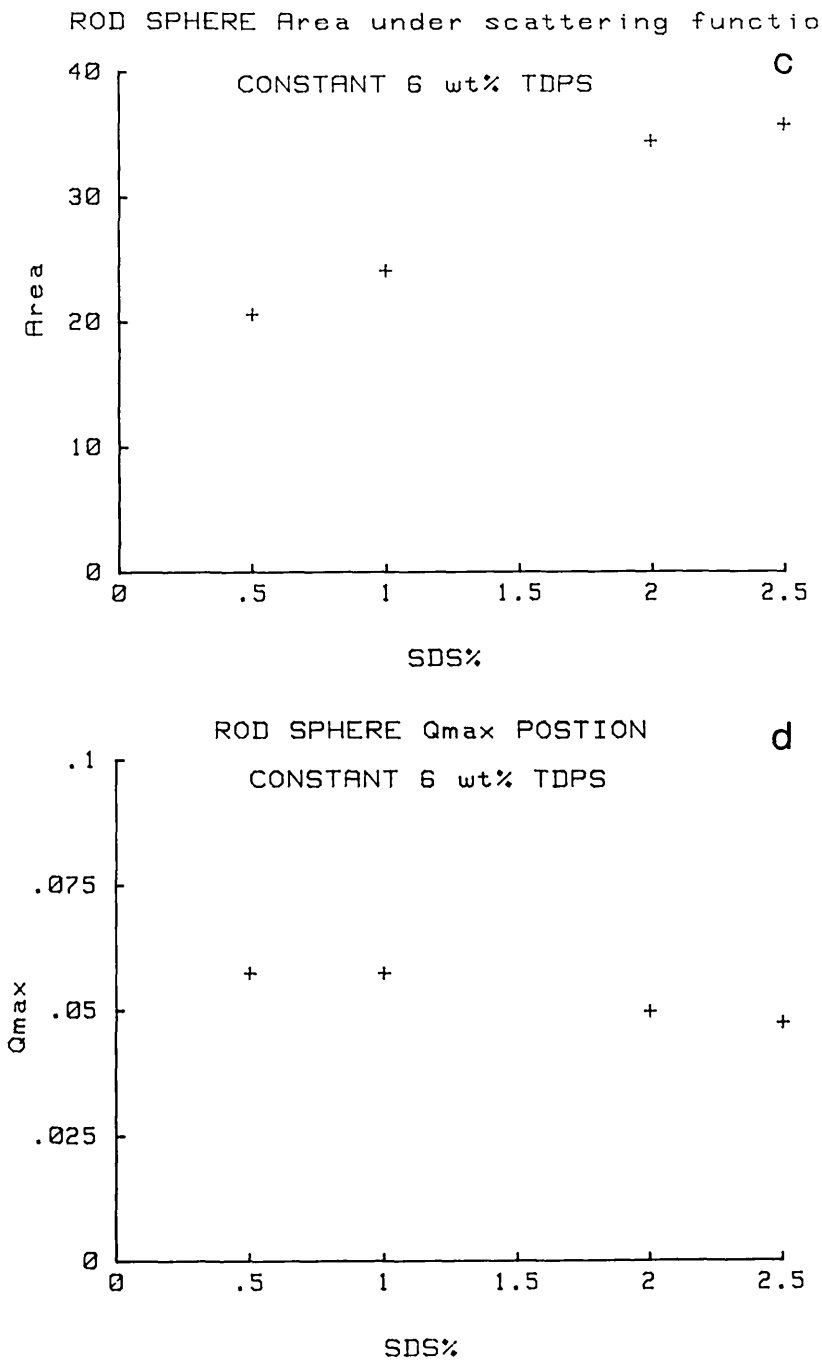


Figure 44: Spectral parameters associated with the data in figure 43.

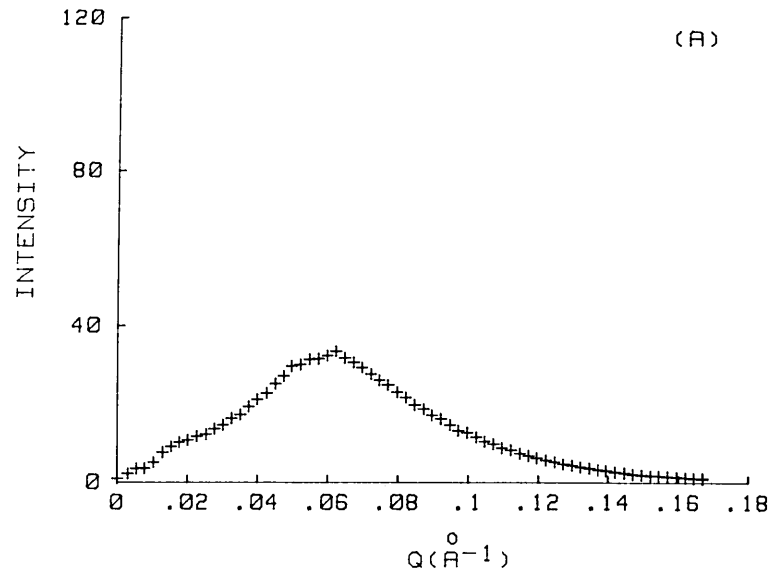
From the form factor equations 2(35) and 2(33) for a sphere and cylinder one can obtain information about the radius of the sphere and the length and radii of the rods. However, in the Q region examined the spectra reside outside the Guinier region $0<QRg<1$ and in theory a straight line should not be fitted to the plots of ln(I) or ln(IQ) against Q^2. Fits of these two functions were however attempted and the results are shown in table 12. These radii are a little small compared to the radius of the SDS micelles previously described (12), which should be similar to this system.

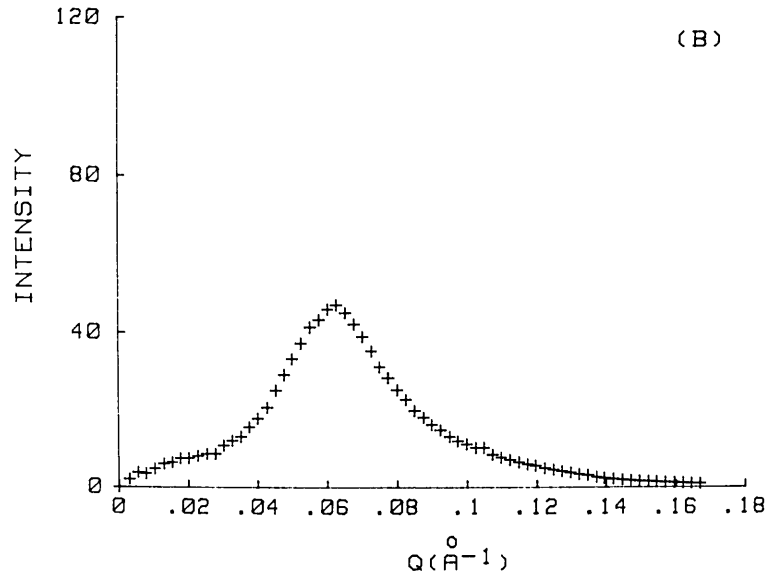
Table 12: Micelle dimension obtained from fits using Guinier plots.

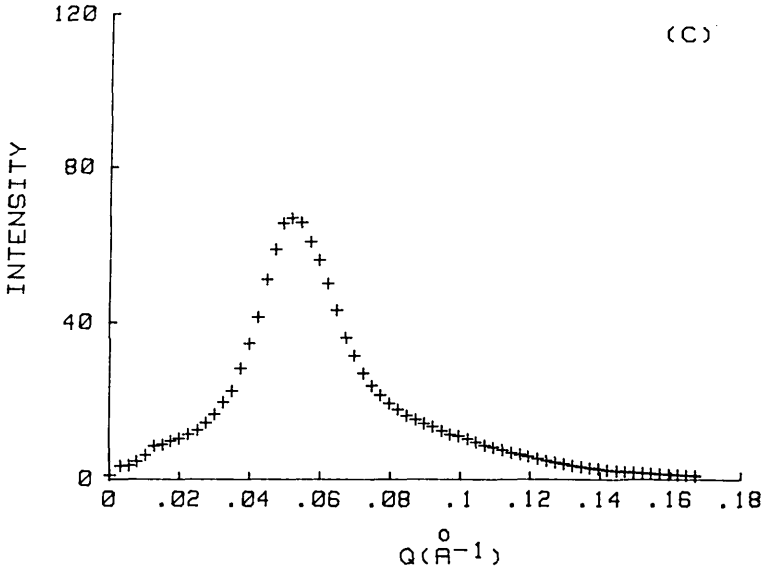
Samples on line 1	1	2	3	4
Radius of sphere (Å)	22.1	22.6	22.0	22.5
Radius of rod (Å)	21.8	21.8	-	23.2

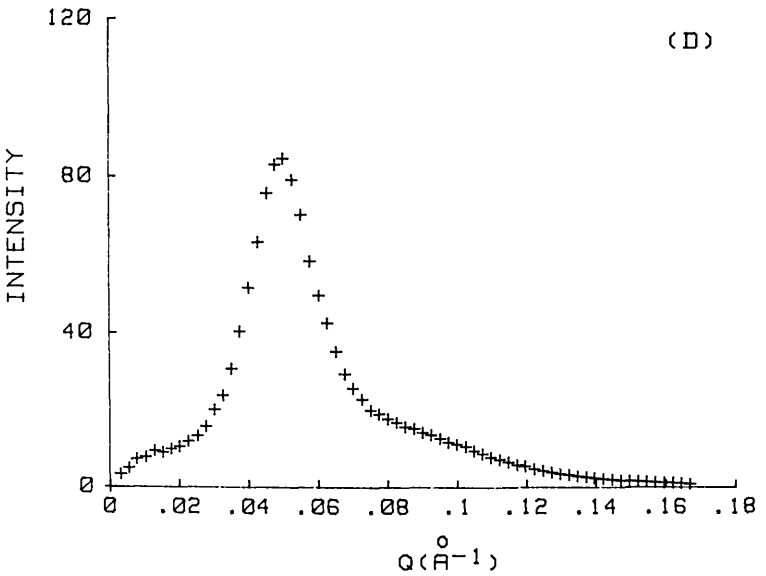
In other systems where interactions produce an interference peak suppression of the peak by electrolyte does not affect the peak position but reduces its magnitude. However, in these system addition of electrolyte alters the peak position dramatically. From the literature (148-150) it does appear that on addition of electrolyte the particles change shape. When the interaction energy was lowered by addition of salt the system can switch from spherical to rod-like micelles or rods can increase in length.

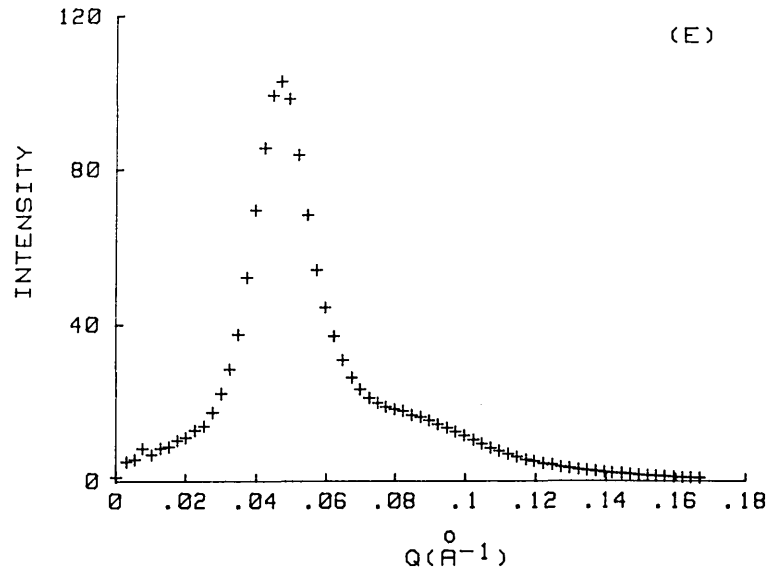
The neutron scattering data (not shown) from line 2 where the TDPS composition is kept constant at 4% (wt%) was very similar to line 1.

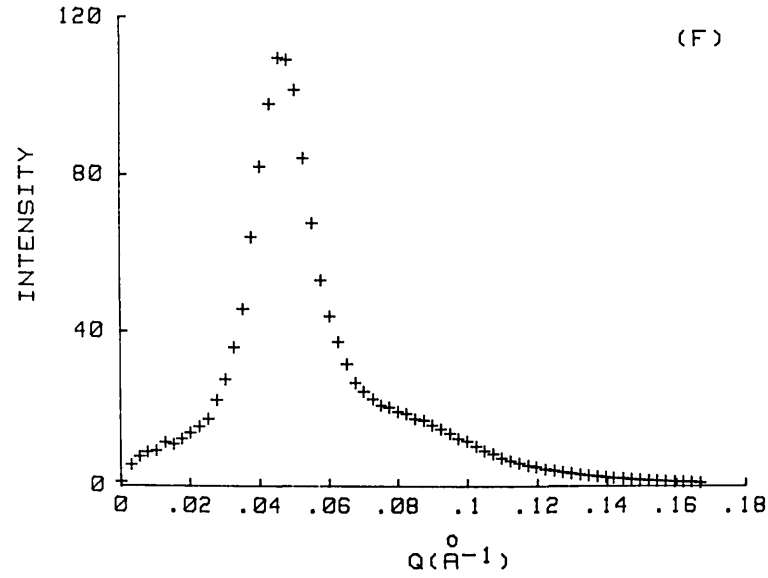

(A)
120
80
40
0
INTENSITY
0 .02 .04 .06 .08 .1 .12 .14 .16 .18
Q(Å⁻¹)

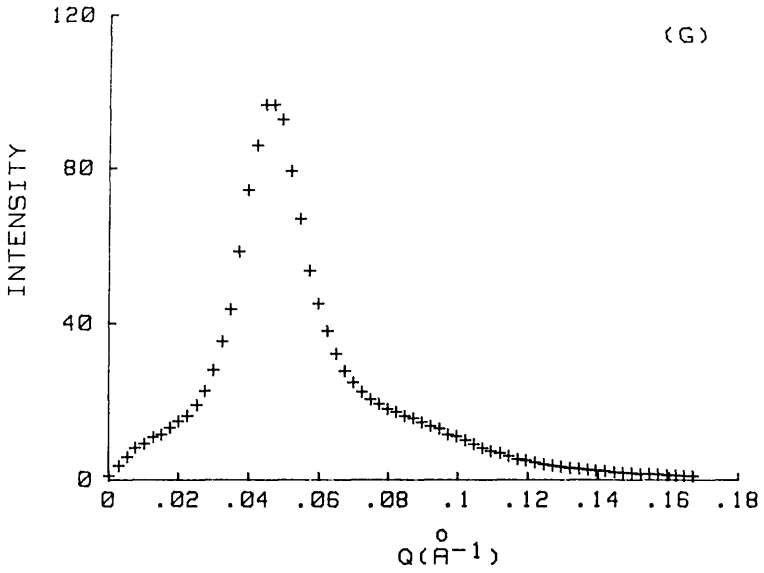

(B)
120
80
40
0
INTENSITY
0 .02 .04 .06 .08 .1 .12 .14 .16 .18
Q(Å⁻¹)

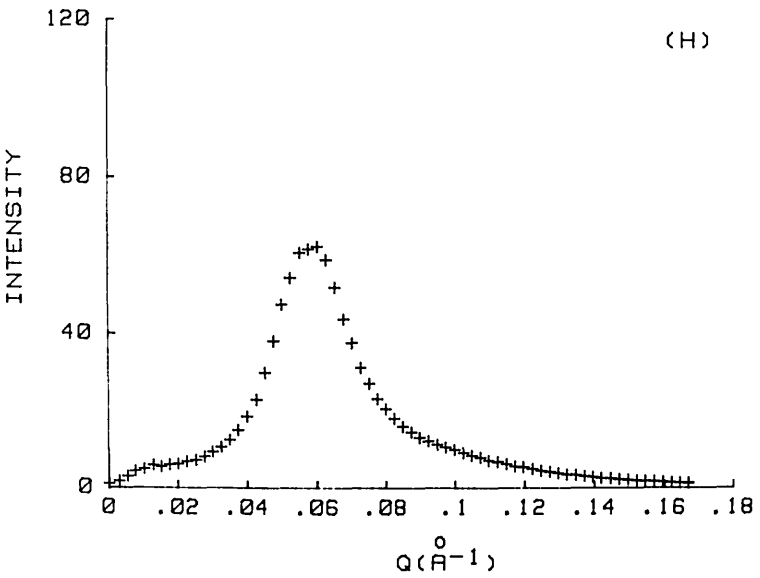

(C)
INTENSITY
120
80
40
0
0 .02 .04 .06 .08 .1 .12 .14 .16 .18
Q(Å⁻¹)


(D)
INTENSITY
120
80
40
0
0 .02 .04 .06 .08 .1 .12 .14 .16 .18
Q(Å⁻¹)


(E)
INTENSITY
120
80
40
0
0 .02 .04 .06 .08 .1 .12 .14 .16 .18
Q(Å⁻¹)


(F)
INTENSITY
120
80
40
0
0 .02 .04 .06 .08 .1 .12 .14 .16 .18
Q(Å⁻¹)


(G)
120
80
40
0
INTENSITY
0
.02
.04
.06
.08
.1
.12
.14
.16
.18
Q(Å⁻¹)


(H)
120
80
40
0
INTENSITY
0
.02
.04
.06
.08
.1
.12
.14
.16
.18
Q(Å⁻¹)

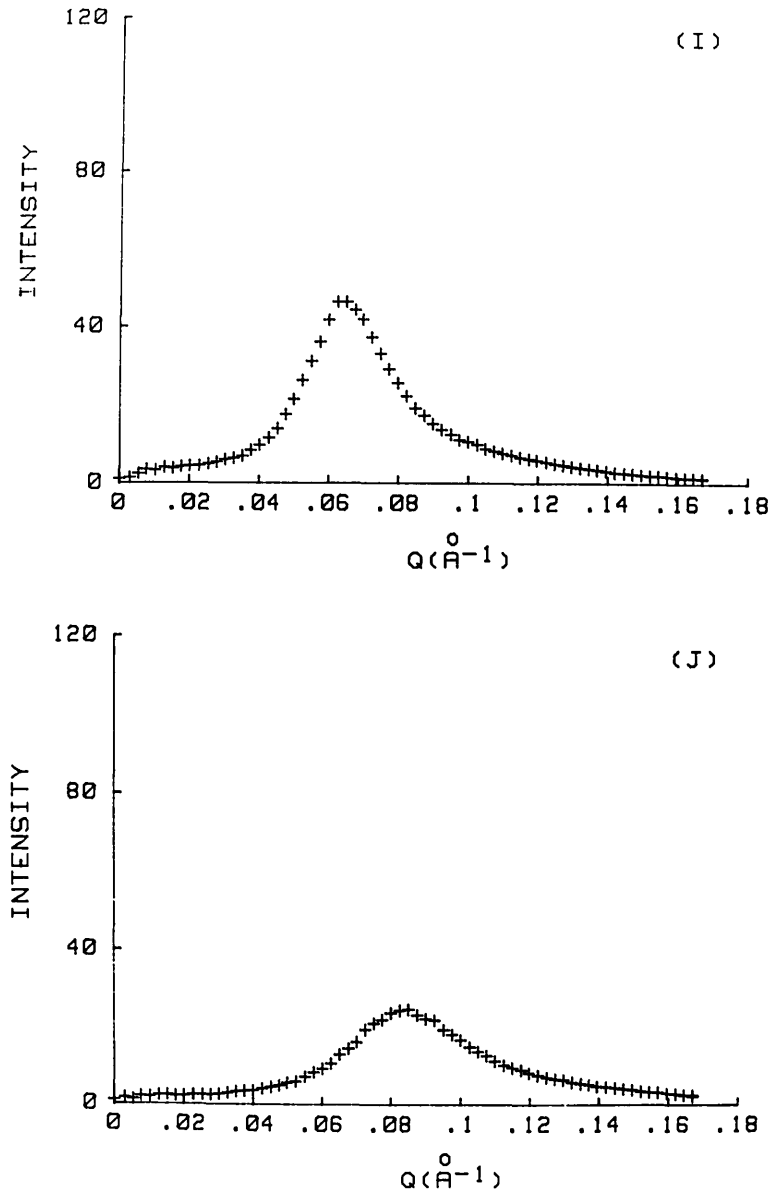
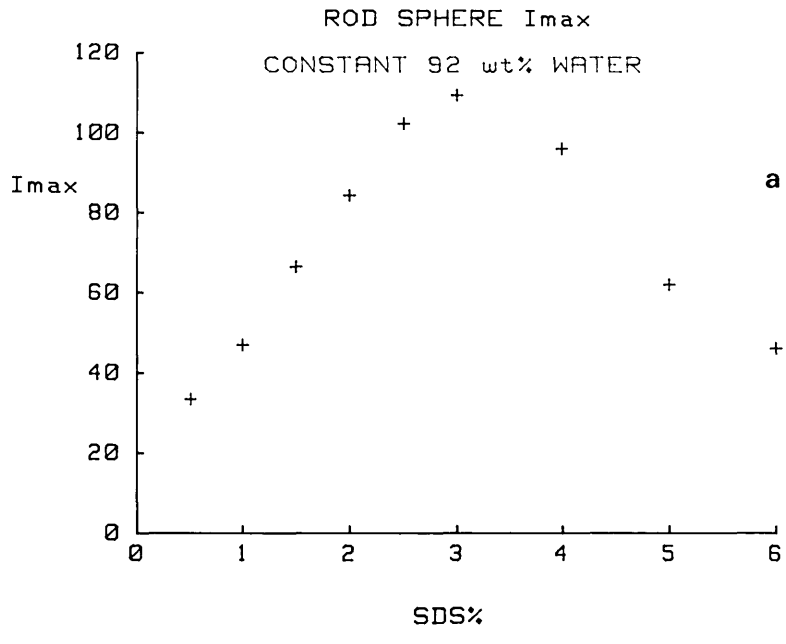
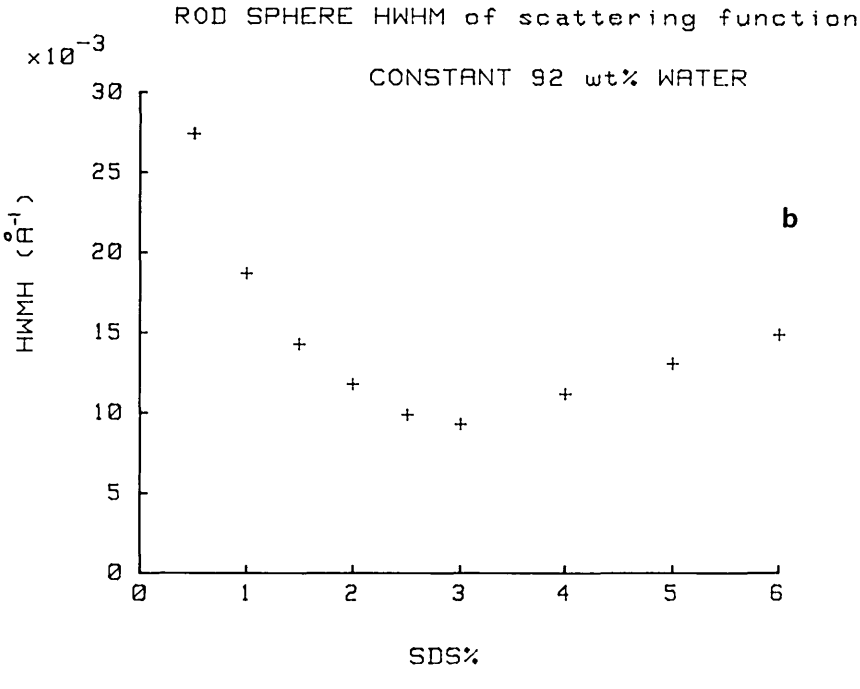


Figure 45: Neutron scattering data at high Q for SDS/TDPS along line 3. The samples (a) 22, (b) 23, (c) 24, (d) 25, (e) 26, (f) 27, (g) 28, (h) 29, (i) 30, (j) 31 (8% SDS) are described in table 11.


ROD SPHERE Imax
CONSTANT 92 wt% WATER
Imax
120
100
80
60
40
20
0
0
1
2
3
4
5
6
SDS%
a


ROD SPHERE HWHM of scattering function
CONSTANT 92 wt% WATER
x10^-3
HWMH (Å^-1)
30
25
20
15
10
5
0
0
1
2
3
4
5
6
SDS%
b

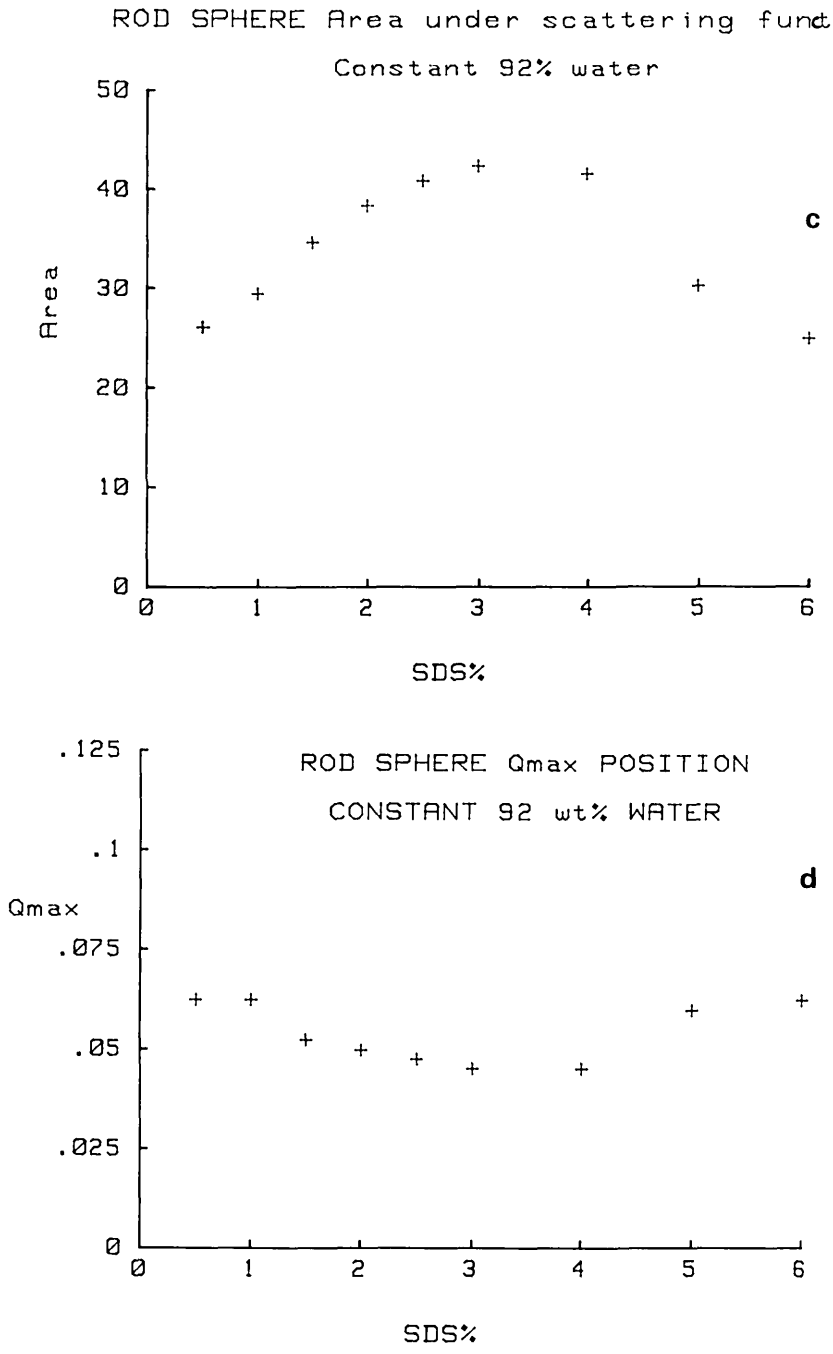


Figure 46: The spectral parameters associated with the data in figure 45 from sample 22-30.

The samples 22-30 on line 3, at constant water, show identical behaviour to line 1. At low SDS concentration the spectrum was broad and the peak was at high Q. As the ratio of surfactant changes the solutions become viscoelastic and changes were seen in the neutron scattering data. As SDS becomes the major component the solution passes through the transition again. The spectrum becomes broad and the peak moves out in Q as seen in Figure 44 and Figure 45. The difference between samples on lines 1 and 3 was that the surfactant concentration of line 1 changes from 4.5% to 6.5% while samples on line 3 have constant concentration of surfactant (6%). Line 4 shows similar behaviour to line 3 (data not shown).

On line 5 micellar solutions were prepared with TDPS only, in the concentration range 0.5%-10%. At 0.5% and 1% the scattering curves were fitted with a P(Q) for a sphere, equation 2(35), with a radius of 22Å convoluted with a Gaussian distribution of radii (half width, half maximum, h.w.h.m. 4.5Å). In this Q range the 0.5% data could be fitted in the Guinier region, equation 2(26). From the slope (figure 47b), a radius of gyration of 19.5Å was obtained. Using equation 2(32) the radius of gyration was converted to the equivalent spherical radius of 25Å. The 1% TDPS sample gave a radius of gyration of 19.7Å, giving a radius of 25.5Å for the micelle when fitted in the Guinier region.

At 10% TDPS, the highest concentration, it was attempted to extract the S(Q) function from the scattering curve, I(Q), by assuming that the 0.5% data was unstructured. The structure factor S(Q) was obtained by dividing the high concentration data by the whole curve for the lowest concentration. However, the S(Q) curve obtained was uncharacteristic, the data at low Q, S(0) was extremely high and there was no apparent peak in the curve. Theoretical calculation assuming a radius of 24Å and using the concentration of surfactant, predicted a peak at a Q value of $0.078Å^{-1}$. The shape of the experimental S(Q) was probably due to the 0.5% data being structured or that the micelles in this system change shape or size as a function of the concentration. Therefore, this method of extracting S(Q) from these data was inappropriate.

(4) Discussion of results

If on altering composition in line 1 the micellar size does not change then the number of particles should increase slightly. Therefore, interparticle spacings should decrease using the relationship $Q \cong 2\pi/d$ and the peak should move to a higher Q value. However, the data does not show this, as the SDS was increased the interparticle spacing increases and therefore it would appear that particles were changing shape. A simple calculation using the exact concentration of surfactants and the interparticle spacing obtained from the peak position indicated that sample 1 had an interparticle spacing of 105Å yielding 8.638×10^{17} particles per ml. The total number of molecules per ml was 1.2546×10^{20}, using these values the number of molecules per particle was estimated to be 158. By assuming each head group occupies $\sim 70Å^2$ the total surface area per particle may be calculated. From the total surface area the radius of the sphere was calculated to be 30Å or if a cylinder was considered then a length of 70Å with radius of 25Å was obtained.

Using the same method with sample 4, though now only considering a cylinder, the parameters are 180Å (length) and 25Å (radius), while samples 27 and 28 both gave lengths of 205Å using a radius of 25Å. The calculation was preformed on all the samples on line 1 and 3. If using this approximate calculation from the peak in I(Q) [Qmax] is correct, then this has given us an estimate for the micelle size assuming the shape to be rod-like or spherical (shown in table 13).

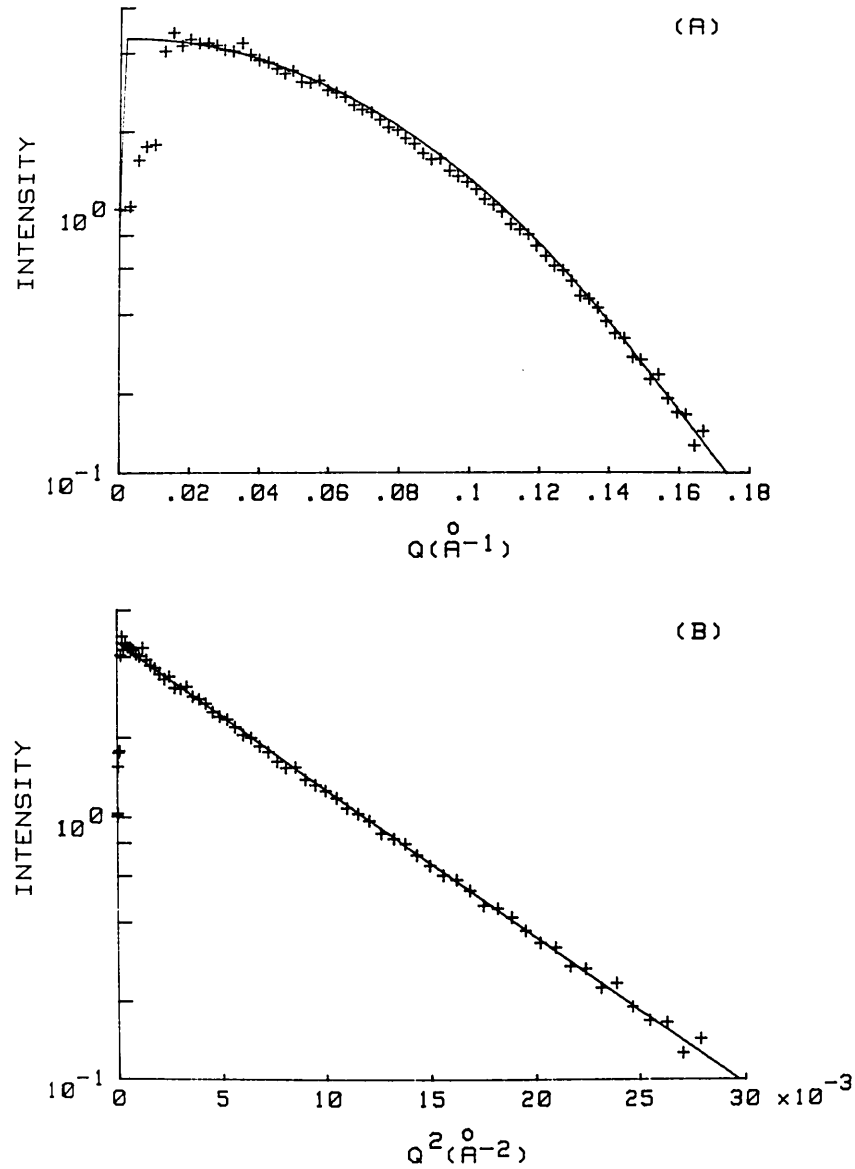


Figure 47: Neutron scattering data for 0.5% TDPS (line 5) fitted with (a) P(Q) using the parameters radius 22Å, h.w.h.m. 4.9, (b) using the Guinier approximation equation 2(28) obtaining a radius of 25Å.

Table 13: Micelles dimersion obtained from the peak in I(Q) data.

Line 1	1	2	3	4
Sphere (radius Å)	30	32	42.6	48
Cylinder (r=25Å) Length (Å)	70	81	145	180

Line 3	22	23	24	25	26	27	28	29	30
Sphere	31	31	40	43	47	50	50	33	32
Cylinder (r=25Å)	76	78	132	150	178	205	205	89	82

A number of the spectra have been fitted to the Hayter-Penfold model (for spherical micelles) with little success. However, one relevant point is worth mentioning; by assuming a P(Q) [equation 2(35)] with radii between 27Å and 40Å, and combining this with the S(Q) function with sensible parameters, the maximum in the data was fitted (the model never fitted the data at high or low Q). From this model a number of micelles per ml was calculated which was extremely close to the estimated value using the surfactant concentration and Qmax.

(5) General Discussion

In all the discussions thus far the transition between the Newtonian and viscoelastic solutions have been thought of as a transition between particle shapes. A spherical particle changes to a rod-like particle. This may be a simplistic view of the transition and other alternatives should be considered.

(i) A nematic transition is a transition from randomly arranged rod-like particles to hexagonally packed domains of rods. One would still, however, expect a viscous material in the randomly arranged rod region.

(ii) A more complex situation would be if in the Newtonian fluid a mixture of rods and spheres were present. Due to the nature of the two surfactants there may be preferential packing in the micelle whereby an SDS molecule would be more stable with TDPS molecules surrounding it and similarly with the TDPS molecules giving a close packed array of alternately packed molecules. At low concentration of one of the surfactants, this surfactant would preferentially enter a growing rod with alternate packing rather than enter micelles made up of the pure major component. The end result would be a small percentage of growing rods (with approximately 50:50 ratio of the surfactants) and almost pure spherical micelles of the major component. At a certain ratio of surfactant the chance of the minor surfactant entering all the spherical micelles is high and produces a system of 100% growing rods. After equilibriating for a period of time these rods form domains of order, which may or may not have similar lengths. The way to prove or disprove this theory of "phase separation" in the Newtonian region would involve a neutron scattering experiment where the spherical micelle of the major component could be contrast matched with the solvent. The observed particles would be the growing rods. If the ratio of surfactant was equal in all the micelles then no particle would be matched out and the final spectra would be exactly the same as before with slightly different intensity due to the contrast of the solvent.

(6) Conclusions and Future Aims

Although the transition to the viscoelastic region can be seen as an abrupt change in the shape of the spectra no details have yet been extracted about the P(Q) of the individual particles (radius or length) on either side of the boundary. The simple calculation using the Qmax has given us some indication of the micelle size if one makes the assumption of shape. However, it is the shape of the micelle that is of interest. The structure S(Q) cannot be removed by dilution or electrolyte so this is the major contribution to the spectra. Future analysis involves computing the P(Q) for a rod over the whole Q range examined. J. Hayter (151) has tried to attempt to adapt his model

to cylinderical micelles, if he were to succeed then all of these data could be modelled by extraction of the P(Q) from the I(Q) producing experimental S(Q). However, until such a development the analysis of the data remains unclear.

A programme of research has commenced recently with the growing interest in these rod-like micellar systems. Drs. Penfold and Hayter have used a theoretical analysis and a simple shear cell with poiseuille flow, constructed from quartz to investigate rod-like micelle solutions. No theory as yet is available for interacting rods under shear. My colleagues, Drs. Cummins and Staples, have designed and built a rheometer which can have radiation (neutron or light) transmitted through it enabling simultaneous measurements of viscosity and scattering in a sheared environment. Together they intend to use the new cell design to study various rod-like systems.

By applying a high shear onto the viscous solutions the rods orient themselves in the direction of flow. By collecting the data on the usual two dimensional detector, information about the micelle shape in two directions may be obtained. Analyses of such data was done by only using the information in a 10° sector perpendicular and parallel to the flow (figure 48).

Initial data modelled by Penfold and Hayter (152, 153) on some rod-like systems seems extremely promising determining the rods dimensions (radius and length). In figure 49 their data for a CTAB solution was shown. This data was only presented to emphasise the vast difference between the TDPS/SDS system (shown later) and another rod-like system (CTAB). Both the spectra and the dimensions of the rod lengths are different. CTAB rods are an order of ten larger than the estimated TDPS/SDS rods dimensions.

When the TDPS/SDS system was highly sheared the peak in the data moved into the sector perpendicular to the flow. The peak also increased in magnitude. In figure 50 the TDPS/SDS system (2% SDS and 6% TDPS) was shown at low and high shear. There was still a peak in the data parallel to the flow.

Even when one degree of freedom was removed from this system little information has been extracted. However, the continuation of the work by the above researchers will, I am sure, result in some extremely fascinating conclusions.

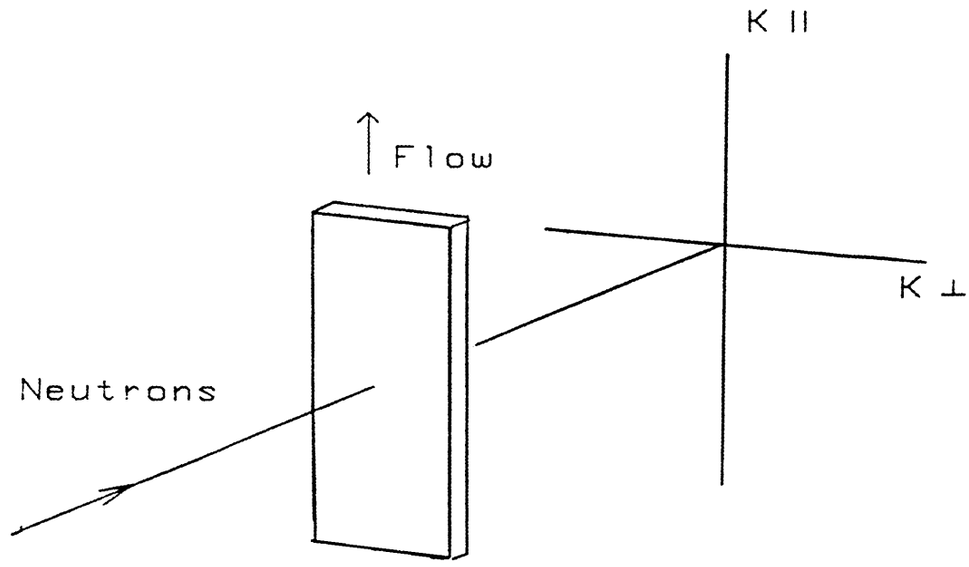


Figure 48: Schematic diagram of the flow in the shear experiments on rod micellar system. K is equal to Q in this diagram.

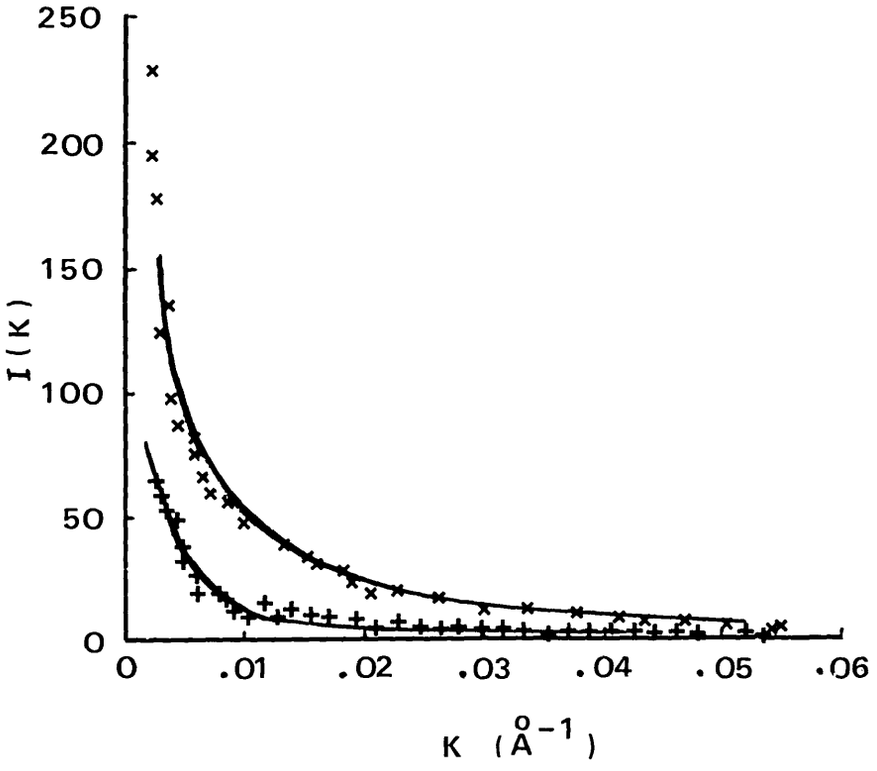


Figure 49: Neutron scattering data perpendicular(+) and parallel(×) to the flow direction for 0.03M CTAB in 0.4M KBr/D_2O. The fits to the data indicate that the micelle dimensions are 3200Å length and 25Å radius. K is equivalent to Q in this diagram.

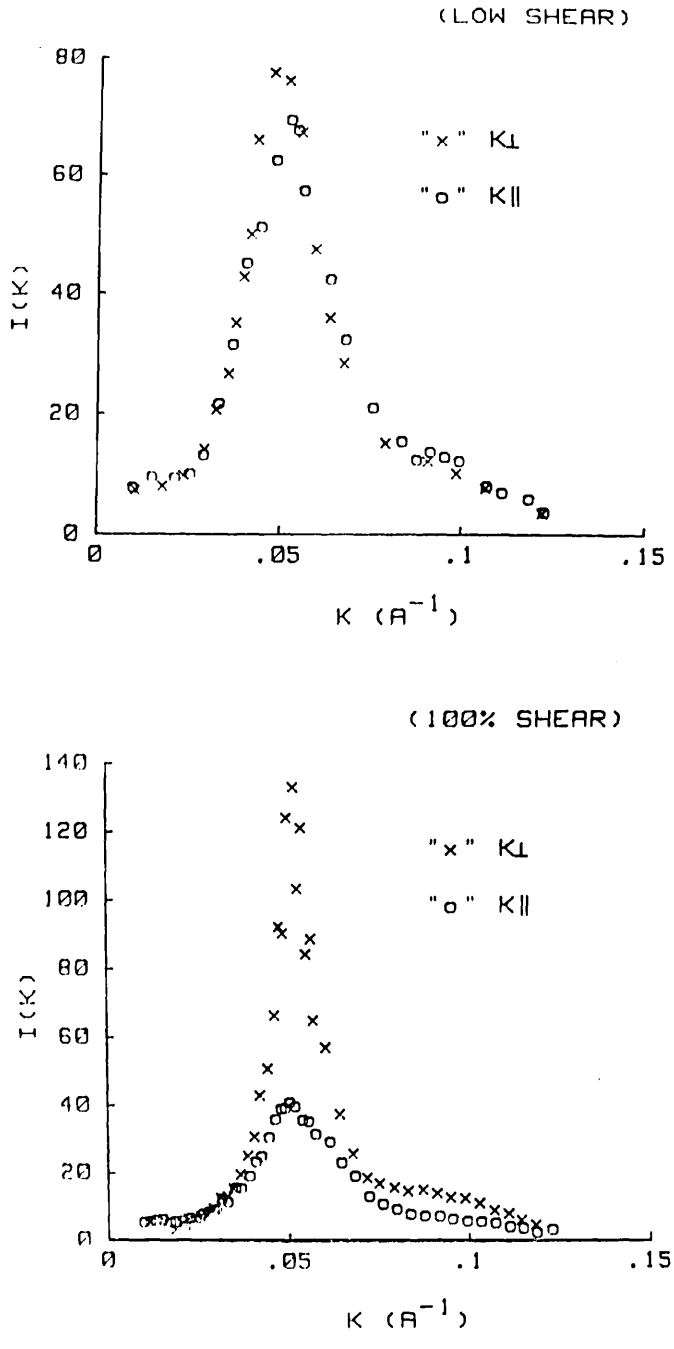


Figure 50: Neutron scattering data perpendicular and parallel to the flow direction for the TDPS/SDS system (2% SDS and 6% TDPS), (a) low shear, (b) high shear. K is equivalent to Q in this diagram.

CHAPTER 1 REFERENCES

1. J.W. McBain, J.W. Laing and A.F. Titley, J.C.S., 115, 1219, 1919.

2. J.W. McBain and C.S. Salmon, J. Amer. Chem., 42, 426, 1920.

3. G.S. Hartley, "Aqueous Solutions of Paraffin Chain Salts", Herman, Paris, 1936.

4. "Microemulsions, Theory and Practice" (Ed. L.M. Prince), Academic Press, New York, 1977.

5. M.L. Corrin, J. Colloid Sci., 3, 333, 1948.

6. K. Shinoda and E. Hutchinson, J. Phys. Chem. 66, 577, 1962.

7. D.G. Hall, Kolloid-Z, Z. Polym., 250, 895, 1972.

8. V.A. Parsegian, Ann. Rev. Biophys. Bioeng., 2, 221, 1973.

9. D.J. Mitchell and B.W. Ninham, J. Chem. Soc. Faraday Trans. 2, 77, 601, 1981.

10. O.W. Howarth, Chem. Soc. Faraday Trans. 1, 71, 2303, 1975.

11. V.A. Parsegian, Trans. Faraday Soc., 62, 848, 1966.

12. J.B. Hayter and J. Penfold, J. Chem. Soc., Faraday Trans. 1., 77, 1851-1863, 1981.

13. H. Rehage and H. Hoffmann, Faraday Discuss. Chem. Soc., 76, 1983.

14. P. Ekwall, L. Mandell and K. Fontell, Mol. Cryst. Liq. Cryst. 8, 157, 1969.

15. P. Ekwall, Advances in Liquid Crystals (Ed. G.H. Brown), Academic Press, New York, San Francisco and London Vol. 1, Ch. 1, p. 1, 1971.

16. V. Luzzati, "Biological Membranes" (Ed. D. Chapman), Academic Press, London and New York, Ch. 3, p. 71, 1968.

17. G.W. Gray and P.A. Winsor, Adv. Chem. Ser., 152, 1, 1976.

18. J.M. Vincent and A.W. Skoulios, Acta Cryst., 20, 432, 1966.

19. S.J. Singer and G.L. Nicholson, Science, New York, 175, 720, 1972.

20. D. Gingell, I. Todd and J. Bailey, J. Cell. Biol., in press.

21. D.A. Rees, J.R. Couchman, C.G. Smith, A. Woods and G. Wilson, Phil. Trans. R. Soc. London. B., 299, 169, 1982.

22. A.G. Lee, N.J.M. Birdsall and J.C. Metcalfe, In "Methods in Membrane Biology" (Ed. E. Korn), Plenum Press, New York, 1974.

23. Y.K. Levine, N.J.M. Birdsall, A.G. Lee and J.C. Metcalfe, Biochemistry, 11, 1416, 1972.

24. P. Solyom and P. Ekwall, Rheol. Acta, 8, 316, 1969.

25. M.J. Groves and A.B. Ahmed, Rheol. Acta, 15, 501, 1976.

26. G.J.T. Tiddy, Ch. 7 in "Nuclear Magnetic Resonance", (Ed. R. Harris), the Chemical Society, London, 4, 233, 1975.

27. H.J. Galla and E. Sackmann, Biochim. Biophys. Acta, 339, 103, 1974.

28. B. Norden, G. Lindblom and I. Jonas, J. Phys. Chem., 81, 2086, 1977.

29. K. Larsson and R.P. Rand, Biochim. Biophys. Acta, 326, 245, 1978.

30. H.C. Van de Hulst, "Light Scattering by Small Particles", Wiley, 1957.

CHAPTER 2 REFERENCES

31. M. Kerker, "The Scattering of Light and Other Electromagnetic Radiation", Academic Press, New York, 1969.

32. "Photon Correlation and Light Beating Spectroscopy", (Eds. H.Z. Cummins and E.R. Pike), Plenum, 1974.

33. B.J. Berne and R. Pecora, "Dynamic Light Scattering", Wiley, New York, 1976.

34. B. Jacrot, Rep. Prog. Phys., 39, 911, 1976.

35. P.A. Egelstaff, "An Introduction to the Liquid State", Academic Press, New York, 1967.

36. G. Oster and D.P. Riley, Acta Cryst., 5, 1, 1952.

37. J.B. Hayter and T. Zemb, Chem. Phys. Lett., 93(1), 91, 1982.

38. D. Bendedouch, S.H. Chen, W.C. Koehler and J.S. Lin, J. Chem. Phys., 76, 5022, 1982.

39. A. Vrij, J.W. Jansen, J.K.G. Dhont, C. Pathamamanoharan, M.M. Kops-Werkhoven and H.M. Fijnant, Faraday, Discuss. Chem. Soc., 76, 1983.

40. H.B. Stuhrmann, J. Appl. Cryst., 7, 173, 1974.

41. O. Kratky and G. Porod, Acta. Physica. Austriaca, 2, 133, 1948.

42. Lord Rayleigh, Proc. Roy. Soc., A90, 219, 1914.

43. D.O. Tinker, Chem. Phys. Lipids, 8, 230, 1972.

44. R. Sergio, S. Aragon and R. Pecora, J. Colloid Interface Sci., 89(1), 170, 1982.

45. D.J. Cebula and R.H. Ottewill, Colloid & Polymer Sci., 260, 1118, 1982.

46. P.N. Pusey, Phil. Trans. R. Soc. Lond., A 293, 429, 1979.

47. J.C. Brown, P.N. Pusey, J.W. Goodwin and R.H. Ottewill, J. Phys., A 8, 664, 1975.

48. P.N. Pusey, J. Phys. A. Math. Gen., 8, 1433, 1975.

49. M. Corti and V. Degiorgio, in "Light Scattering in Liquids and Macromolecular Solutions", (Eds. V. Degiorgio, M. Corti and M. Giglio), Plenum Press, New York, 1980, p.111.

50. M. Corti and V. Degiorgio, J. Phys. Chem., 85, 711, 1981.

51. M.B. Weissman, J. Chem. Phys., 72, 231, 1980.

52. P.N. Pusey, in "Light Scattering in Liquids and Macromolecular Solutions", (Eds. V. Degiorgio, M. Corti and M. Giglio), Plenum Press, New York, 1980.

CHAPTER 3 REFERENCES

53. B.V. Derjaguin and L. Landau, Acta. Physiochim., 14, 633, 1941.

54. E.J.W. Verwey and J.Th.G. Overbeek, "The Theory of the Stability of Lyophobic Colloids", Elsevier, Amsterdam, 1948.

55. B.V. Derjaguin, Trans. Fara. Soc., 18, 85, 1954.

56. L.M. McCartney and S. Levine, J. Colloid Interface Sci., 30, 345, 1969.

57. L.M. Barclay and R.H. Ottewill, Spec. Discuss. Faraday Soc., 1, 138, 1970.

58. V.A. Parsegian, N.L. Fuller and R.P. Rand, Proc. Natl. Acad. U.S.A., 76, 2750, 1979.

59. B. Vincent, J. Colloid Interface Sci., 42, 270, 1973.

60. D.J. Cebula, R.H. Ottewill, J. Ralston and P.N. Pusey, J. Chem. Soc. Faraday Trans., 77, 2585, 1981.

61. L.J. Magid, R. Triolo, J.S. Johnson and W.C. Koehler, J. Phys. Chem., 86, 164, 1982.

62. J.K. Percus and G.J. Yevick, Phys. Rev., 110, 1, 1958.

63. N.W. Ashcroft and J. Lekner, Phys. Rev., 45, 33, 1966.

64. J.A. Barker and D. Henderson, Rev. Mod. Phys., 48, 587, 1976.

65. J.B. Hayter and J. Penfold, J. Chem. Soc. Faraday Trans. 1, 77, 1851, 1981.

66. J.B. Hayter and J. Penfold, Colloid and Polymer Sci., 261, 1022, 1983.

67. J.B. Hayter and J. Penfold, Mol. Phys., 42, 109, 1981.

68. J.B. Hayter and M. Zulauf, Colloid and Polymer Sci., 260, 1023, 1982.

CHAPTER 4 REFERENCES

69. G. Zaccai and B. Jacrot, Ann. Rev. Biophys. Bioeng., 12, 139, 1983.

70. A. Maconnachie and R.W. Richard, Polymer, 19, 739, 1978.

71. J.S. Higgins and Stein, J. Appl. Crystallogr., 11, 346, 1978.

72. R.H. Ottewill, Chapter 7 and 9, "Colloidal Dispersions", (Ed. J.W. Goodwin), Royal Soc., Chem. Special Publication No. 43, 1981.

73. K. Ibel, J. Appl. Crystallogr., 9, 296. 1976.

74. P.N. Pusey, Chapter 6, "Colloid Dispersions", (Ed. J.W. Goodwin), Royal Soc. Chem. Special Publication No. 43, 1981.

75. B. Chu, "Laser Light Scattering", Academic Press, New York, 1974.

76. P.N. Pusey and J.M. Vaughan, "Dielectric and Related Molecular Processes", (Ed. M. Davies), Vol. 2., The Chem. Soc., London, 1976.

77. A.J.F. Siegert, MIT Rad. Lab. Rep. No. 465, 1943.

78. B. Chu, Physica. Scripta., 19, 458, 1979.

79. S.W. Provencher, J. Hendrix, L. DeMaeyer and N. Paulussen, J. Chem. Phys., 69, 4273, 1978.

80. N. Ostrowski, D. Sornette, P. Parker and E.R. Pike, Optoca Acta., 28, 1059, 1981.

81. D.E. Koppel, J. Chem. Phys., 57, 4814, 1972.

CHAPTER 5 REFERENCES

82. D.A. Tyrrell, T.D. Heath, C.M. Colley and B.E. Ryman, Biochim. Biophys. Acta, 457, 259, 1976.

83. D. Papahadjopoulos, Ann. N.Y. Acad. Sci., 308, 1978.

84. J.N. Israelachvili, D.J. Mitchell and B.W. Ninham, Biochim. Biophys. Acta., 470, 185, 1977.

85. E.G. Finer, A.G. Flook and H. Hauser, Biochim. Biophys. Acta., 260, 49, 1972.

86. C. Huang, Biochem. 8, 344, 1969.

87. E.P. Day, J.T. Ho, R.K. Kunze and S.T. Sun, Biochim. Biophys. Acta., 470, 503, 1977.

88. J. Goll, F.D. Carlson, Y. Barenholz, B.J. Litman and T.E. Thompson, Biophys. J. 38, 7, 1982.

89. W. Knoll, J. Haas, H.B. Stuhrmann, H.H. Fuldner, H. Vogel and E. Sackman, J. Appl. Crystallogr., 14, 191, 1981.

90. V. Luzzati and F. Husson, J. Cell. Biol. 50, 187, 1962.

91. M. Eisenberg, T. Gresalfi, T. Riccio and S. McLaughlin, Biochem. 18, 5213, 1979.

92. C. Huang and J.T. Mason, Proc. Natl. Acad. Sci. USA, 75, 308, 1978.

93. S. Nir and J. Bentz, J. Colloid Interface Sci. 65, 399, 1978.

94. S. Nir, J. Bentz and N. Duzgunes, J. Colloid Interface Sci. 84, 266, 1981.

95. M. Koter, B. de Kruijff and L.L.M. van Deenen, Biochim. Biophys. Acta., 514, 255, 1978.

96. J. Lansmann and D.H. Haynes, Biochim. Biophys. Acta., 394, 335, 1975.

97. J. Wilschut, N. Duzgunes and D. Papahadjopoulos, Biochem. 20, 3126, 1981.

98. D.M. Le Neveu, R.P. Rand, V.A. Parsegian and D. Gingell, Biophys. J., 18, 209, 1977.

99. A.C. Cowley, N.L. Fuller, R.P. Rand and V.A. Parsegian, Biochem. 17, 3163, 1978.

100. R.P. Rand, Annu. Rev. Biophys. Bioeng. 10, 277, 1981.

101. M.E. Loosley-Millman, R.P. Rand and V.A. Parsegian, Biophys. J., 40, 221, 1982.

102. J.A. Beunen and L.R. White, Colloids and Surfaces, 3, 371, 1981.

103. W.R. Morrison, Anal. Biochem. 7, 218, 1964.

104. S. Komura, Y. Toyoshima and T. Takeda, Jpn. J. Appl. Phys. 21, 1370, 1982.

105. F.C. Chen, A. Chrzeszczyk and B. Chu, J. Chem. Phys. 64, 3403, 1976.

106. D.P. Riley and G. Oster, Faraday Discuss. Chem. Soc. 11, 107, 1951.

107. B.A. Cornell, J. Middlehurst and F. Separovic, Biochim. Biophys. Acta., 598, 405, 1980.

108. R.H. Ottewill and R.A. Richardson, Colloid Polym. Sci., 260, 708, 1982.

109. A. Vrij, J. Chem. Phys. 71, 3267, 1979.

110. A. Vrij, J. Chem. Phys., 69, 1742, 1978.

111. H.M. Fijnaut, C. Pathmamanoharan, E.A. Nieuwenhuis and A. Vrij, Chem. Phys. Lett., 59, 351. 1978.

112. P. van Beurten and A. Vrij, J. Chem. Phys., 74, 2744, 1981.

113. M.M. Kops-Werkhoven and H.M. Fijnaut, J. Chem. Phys., 77, 2242, 1982.

114. M.M. Kops-Werkhoven, C. Pathmamanoharan, A. Vrij and H.M. Fijnaut, J. Chem. Phys., 77, 5913, 1982.

115. D.J. Cebula, D.Y. Myers and R.H. Ottewill, Colloid Polym. Sci. 260, 96, 1982.

116. J. Goll, F.D. Carlson, Y. Barenholz, B.J. Litman and T.E. Thompson, Biophys. J. 38, 7, 1982.

117. F.C. Chen. A. Chrzeszczyk and B. Chu, J. Chem. Phys., 64, 3403, 1976.

118. A.L. Larrabee, Amer. Chem. Soc. 18, 3321, 1979.

119. Y.M. Tricot, D.N. Furlong, W.H.F. Sasse, P. Davis and I. Snook, Austr. J. Chem. 36, 609. 1983.

120. Y.M. Tricot, D.N. Furlong, W.H.F. Sasse, P. Davis, I. Snook, W. van Megen, J. Colloid Interface Sci., to be published.

121. N.F. Carnahan and K.E. Starling, J. Chem. Phys. 51, 635, 1969.

122. A. Vrij, E.A. Nieuwenhuis, H.M. Fijnaut and W.G.N. Agterof, Faraday Discuss. Chem. Soc., 65, 101, 1978.

123. B.J. Ackerson, J. Chem. Phys., 64, 242, 1976.

124. P.N. Pusey and J.M. Vaughan, Dielectric and Related Molecular Processes (Specialist Periodical Report, The Chemical Society, London 1975), Vol. 2, Chap. 2, pp. 48-105.

CHAPTER 6 REFERENCES

125. K. Dorn, E.V. Patton, R.T. Klingbiel, D.F. O'Brien and H. Ringsdorf, Makromol. Chem. Rapid Commun., 4, 513, 1983.

126. K. Dorn, R.T. Klingbiel, D.P. Specht, P.N. Tyminski, H. Ringsdorf and D.F. O'Brien, J. Am. Chem. Soc., 106, 1627, 1984.

127. H. Gaub, E. Sackmann, R. Buschl and H. Ringsdorf, Biophys. J., 45, 725, 1984.

128. N. Wagner, K. Dose, H. Koch and H. Ringsdorf, Febs. Lett., 132, 313, 1981.

129. T. Kunikate, N. Nakashima, K. Takarabe, M. Nagai, A. Tsuge and H. Yanagi, J. Am. Chem. Soc., 103, 5945, 1981.

130. S.L. Regen, A. Singh, G. Oehme and M. Singh, J. Am. Chem. Soc., 104, 791, 1982.

131. S.L. Regen, Polymer News, 10, 68, 1984.

132. B. Hupfer and H. Ringsdorf, "Polymer Science Overview" (Ed. A. Stahl), ACS Symposium Series, 175, 209, 1981.

133. J.H. Fendler, Acc. Chem. Res., 13, 7, 1980.

134. S. Hayashida, K. Takarabe, M. Fujiki and T. Kunitake, Polymer Preprints, Japan, 28(1), 107, 1979.

135. S.L. Regen, J.S. Shin and K. Yamaguchi, J. Am. Chem. Soc. 106, 2446, 1984.

136. S.L. Regen, B. Czech and A.J. Singh, J. Am. Chem. Soc. 102, 6638, 1980.

137. P. Debye, Ann. Physik. 46, 809, 1915.

138. G. Porod, Kolloid-Z, 83, 124, 1951.

CHAPTER 7 REFERENCES

139. H. Hoffmann, H. Rehage, G. Platz, W. Schorr, H. Thurn and W. Ulbricht, Colloid Polym. Sci., 260, 1042, 1982.

140. H. Hoffmann, G. Platz, H. Rehage, W. Schorr and W. Ulbricht, Ber. Bunsenges, Phys. Chem., 85, 255, 1981.

141. H. Hoffmann, G. Platz, H. Rehage, K. Reizlein and W. Ulbricht, Makromol. Chem., 182, 451, 1981.

142. H. Hoffmann, G. Platz and W. Ulbricht, J. Phys. Chem., 85, 1418, 1981.

143. W. Schorr and H. Hoffmann, J. Phys. Chem., 85, 3160, 1981.

144. H. Hoffmann, G. Platz, H. Rehage and W. Schorr, Ber. Bunsenges, Phys. Chem., 85, 877, 1981.

145. S. Gravsholt, J. Colloid Interface Sci., 57, 576, 1976.

146. J. Ulmius, H. Wennerstrom, L.B.A. Johansson, G. Lindblom and S. Gravsholt, J. Phys. Chem., 83, 2232, 1979.

147. M. Doi and S.F. Edwards, J. Chem. Soc. Faraday Trans. 2, 74, 918, 1978.

148. C.A. Barker, D. Saul, G.J.T. Tiddy, B.A. Wheeler and E. Willis, J. Chem. Soc. Faraday Trans. 1, 70, 154, 1974.

149. D. Saul, G.J.T. Tiddy, B.A. Wheeler and E. Willis, J. Chem. Soc. Farraday Trans. 1, 70, 163, 1974.

150. G.J.T. Tiddy and B.A. Wheeler, J. de Physique, Colloque C1, 36, C1-167, 1975.

151. J. Hayter, private communication.

152. J. Penfold, unpublished data.

153. J.B. Hayter and J. Penfold, J. Phys. Chem., 88, 4589, 1984.